NASA Contractor Report 159246



# Performance and Noise of a Low Pressure Ratio Variable Pitch Fan Designed for General Aviation Applications

F. B. Metzger
R. W. Menthe
C. J. McColgan

January 31, 1980

Prepared for NASA Langley Research Center,
Hampton, Va. Under Contract
NAS1-13774

HAMILTON STANDARD

Division of UNITED TECHNOLOGIES

# Performance and Noise of a Low Pressure Ratio Variable Pitch Fan Designed for General Aviation Applications

F. B. Metzger
R. W. Menthe
C. J. McColgan

January 31, 1980

Prepared for NASA Langley Research Center,
Hampton, Va. Under Contract
NAS1-13774

HAMILTON STANDARD

Division of
UNITED
TECHNOLOGIES

Index

## ABSTRACT

A limited study has been conducted to establish the performance and noise characteristics of a low design tip speed (168 m/s, 550 ft/sec) low pressure ratio (1.04) variable pitch fan which was tested in the NASA Langley 30X60 tunnel. This fan was designed for minimum noise when installed in the tail mount location of a twin engine aircraft which normally has both nose and tail mounted propulsors. For the tests discussed in this report the propeller normally mounted on the nose of the aircraft was removed.

Measurements showed the fan noise to be very close to predictions made during the design of the fan and extremely low in level (65 dBA at 1000 ft) with no acoustic treatment. This is about 8 dB lower than the unshrouded 2 blade propeller normally used in this installation. On the basis of tests conducted during this program it appears that this level could be further reduced by 2 dBA if optimized acoustic treatment were installed in the fan duct. Even the best of the shrouded propellers tested previously were 7 dB higher in level than the )-Fan without acoustic treatment.

It was found that the cruise performance of this fan was within 5% of the predicted efficiency of 72%. Evaluation of the performance data indicated that disturbances in the inflow to the fan were the probable cause of the reduced performance. Exhaust flow from the simulated engine which passed through the root sections of the blades is an area of particular concern. While a retwist of the inboard sections of the blades on the fan is predicted to overcome some of this deficiency it appears that the better inflow characteristics of a tractor mounted fan might provide even greater gains in performance. As expected, the low pressure ratio fan efficiency was lower than that of the unshrouded propeller but not substantially lower than that of the larger diameter shrouded propeller and substantially higher than could be achieved with high bypass ratio turbofans.

Although the analysis work discussed in this report was limited, the relatively good agreement between predicted and measured noise and performance demonstrated in this program provides confidence in the design methodology used and indicates that this methodology should be successful in tailoring a low pressure ratio fan to other installation and performance requirements.

## SYMBOLS

| | |
|---|---|
| b | wing span, 10.851 m (35.60 ft.) |
| B | number of propeller blades |
| $\bar{c}$ | wing mean aerodynamic chord, 1.490 m (4.89 ft.) |
| D | propulsor diameter, m (ft.) |
| $C_D$ | aircraft drag coefficient, drag/q S |
| $C_L$ | aircraft lift coefficient, lift/q S |
| $C_m$ | aircraft pitching-moment coefficient, pitching moment/q S$\bar{c}$ |
| $C_P$ | propeller power coefficient, $\frac{2\pi Q}{\rho n^2 D^5}$ |
| $C_T$ | propeller thrust coefficient along Q-Fan rotational axis, $\frac{T}{\rho n^2 D^4}$ |
| $C_T'$ | airplane thrust coefficient, $\frac{T}{q\ S}$ |
| E or E(t) | instantaneous hot wire voltage |
| $\bar{E}$ | mean component of hot wire voltage $\quad \bar{E} = \lim_{T\to\infty} \frac{1}{T} \int_0^T E(t)\, dt$ |
| e' or e'(t) | fluctuating component of hot wire voltage $\quad e'(t) = E(t) - \bar{E}$ |
| hp | shaft horsepower, watts $\frac{ft\text{-}lb}{sec}$ |
| J | propeller advance ratio, $\frac{V}{nD}$ |
| n | propeller revolutions per second |
| N | propeller revolutions per minute |
| $P_R$ | pressure ratio, exit total pressure/free stream total pressure |
| $q_o$ | tunnel dynamic pressure, $N/m^2$ ($lb./ft.^2$) |
| Q | propeller torque, N-m (lb.-ft.) |
| r | radius station of propeller, m (ft.) |
| rpm, RPM | propeller rotation speed, rev./min. |
| R | propeller radius, m (ft.) |

| | |
|---|---|
| $R(\tau)$ | autocorrelation coefficient of hot wire voltage signal E (defined in text) |
| $R'(\tau)$ | autocorrelation coefficient of fluctuation voltage e' (defined in text) |
| S | wing area, 16.258 $m^2$ (175.00 $ft.^2$) |
| T | propeller thrust, Drag (prop off) - Drag (prop operating) |
| u' | velocity fluctuation component parallel to aircraft centerline |
| v' | velocity fluctuation component transverse to aircraft centerline |
| V | velocity, m/sec. (ft./sec.) |
| $\omega_c$ | corrected inlet flow/fan area, Kg/(Sec-$m^2$) |
| $\alpha$ | aircraft angle of attack, $\alpha_{AC}$ corrected for wall effects deg (Q-Fan shaft axis is used as zero reference) |
| $\alpha_{AC}$ | geometric angle of attack, deg (angle between Q-Fan shaft axis and horizontal) |
| $\beta_{3/4}$ | propeller blade angle at 75% R |
| $\delta_f$ | flap deflection angle, deg |
| $\eta$ | propeller propulsive efficiency, $\frac{C_T}{C_P}\frac{V}{nD}$ |
| $\theta$ | circumferential position around Q-Fan duct in degrees (see Figure 2) |
| $\rho$ | mass density of air |

## INTRODUCTION

In the past, the propellers of General Aviation Aircraft have been designed for near maximum performance, minimum weight and minimum cost. This generally resulted in selection of a two-blade propeller operating at a high tip speed with direct drive piston engines providing the power. With the necessity to meet noise certification requirements, there has been considerable effort to find viable alternatives to the two-blade propellers. One direction that has proved successful is the use of a smaller diameter propeller with more blades. This causes some penalty in weight and cost but does not necessarily result in a performance penalty as long as the increase in number of blades and the reduction in diameter is limited. Another approach is to reduce noise by the use of a geared engine to reduce the RPM and thus allow reduction of tip speed with a larger diameter propeller. A third approach is to use a shroud around a propeller. This shroud enhances low speed thrust and allows use of a smaller diameter lower tip speed propulsor. An interesting fourth approach studied in this program is the use of a small diameter, low tip speed low pressure ratio quiet fan (Q-Fan). While this device is somewhat like the shrouded propeller there are several differences. First, the struts in a shrouded propeller do nothing but support the shroud. Support struts (inlet guide vanes) for the shroud of the Q-Fan also straighten the outlet flow to enhance thrust. Shrouded propellers generally have 5 or fewer narrow chord blades. The Q-Fan has 7 or more wide chord blades. The considerably smaller diameter of the Q-Fan allows it to operate at higher RPM than a shrouded or unshrouded propeller. This could eliminate the requirement for a gear box in a low tip speed quiet installation. If a gear box were required the gear ratio would be reduced in a Q-Fan installation and, therefore, gear box reliability problems would be minimized. It should also be noted that the Q-Fan, like the turbofan, offers the opportunity to install noise suppression material in the duct.

The purpose of the program discussed in this report was to establish the potential of the Q-Fan as a quiet propulsor for General Aviation Aircraft. Both noise and performance characteristics were measured in the 30 ft. x 60 ft. tunnel at NASA Langley. Diagnostic measurements in and around the fan were obtained to allow evaluation of predicted versus measured noise and performance. In this report a limited analysis of the noise and performance

data obtained in the test is discussed. Also, the Q-Fan results are compared with previous tests of two-blade unshrouded and three-blade and five-blade shrouded propellers.

## AIRCRAFT AND LOW PRESSURE RATIO FAN DESCRIPTION

Testing was conducted in the NASA Langley 30 x 60 tunnel. The test aircraft was the Cessna 327 twin-engine twin boom aircraft of Figure 1 which had previously been tested with shrouded and unshrouded propellers (see Ref. 1). For this test the Q-Fan, a low pressure ratio fan with inlet guide vanes, was mounted in a pusher configuration on the fuselage (see Figure 1). During this test program and during the Ref. 1 testing the forward propeller was not installed.

The Q-Fan tested had a 35-inch diameter 7-bladed rotor with manually adjustable blade pitch setting, and 9 fixed inlet guide vanes. The Q-Fan shroud was supported only by the inlet guide vanes. Figure 2 shows a schematic of the Q-Fan, including the location of instrumentation of the model. The Q-Fan rotor assembly is shown in Figure 3. For part of the test program the acoustic treatment on the aft duct section as shown in Figure 4 and the aft centerbody as shown in Figure 5 were exposed to determine the noise reduction potential of such treatment. For this test program the treatment consisted of perforated plate over an open cell polyurethane foam bulk absorber. In a flight application, perforated plate or porous metal over honeycomb might be used. The Q-Fan was designed to meet the following two aircraft operating requirements:

a) 75 MPH, sea level, std. day, takeoff thrust of 587 lbs., and
b) 185 MPH, 7500 ft., std. day, cruise thrust of 248 lbs.

These design points resulted in the following fan pressure ratios ($P_R$) and corrected ($\omega_c$) flows:

Takeoff: $P_R = 1.043$, $\omega_c = 102.5$ Kg/(sec·m$^2$) (21 lb/(sec·ft$^2$)
Cruise: $P_R = 1.037$, $\omega_c = 128.3$ Kg/(sec·m$^2$) (26.3 lb/(sec·ft$^2$)

The design tip speed was 168 m/s (550 fps). Blade geometric characteristics for the rotor and guide vanes are shown in Figures 6 & 7, respectively.

For the test discussed in this report the fan was driven by a 450 kW variable speed electric motor. In order to simulate an actual internal combustion

engine installation, engine cooling air was allowed to enter the aircraft via the cooling air inlet on top of the fuselage which can be seen in Figure 1. This air was discharged through a 3.8 cm (1.5 inch) high annular opening at the end of the fuselage, between the inlet guide vanes and the rotor. The design of the inboard sections of the fan rotor blades included consideration of the mixing of the exiting cooling air flow with the flow external to the fuselage, which occurs within the duct upstream of the rotor.

## ACOUSTIC INSTRUMENTATION AND TEST PROCEDURES

Fan noise and fan noise diagnostic information were obtained in this test program. Acoustic instrumentation included pole-mounted microphones as shown in Figure 8 to measure propulsor-generated noise. Half inch Bruel & Kjaer microphones fitted with aerodynamically shaped nose cones were used for the tests.

Blade-mounted pressure transducers and hot wire anemometers were installed to measure flow parameters directly related to noise generation by the fan. The pressure transducers were mounted at four locations on one blade as shown in Figure 9. Blade surface pressures were sensed by Kulite transducers mounted flush with the blade surface. The transducer signals were recovered via a rotating amplifier and slipring system.

Two hot wire anemometers were mounted in the airstream; one 16.6 in. ahead of the duct leading edge, and one at the leading edge of the inlet guide vane as shown in Figure 2. The hot wire anemometers used were Thermo-Systems model 1241-T1.5 cross wire probes oriented so they would respond to axial and circumferential velocity components (velocities parallel to the fuselage surface). The probes were mounted so they could be traversed radially as shown in Figure 2.

DC coupling was used for the hot wire anemometer signals, due to the fact that a large proportion of the turbulent fluctuations occur at frequencies below 2Hz. The unmodified hot wire signal contained a mean flow component and a relatively small fluctuating turbulence component. The DC component was suppressed prior to recording in order to improve the signal to noise ratio for the fluctuation signal, and the suppression voltage used was recorded on log sheets. Tape recorder amplifier gains were also recorded on the log sheets.

The microphone signals were recorded on a 14 channel FM tape recorder using AC coupling (20-15K Hz). Blade pressure and hot wire signals were recorded on a similar 14 channel tape recorder. Record times were one minute for the hot wire signals (when recorded) and 30 seconds for the other signals.

In the acoustic test phase of the program, microphone and blade pressure data were recorded on tape for the operating conditions in Table I.

Following the acoustic tests with the wings removed, hot wire data were recorded for the conditions listed in Table II. The blade pressure and hot wire measurements provide diagnostic information concerning the turbulence and mean velocity profile of the air entering the fan rotor.

## AERODYNAMIC INSTRUMENTATION AND TEST PROCEDURES

Overall aircraft performance, fan performance, and fan diagnostic performance measurements were obtained during this test program. The overall airplane performance was measured using the wind tunnel force balance system. The airplane lift, drag, and sideslip forces and pitch, roll, and yaw moments were determined from the force balance data. Q-Fan drive power was supplied by an electric motor located in the fuselage and fan power absorption was determined from a calibration curve of minimum motor current versus torque.

Pneumatic instrumentation of the Q-Fan was provided for assessment of Q-Fan performance. This instrumentation is detailed in the Figure 2 schematic and consisted of the following:

a. three rows of static taps, located axially, on the fuselage cowl at 352°, 188° and 278° (0° is at the top of the fuselage) circumferential position,
b. 3 inlet rakes (static and total pressure taps) at 0°, 180°, and 270° circumferential position,
c. 1 vane rake,
d. duct surface taps (along the internal and external surfaces) at 0° and 270° circumferential positions,
e. 3 exit rakes (static and total pressure taps) at 0°, 180° and 270° circumferential positions.

The Q-Fan propulsion system tested in the program and discussed in this report included a modification of the fuselage cowl boattail configuration forward of the fan to match the fan and fan duct flow requirements. Because of the changes to the aft fuselage cowl boattail configuration, it was planned that a test of the aircraft with the fan removed would be conducted in order to obtain "bare" aircraft performance. Due to a limited amount of tunnel test time this was not possible, and it was necessary to use the "bare" aircraft performance from the Ref. 1 test with the aft unmodified fuselage cowl boattail. NASA believes that the boattail change will have only a minor effect on the "bare" aircraft performance, but the lack of "bare" aircraft performance for the Q-Fan configuration does introduce some uncertainty in the test results.

During the entire Q-Fan test the aircraft was attached to the support struts as shown in Figure 10. Drag of the bar between the fuselage landing gear struts was measured and corrected out of the data. Static testing was done with the aircraft yawed 90° to the tunnel axis and a cloth curtain drawn across the wind tunnel test section entrance throat. This procedure prevented the Q-Fan slipstream from recirculating through the tunnel passages and back to the aircraft. All tests were conducted with the elevator (horizontal tail surface) locked in the undeflected position.

Table III shows a summary of all performance test conditions. The maximum continuous RPM attainable with the electric fan drive motor was 3350 RPM, which was only 93% of the design RPM of 3600. Tunnel speed was restricted to about 100 fps in order to reduce aircraft loads, and limit tunnel drive motor vibrations. Thus, for aircraft cruise conditions, the Q-Fan performance derived from non-dimensionalized data is based on relatively light loadings and is subject to some scatter. Also, since the Q-Fan thrust is determined by subtracting the base (Q-Fan removed) aircraft drag from the drag with the Q-Fan operating, small errors in drag measurements are magnified when the thrust is calculated. This situation is aggravated as the Q-Fan thrust (loading) is reduced.

The aerodynamic data has been corrected for support strut tares, bouyancy, and airflow angularity. These tests were conducted with a non-porous ground board installed in the tunnel beneath the model. Wall corrections, obtained from the theory of Ref. 2, were therefore applied directly to the data.

## DATA ANALYSIS PROCEDURES

The analysis procedures used for the acoustic data and related diagnostic data and the aerodynamic performance and related diagnostic data are discussed below.

Noise Data - The microphone data were reduced using 1/3 octave band and narrow band analyzers. A General Radio model 1920 real time analyzer was used to obtain 1/3 octave band plots (25 Hz to 20 kHz analysis) and A-weighted sound levels. Narrow band analysis from 0-10KHz (30 Hz bandwidth) were obtained using a Spectral Dynamics Model SD 301C analyzer. These allowed determination of propulsor noise levels and comparison with previously tested configurations.

Blade Pressure Data - The blade surface pressures are of interest for diagnosing the mechanisms of fan noise generation. They provide information about the structure of non-uniform flow entering the rotor as discussed in this section. The principle employed is that, as a blade rotates and chops through a disturbance in the inflow, it responds with a pressure pulse whose timing and length can be related to the location and size of the disturbance. A method of data reduction has been developed in which waveforms of the blade pressure signals are plotted in an especially revealing format and statistical calculations are performed which can be interpreted in terms of turbulence properties.

Types of inflow disturbances include fixed flow distortion due to installation effects or influence of upstream stators and random distortion such as turbulence generated by the motion of air in the wind tunnel or turbulence generated in the fuselage boundary layer or the inlet shroud boundary layer upstream of the rotor tips. Tests were conducted with and without wings at various tunnel speeds to study these effects on the Q-Fan.

To introduce blade pressure wave form plots as inlet distortion space-time histories, the waveforms recorded during a previous test with another Q-Fan having an intentional inlet disturbance from an installed post are shown in Figure 11. The instrumented blade chops through the distortion post's wake once per revolution producing a once per revolution blade pressure

pulse. The resulting waveforms from the mid blade transducer are shown in the lower part of the figure. Each trace in this plot represents the pressure signal during one revolution, starting and ending as the instrumented blade passes through the bottom of its rotation. Fifty-one traces from 51 consecutive revolutions are shown. The influence of the distortion post mounted in the top of the inlet is clearly seen at the center of the plot, which represents the 180° or top location in the inlet. Thus, the waveform plotting technique accurately shows the location and size of the inlet disturbance in the circumferential sense.

In order to generate Figure 11, analog tape data were digitized using a special clock with a frequency multiplier which generated exactly 150 equally spaced pulses per pulse of the once-per-revolution pipper. The 150 clock pulses caused the blade pressures to be digitized at 150 angles of rotation. Because the clock output is phase locked to the input pipper, the samples are obtained at the same location in the inlet during each revolution. That is, sample number 75 is always obtained as the blade passes through 180°.

Hot Wire Data

In Refs. 3 and 4, the inflow turbulence characteristics which are important for noise generation in fans are discussed. The mean velocity and turbulence intensity entering the fan were determined in this study. The procedures required to determine the values of u' and v' from the recorded data are described in Ref. 5, from which the following discussion is derived.

The output from a hot wire anemometer channel is a voltage signal consisting of a mean component, $\bar{E}$, and a fluctuating component, e'. For the purpose of determining the turbulence properties of the flow, e' is the quantity of interest. However, the mean component (DC voltage) is generally much larger than the fluctuating component of the signal, so the accuracy of the record and playback system in reproducing the fluctuation is jeopardized if the unmodified signal is recorded. Suppressing the DC component allows recording e' at a much higher gain, resulting in a large improvement in signal-to-noise ratio (on the order of a factor of 500 for the present investigation).

From Ref. 5, the principal analysis method for determining the turbulence properties is the auto-correlation procedure. In order to determine the turbulence intensity of the tunnel flow, auto-correlograms of the signals were obtained for the hot wire pair.

The sum of the signals from the hot wire (referred to as A + B) was assumed to be proportional to the axial velocity component, and the difference signal (referred to as A - B) to be proportional to the lateral velocity component. For high levels of turbulence, these relationships are only approximate, but they are adequate for the present investigation.

In order to determine the turbulence intensity, it is first necessary to examine a typical auto-correlation function as shown for the sum signal (A + B) of the probe in Figure 12.

The correlation function $R(\tau)$ is related to the time delay $\tau$, as follows;

$$R(\tau) = \frac{1}{T}\int_0^T E(t)\,E(t+\tau)\,dt, \tag{1}$$

where E is the hot wire voltage signal due to flow.. It is assumed that E is made up of mean signal, $\bar{E}$, and a time dependent voltage, e', so that the following relationships hold;

$$E(t) = \bar{E} + e'(t) \tag{2}$$

$$\frac{1}{T}\int_0^T E(t)\,dt = \bar{E}, \tag{3}$$

and

$$\frac{1}{T}\int_0^T e'(t)\,dt = 0, \tag{4}$$

where T is the period for data analysis.

Then, by substituting (2) into (1) . . . . . .

$$R(\tau) = \frac{1}{T}\int_0^T (\bar{E} + e'(t))(\bar{E} + e'(t+\tau))\,dt, \tag{5}$$

or

$$R(\tau) = \frac{1}{T}\left[\int_0^T \bar{E}^2\,dt + \int_0^T e'(t)\,e'(t+\tau)\,dt + \bar{E}\left[\int_0^T e'(t)\,dt + \int_0^T e'(t+\tau)\,dt\right]\right] \tag{6}$$

The first term in (6) is just the square of the mean value of the signal. The second is the auto-correlation of the fluctuating component. The third term is identically zero from Equation (4) and the last term can be neglected if it is assumed that:

$$\frac{1}{T}\int_0^T e'(t)\,dt = \frac{1}{T}\int_\tau^{T+\tau} e'(t)\,dt \tag{7}$$

The assumption in Equation (7) is valid if the length of the data records allows sufficient time for averaging. The correlation coefficient then becomes:

$$R(\tau) = \bar{E}^2 + R'(\tau) \tag{8}$$

Where $R'(\tau)$ is the desired correlation coefficient of the fluctuating components,

$$R'(\tau) = \frac{1}{T}\int_0^T e'(t)\,e'(t+\tau)\,dt \tag{9}$$

The correlogram in Figure 12 is the sum of the auto-correlogram for the fluctuating component and the square of a mean DC voltage (from Equation (9)). Since the turbulence signal is not correlated for large values of $\tau$, the second term in Equation (10) approaches zero and the correlation function approaches the square of the mean value, $\bar{E}^2$.

$\bar{E}$ is the voltage from the hot wire which represents the mean flow velocity. Although DC suppression was used to reduce this mean component during data recording, it was generally not perfectly cancelled. Thus, in the correlograms, the asymptotic values were not zero, but approached a value $\bar{E}^2$ which represents the difference between the true mean flow velocity and the amount of DC suppression used. The residual mean value was subtracted in each analysis to obtain the auto-correlation curve for the fluctuating velocity component (this was simply done by drawing a new reference line at $\bar{E}^2$, as shown in Figure 12). The mean-square turbulence intensity is proportional to the auto-correlation at zero time delay. ($\tau$ = 0) less the residual mean square value.

Aerodynamic Data - In general, the data analysis for the Q-Fan is similar to that used for evaluation of the shrouded and unshrouded propellers of Ref. 1. Computer processing of the data acquired during the aerodynamic portion of the program was done by NASA. Wall and jet boundary corrections based on the Ref. 2 report are part of the data reduction computer program, and were therefore included in the data reduction.

## ACOUSTIC RESULTS

The acoustic results are summarized below. For certification, the A-weighted noise level at a 1000 ft. sideline is the criterion used to determine the acceptability of an aircraft/power plant combination. Therefore, most of the data presented will be A-weighted sound pressure levels (for the frequency range 25 to 20 k[illegible]). Before proceeding with the discussion it should be noted that the previous propulsor tests (2-blade unshrouded propeller and 3 and 5-blade shrouded propellers) used microphone arrays at a 19 ft. measuring radius centered on the propulsor. As can be seen in Figure 8, the microphone array was centered on the aircraft. Therefore, some of the Q-Fan data have been corrected to the same measuring distance as the previous propulsor tests for ease of comparison with the previous data. The magnitudes of the corrections are given in Table IV.

Forward Flight Effect - The effect of forward flight on fan noise at two directivities is shown in Figure 13 for the wings on configuration. It can be seen that the noise is only a weak function of simulated flight speed for these directivities. The change in propulsor inflow as the aircraft moves from a static to flight condition usually results in a significant noise reduction. This did not occur in the Q-Fan test due to two factors. First, the inflow to the blade row was always distorted due to the wakes of the inlet guide vanes. Distortion due to inlet turbulence related to the normal atmosphere (which is expected to decrease with forward flight speed) thus had a relatively small effect on the noise generation. In addition, the power absorbed by the fan was reduced only slightly be the change from static to forware flight conditions. Therefore, the blade loading did not change enough to cause a large change in the radiated noise.

It should be noted that at the highest tunnel speed, the tunnel background noise is high enough to affect the measured propulsor noise levels. For this reason, the 72.5 ft/sec tunnel speed was selected for simulated flight data analysis whenever possible.

Dependence of Noise on Operating Condition - The maximum noise generated by the fan depends on blade angle and RPM as shown in Figure 14. The data shown were obtained for the wings off configuration since the range of operating

conditions available is much greater than for the wings on configuration (see Table I). The noise trends in Figure 14 are expected to hold for the case with wings on in forward flight, i.e., the change in blade loading due to changing blade angle from 28 to 33 degrees at 2500 fan RPM should cause the noise to increase by 2 dB for a given flight speed and airplane configuration.

The data shown represent the maximum sound level for the two microphones selected. Analysis of the data at different directivities may show somewhat different results.

Comparison of Measurement with Prediction - The noise generated by interaction of the Q-Fan rotor with wing wakes and IGV wakes was predicted on a 1/3 octave band power level basis. This prediction was corrected to the nominal 30 ft. measuring radius for the peak noise location and is shown in Figure 15a. The total predicted spectrum is compared to wings on data in Figure 15b. It can be seen that the prediction matched the data fairly well except in the frequency range from 3K to 8K, where it is several dB high. Since the A-weighted level for the spectrum was controlled by the levels of the blade passage tone and its harmonics, the agreement between predicted and measured A-weighted levels is considered satisfactory. When the wings were removed, the noise spectrum was expected to resemble that shown for the IGV prediction (Figure 15a). The result is shown in Figure 15c, where it can be seen that the noise did not behave as expected. This is discussed in the next section.

Effect of Wing Removal - From Figure 15c, it can be seen that the tone noise levels are much higher than was predicted for the wings removed case, and are, in fact, higher than the levels for the wings on case. The reason for the noise increase is best illustrated by time history plots of the blade pressure transducer signals. Figures 16 through 18 show the changes in inflow structure with changing aircraft configuration and flight speed.

In Figure 16, it can be seen that, at zero flight speed, the only regular disturbances are caused by the inlet guide vanes. With simulated forward

flight (Figure 17) disturbances from the wings and landing gear brace become evident. Removing the wings (Figure 18) does not eliminate the wing disturbances, but in fact appears to cause an increase in the disturbance level (as is evident in the mid-blade transducer plots).

Figure 19 shows the configuration of the stub wings which were used to fair the fuselage mounting points for the wings. The span of this wing is about 6 inches, so that a vortex shed from its tip will pass approximately through the mid-blade area of the rotor. This type of disturbance is effective in generating noise, so the expected noise reduction did not occur when the wings were removed.

Further investigation of the wings on/wings off data would give better insight on the noise generating mechanisms in the Q-Fan and possibly form a basis for predicting the noise due to other types of inflow distortion sources.

Acoustic Treatment Effect - The maximum acoustic treatment effect was derived from information presented in Figure 20. Although there were no measurements taken to directly compare the noise spectra with and without both the spinner and duct treatment, measurements were made with the spinner treatment both covered and uncovered. This data is shown by the symbols in Figure 20. The average of these measurements was summed with the predicted duct treatment attenuation to estimate the estimated total attenuation values. These values were applied to a noise spectrum similar to that in Figure 21 and the resulting 1/3 octave band levels were A-weighted and summed logarithmically. By this analysis it is estimated that the treatment included in the Q-Fan tested is capable of reducing the fan noise by about 2 dBA. The total attenuation is a fairly rough estimate, since the treatment effects were only studied at one directivity and not in great depth. Also, to achieve the maximum attenuation, the treatment would have to be placed so that the maximum noise radiation directivity would be affected (probably in the fan inlet duct and center body sections).

Q-Fan Directivity - A typical 1/3 octave band spectrum with A-weighted and linear SPL values for the Q-Fan is shown in Figure 21. The A-weighted

level from such spectra were used in conjunction with the radius corrections of Table IV to obtain the typical directivity pattern shown in Figure 22. The peak noise is seen to occur at microphone #4 (60.1° from directly ahead of the fan). The noise level at the microphone 4 directivity was found to control the peak 10 'O' sideline noise.

Effect of Angle of Attack - The effect of increasing angle of attack from 0. to 4 degrees is shown in Figure 23. It can be seen that the major effect is an increase in the 1/3 octave band containing the 2 x BPF harmonic. However, the A-weighted spectrum level is affected only a small amount. Similar comparisons should be made at other directivity points and at the higher attack angles available (8 and 12 degrees).

Effect of Aircraft Angle on Attack and Flap Setting - The effect of increased angle of attack and flaps is shown in Figure 24. However, the flap data were taken at a tunnel speed of 99 fps, with resulting background noise problems. It can be seen in Figure 24 that the background noise level is high enough to increase the measured levels at low and intermediate frequencies. It might be possible in a further study to estimate the effect of flaps on the basis of tone levels derived from narrow band data analyses.

Hot Wire Results - The hot wire anemometer provides the mean velocity and turbulence intensity for discrete points in the flow field. The locations of the hot wire probes are shown in Figure 2. The probes were installed so they could be moved to different distances from the fuselage. Four insertion distances were selected (0.5, 5.5, 7.0, and 8.5 inches from the fuselage wall), which approximately agree with the radial locations of the pressure transducers on the rotor blade.

Velocity and turbulence intensity profiles obtained from the hot wire probes are shown in Figure 25. Also included is the velocity profile obtained from the inlet rake (see Figure 2).

The mean velocity profiles in Figure 25 show that the flow becomes more distorted as it approaches the rotor row. The profile at hot wire probe location E is very smooth, while the inlet rake (close to the duct leading

edge) shows more distortion, and the velocity profile at the vane leading edge (probe location D), shows a large velocity variation from the fuselage surface to the duct surface. These data were obtained for a tunnel speed of 99 FPS and 3350 fan RPM. Further investigation of the hot wire data and comparison with the pressure data should be done to determine the influence of the inlet velocity profile on fan performance.

The turbulence intensity profiles shown at the bottom of the figure indicate high levels near the fuselage surface (due to the turbulent boundary layer), and a peak in the profiles at the 78% probe insertion position. The peak at 78% corresponds approximately to the location of the tip of the stub wing (installed when the wings were removed). The higher disturbance levels are probably due to the tip vortex of the stub wing. Investigation at static conditions, however, would be necessary to verify this supposition.

Comparison with Previous Tests - The noise levels from the Q-fan and several previously tested shrouded and unshrouded propellers were extrapolated to a 1000 ft. sideline for comparison purposes. In the case of the Q-Fan, the peak A-weighted noise level (microphone #4 in Figure 8) was used. The 1/3 octave band spectrum for this microphone which is at a radius of 30.1 ft from the propulsor center, is shown in Figure 21. In the narrow band analysis (Figure 23) for this microphone it can be seen that the spectral peaks are due to tones at blade passage frequency and its harmonics.

The extrapolation to a 1000 ft. sideline consists of adding a distance correction $\left(20 \log_{10} \frac{R}{1000}\right)$ and an operating condition correction (from Figure 14). The data were taken for $28^{\circ}$ blade angle and 3350 fan RPM, while the design condition is $33^{\circ}$ blade angle and 3600 fan RPM. From Figure 14, the level at the design condition is 4.5 dB higher than at the condition tested (by extrapolation). The resulting A-weighted noise level is presented in Figure 24 along with those from shrouded and unshrouded propellers (Ref. 1). It can be seen that the Q-Fan is 7 dB quieter than the lowest noise propeller configuration. Also the predicted level (done during the fan design) agrees very well with the extrapolated level based on measurements. As indicated earlier in the discussion a further reduction of 2 dB appears feasible by installing acoustic treatment in the duct.

The above discussion treated the Q-Fan with inlet guide vanes in a pusher configuration. The Q-Fan was shown to be a quiet device relative to other propulsors in this study. However, mounting the Q-Fan in a tractor configuration with outlet guide vanes would be expected to result in a significantly lower noise level than the pusher configuration with inlet guide vanes. The primary considerations responsible for this are as follows.

First, in a tractor configuration the wing wakes and inlet guide vane wakes would not interact with the rotor, so the high levels of fluctuating lift which cause relatively high noise radiation would be absent. The rotor wakes would impinge on the outlet guide vanes, but these are less efficient radiators. Second, the wing wakes which can interact with the rotor in a pusher configuration are absent on a tractor installation. Therefore, a tractor configuration might be as much as 10 dB quieter than a pusher installation.

## AERODYNAMIC RESULTS

The data recorded during most of the aerodynamic testing consisted of both force and pneumatic measurements. While the pneumatic data recorded was sufficient to determine the Q-Fan thrust, it was decided that the force data would be used in this report in order to be consistent with the data which was obtained in previous tests of unshrouded and shrouded propellers (see Ref. 1). Therefore, unless otherwise noted, all performance data in this report is based on force measurements.

The performance data are presented in the following sections. The "Basic Data" section results from a compilation of all the zero angle of attack, flaps retracted, wings on, data taken during the test. Performance in the "Angle of Attack Effect" and "Flap Effect" sections at zero angle of attack, and flaps retracted was based on data taken during the sequence of testing of a particular configuration.

Basic Data - The installed performance of the Q-Fan is shown in Figures 28 - 31 with wings on, at zero angle of attack, and with flaps retracted. Figure 28 shows the test static performance. The non-dimensionalized static performance data are seen to collapse to a smooth curve. The maximum efficiency achieved by the Q-Fan is shown in Figure 29 to be 67% while the predicted maximum efficiency level was 72%. This performance difference will be discussed in more detail later. Figure 30 shows very little scatter in the thrust data taken over the course of the test. The scatter in the power measurements showed in Figure 31 is probably due to the light loading on the Q-Fan and the procedure used to establish motor current. This scatter in power measurement results in some scatter in the efficiency levels (Figure 29).

The velocity profile at the shroud entrance is shown in Figures 32 and 33 for the aircraft at zero angle of attack with flaps retracted. The data shows that the asymmetrical fuselage creates only a small circumferential variation in the velocity except in the area near the shroud, and that the circumferential variation increases as the free stream velocity increases. The inlet velocity profiles were similar to those used to design the Q-Fan.

These gradients in inlet velocity are primarily responsible for the variations in shroud exit total pressures shown in Figures 34 and 35. The sharp reduction in exit total pressure near the centerbody will be discussed later. Shroud internal and external pressure variations with velocity and axial position are presented in Figures 36 and 37. The discontinuity in the internal static pressure between 40 and 62.5% shroud chord results from the static pressure ride through the rotor. No taps were installed on the shroud at the blade tip.

Angle of Attack Effects - The effect of aircraft angle of attack on the Q-Fan performance is illustrated for the 33° blade angle in Figures 38-40. Figure 38 shows that increasing the aircraft angle of attack to 12° results in approximately a 2% loss in efficiency. This result is contrary to the Ref. 1 propeller and shrouded propeller test data which showed an increase in efficiency as aircraft angle of attack was increased. The Q-Fan performance calculations also show an increase in efficiency as angle of attack is increased. The reason for this trend may be associated with bare aircraft tares. Possibly, further study of the pressure data will provide insight on the cause of the observed trend. A comparison of Figures 41 and 33, and Figures 42 and 35 reveals that the angle of attack has only a minor influence on the inlet velocity profiles and the exit total pressure profiles.

The shroud surface pressure coefficients are shown in Figure 43 for the 12° angle of attack case. A comparison of Figure 43 with the 0° angle of attack surface pressure coefficients in Figure 37 indicates that the flow remains attached to the shroud at 12° angle of attack, and is nearly identical to the flow at 0° angle of attack. The pressure data indicates that the performance level should not change due to angle of attack, and thus the 2% performance loss is unexplained.

Flap Effects - The effect of flap deflection on fan performance is small, as shown in Figures 44 - 46. A considerable amount of asymmetry exists in the fan inlet flow profiles and in the total pressure profiles at the duct exit, Figures 47 and 48 respectively. The change in the velocity distribution at 180° with 30° flap is apparently caused by the increased downwash. This circumferentially asymmetric flow actually results in slight

increase in fan efficiency at 30° flap deflection. Figure 49 indicates that the flap deflection has reduced the external shroud surface velocity at 270° circumferential position, contributing to the slight performance increase.

Wings on-Wings Off - A comparison of Q-Fan performance with wings on and wings off is shown in Figure 50. The efficiency was based on the pressure data, because the wings off efficiency levels based on force are inexplicably greater than 100% in some instances. As expected, Figure 50 shows the wings have virtually no effect on the Q-Fan performance.

Comparing pressure data taken with the wings removed in Figure 51 with wings on data, Figure 33, shows some reduction in inlet velocity near the shroud at $\theta = 0^{\circ}$. The exit totals with wings-off, Figure 52, are, as expected, very similar to the wings-on totals. The shroud surface pressures, Figure 53 show an unexplained discontinuity near the shroud leading edge with wings removed which may be associated with the vortex flow off the wing stubs.

Force vs Pressure Measurements - The pressure measurements recorded during the test were also used to calculate the Q-Fan thrust. Since the external shroud friction drag and the tail cone drag were not included in the pressure measurements, their magnitude was calculated and included in the thrust calculated from the pressure measurements. Q-Fan efficiency was then obtained using the thrust calculated from measured pressures and using the power obtained from the calibration of minimum motor current vs. torque. Figure 54 shows the pressure-thrust calculations to be significantly less than the force measurements. The agreement becomes better as the Q-Fan loading is increased (lower advance ratios). The reason for this discrepancy has not been established from the limited analysis permitted within the scope of this program. A more rigorous study of the data reduction procedures may provide further enlightenment on the validity of these results.

Pre-Test Calculations - Performance estimates were made for the Q-Fan prior to testing, and are shown compared to the test data in Figures 55 - 58. Test static thrust is about 7% below the design value, while take-off (75 mph) efficiency is 1 unit of efficiency below the design value and test cruise

(185 mph) efficiency is 5 units below the design value. Figures 57 and 58 show an increasing discrepancy between the calculated and the test blade angle as the angle is increased. Further analysis is required to explain these results. The exit total pressure profiles shown in Figures 34-35 indicate that a fall-off in total pressure is occurring at the rotor root which is probably associated with flow conditions in the inboard sections of the Q-Fan. Most likely, the quantity and mixing of the cooling exit air with the flow coming through the inlet guide vanes was not as predicted during the fan design and is causing the rotor inboard sections to be poorly loaded.

Also contributing to the loss in fan performance is the relatively high level of turbulence in the engine cooling duct exit flow recorded by the blade pressure transducers at the blade root and shown in Figures 16-18.

Influence of the Q-Fan on Aircraft Characteristics - The effects of the Q-Fan on the aerodynamic characteristics of the aircraft are shown in Figures 59-63. The operation of the Q-Fan provides some increase in lift curve slope and maximum $C_L$ as thrust level is increased. Aircraft pitching moment is virtually unaffected by changes in Q-Fan thrust. Figure 61 shows that a similar increase in lift occurs when flaps are extended. The pitching moment is again unaffected by changes in thrust level with flaps extended.

Comparative Performance - In order to compare the performance of the Q-Fan with that of the propulsors tested on the same aircraft during the Ref. 1 tests, the shaft horsepower required for aircraft cruise at 160 MPH, 7500 ft altitude was calculated for each of these propulsors.

The required cruise thrust for the aircraft was obtained from the Figure 64 thrust required ( = drag) curve, developed from the current test data for a 3500 lb. gross weight aircraft operating at 7500 ft.

It is basic aerodynamics that for subsonic operation, a well designed propeller will always be more efficient in cruise than a shrouded propeller or fan due to the shroud drag and higher disk loading of the latter propeller types. Thus, it was not surprising that the results of this study,

shown in Table V, indicated that the propeller has a significantly higher efficiency than the shrouded propeller or Q-Fan. Therefore, use of a shrouded propulsor for aircraft of this type must be predicated on requirements other than performance, such as constraints on propulsor diameter, or acceptable noise levels. If a shrouded propulsor were considered for an aircraft of this type then a high pressure ratio turbo-fan would probably also be considered, and for this reason an analytical estimate of the power required to propel the aircraft with an 1.5 PR fan was estimated. It can be seen that the estimated power and efficiency of a turbofan in this application is considerably worse than any of the other propulsors tested. Thus, if a small diameter quiet propulsor is of interest for this class of aircraft then the Q-Fan appears to be a more efficient choice than a turbofan.

The effects of the Q-Fan on aircraft lift characteristics were nearly identical with those of the Ref. 1 propeller:

a) Lift curve slope was increased slightly with flaps retracted.
b) Lift and lift curve slope were increased slightly with flaps extended.

The Q-Fan showed no effect on aircraft pitching moment when thrust was increased, whereas the propeller normal force resulted in an increased nose down pitching moment when thrust was increased.

## CONCLUSIONS

The amount of data analyzed from the Q-Fan test and the amount of analysis of this data was severely restricted. Therefore, the following conclusions should be considered preliminary until a more thorough study of the test results is conducted.

The preliminary acoustic conclusions are as follows:

1. The fan met the noise objectives set during its design. Based on test data the noise level was extrapolated to be 65 dBA for a 1000 ft. flyover without duct acoustic treatment. This compares with levels of 72 to 75 dBA for the unshrouded and shrouded propellers tested in an earlier program on the same aircraft. With cleaner inflow to the fan such as that found in a tractor (with exit guide vanes) rather than a pusher (with inlet guide vanes) installation lower levels could be achieved.

2. There is the potential for 2 dBA reduction in the above levels by use of duct acoustic treatment.

3. Inlet disturbances created by stub wings used for the wings-off testing caused noise increases over the conditions with the wings on.

4. Limited evaluation indicates that aircraft angle of attack and deployment of flaps increase the Q-Fan noise by a small amount.

5. The hot-wire anemometry data shows the presence of distortion upstream of the fan rotor. Reduction of this distortion could lead to lower noise levels and may also improve aerodynamic performance.

The aerodynamic conclusions are as follows:

1. Maximum propulsive efficiency derived in this limited study of the Q-Fan was about 5% less than the 72% predicted during the design phase.

There is some question about the accuracy of the measurements but it is possible that differences between anticipated and actual blade root flow caused some loss in efficiency.

2. Propulsive efficiency of the Q-Fan was less than that of the unshrouded propeller tested earlier, similar to that of the shrouded propeller tested earlier, but significantly greater than a high bypass ratio turbofan would be for this application.

3. Aerodynamic characteristics of the aircraft with the Q-Fan installed were nearly identical to those of the aircraft with the propeller.

4. Limited study of the data indicates that an improvement in rotor blade root design would probably improve the maximum Q-Fan efficiency.

## REFERENCES


1. McLemore, H. C., and Pegg, R. J., "Aeroacoustic Wind-Tunnel Tests of a Light Twin-Boom General-Aviation Airplane With Free- or Shrouded-Pusher Propellers," NASA TM-80203, 1980.

2. Heyson, H.H., "Use of Superposition in Digital Computers to Obtain Wind Tunnel Interference Factors for Arbitrary Configurations, with Particular Reference to V/STOL Models," NASA TR-R-302, 1969.

3. Hanson, D.B., "Measurements of Static Inlet Turbulence," AIAA Paper No. 75-467, March 1975.

4. Hanson, D.B., "The Spectrum of Rotor Noise Caused by Atmospheric Turbulence." Journal of Acoustic Society of America, Vol. 56, No. 1, July 1974.

5. Hinze, J.O., Turbulence, Chapter 1, p. 40-42, McGraw-Hill Book Company, New York, 1959.

# TABLE I

## Test Configuration and Operating Conditions for Acoustic Tests of the Cessna 327 Q-Fan

| Test Sequence | Description | Blade Angle β | Tunnel RPM | Tunnel Speed | Q-Fan RPM: Free Wheeling | 1000 | 1500 | 2000 | 2500 | 3000 | 3150 | Wings | Acoustic Treatment | Aircraft Angle of Attack: 0° | 4° | 6° | 8° | 10° | 12° | Flap Angle: 0° | 20° | 30° |
|---|---|---|---|---|---|---|---|---|---|---|---|---|---|---|---|---|---|---|---|---|---|---|
| | | | 0 | 0 | | X | X | X | X | X | X | on | Covered | X | | | | | | X | | |
| I | Reference Test Low Blade Angle With Treatment Covered Wings On | 28° | 54 | | | | | | | | | | | | | | | | | | | |
| | | | 75 | | Free Wheeling | | | | | | | | | | | | | | | | | |
| | | | 100 | | | | | | | | | | | | | | | | | | | |
| | | | 138 | | | | | | | | | | | | | | | | | | | |
| | | | 190 | | | | X | X | X | | X | | | | | | | | | | | |
| II | Angle of Attack Effect | | 190 | | | | | | | | | | | | X | X | X | X | X | | | |
| | | | 140 | | | | | | | | | | | | | X | | | | | X | |
| III | Flap Angle Effect | | 190 | | | | | | | | | | | | | | | | X | | | |
| | | | 190 | | | | | | | | | | | | | | | | | | | |
| | | | 0 | | | X | X | X | X | X | X | off | Uncovered | X | | | | | | X | | X |
| | | | 50 | | | | | | | | | | | | | | | | | | | |
| IV | Reference Test With Treatment Uncovered and Wings Off | | 75 | | | | | | | | | | | | | | | | | | | |
| | | | 100 | | | | | | | | | | | | | | | | | | | |
| | | | 140 | | | | | | | | | | | | | | | | | | | |
| | | | 190 | | | | X | | X | X | X | | | | | | | | | | | |
| | | 38° | 0 | | | X | | X | X | X | X | | | | | | | | | | | |
| | | | 50 | | | | | | | | | | | | | | | | | | | |
| V | Reference Test High Blade Angle | | 75 | | | | | | | | | | | | | | | | | | | |
| | | | 100 | | | | | | | | | | | | | | | | | | | |
| | | | 140 | | | | | | | | | | | | | | | | | | | |
| | | | 190 | | | | X | X | X | X | X | | | | | | | | | | | |
| | | 33° | 0 | | | X | X | X | X | X | X | | | | | | | | | | | |
| | | | 50 | | | | | | | | | | | | | | | | | | | |
| VI | Reference Test Medium Blade Angle Treatment | | 75 | | | | | | | | | | | | | | | | | | | |
| | | | 100 | | | | | | | | | | | | | | | | | | | |
| | | | 140 | | | | | | | | | | | | | | | | | | | |
| | | | 190 | | | | X | X | X | X | X | | | | | | | | | | | |
| | | | 190 | | | | | | | | | | | | | X | | X | X | | | |
| VII | Angle of Attack Effect Wings Off | | 100 | | | | | | | | | | | | | | | | | | | |
| | | | 140 | | | | | | | | | | | | | | | | | | | |
| | | | 0 | | | X | X | X | X | X | X | | Covered | X | | | | | | | | |
| | | | 50 | | | | | | | | | | | | | | | | | | | |
| VIII | Reference Test Treatment Covered Wings Off | | 75 | | | | | | | | | | | | | | | | | | | |
| | | | 100 | | | | | | | | | | | | | | | | | | | |
| | | | 140 | | | | | | | | | | | | | | | | | | | |
| | | | 190 | | | | X | X | X | X | X | | | | | | | | | | | |

Note (1) Actual test RPM is 3344

| Data Analyzed | | Desired Additional Analysis |
|---|---|---|
| Noise | 1/3 OB 2 mics | X |
| | 1/3 OB directivity | |
| | narrowband 2 mics | |
| Blade surface pressure | 4 channels digitize done | |
| | 4 channels narrowband | |

# TABLE II

Test Configuration and Operating Conditions for Hot Wire Anemometry Measurements on the Cessna 337
(All Tests with no Winge, Treatment Covered, 0° Angle of Attack and 0° Flap Angle)

| Test Sequence | Description | Blade Angle β | Tunnel RPM | Tunnel Speed | Q-Fan RPM: Free Wheeling | 1000 | 1500 | 2000 | 2500 | 3000 | 3350 | Distance from Fuselage to Hot Wire Probe in inches: 0.5 | 5.5 | 7 | 8.5 |
|---|---|---|---|---|---|---|---|---|---|---|---|---|---|---|---|
| | | 33° | 0 | | | | | | | | X | X | | | |
| | | | 75 | | | | | | | | | | | | |
| | | | 140 | | | | | | | | | | | | |
| | | | 190 | | | | | | | | | | | | |
| AI | Turbulence Distribution at 33° Blade Angle | | 75 | | | | | | | X | | | X | | |
| | | | 140 | | | | | X | X | X | X | | | | |
| | | | 190 | | | | | X | X | X | X | | | | |
| | | | 0 | | | | | | X | X | X | | | | |
| | | | 0 | | | | | | | | X | | | X | |
| | | | 75 | | | | | | | | | | | | |
| | | | 140 | | | | | | | | | | | | |
| | | | 190 | | | | | | | | | | | | |
| | | | 0 | | | | | | | | | | | | X |
| | | | 75 | | | | | | | | | | | | |
| | | | 140 | | | | | | | | | | | | |
| | | | 190 | | | | | | | | | | | | |
| AII | Turbulence Distribution at 28° Blade Angle | 28° | 0 | | | | | | | | | X | | | |
| | | | 75 | | | | | | | | | | | | |
| | | | 140 | | | | | | | | | | | | |
| | | | 190 | | | | | | | | | | | | |
| | | | 0 | | | | | X | X | X | | | X | | |
| | | | 140 | | | | | | | | | | | | |
| | | | 75 | | | | | | | | | | | | |
| | | | 190 | | | | | | | | | | | | |
| | | | 0 | | | | | | | | | | | X | |
| | | | 75 | | | | | | | | | | | | |
| | | | 140 | | | | | | | | | | | | |
| | | | 190 | | | | | | | | | | | | |
| | | | 0 | | | | | | | | | | | | X |
| | | | 75 | | | | | | | | | | | | |
| | | | 140 | | | | | | | | | | | | |
| | | | 190 | | | | | | | | | | | | |
| | | 38° | 0 | | | | | | | | | X | | | |
| AIII | Turbulence Distribution at 38° Blade Angle | | 75 | | | | | | | | | | | | |
| | | | 140 | | | | | | | | | | | | |
| | | | 190 | | | | | | | | | | | | |
| | | | 0 | | | | | X | X | X | | | X | | |
| | | | 140 | | | | | | | | | | | | |
| | | | 75 | | | | | | | | | | | | |
| | | | 190 | | | | | | | | | | | | |
| | | | 0 | | | | | | | | | | | X | |
| | | | 75 | | | | | | | | | | | | |
| | | | 140 | | | | | | | | | | | | |
| | | | 190 | | | | | | | | | | | | |
| | | | 0 | | | | | | | | | | | | X |
| | | | 75 | | | | | | | | | | | | |
| | | | 140 | | | | | | | | | | | | |
| | | | 190 | | | | | | | | | | | | |

Data Analyzed
Correlograms

## TABLE III

### AERODYNAMIC TEST CONDITIONS

| AIRCRAFT CONFIGURATION | TUNNEL SPEED m/s, (ft/sec) | FLAP ANGLE (DEG.) | ANGLE OF ATTACK, (DEG.) | Q-FAN BLADE ANGLE, (DEG.) | Q-FAN RPM RANGE |
|---|---|---|---|---|---|
| WINGS ON | 0 (0) | 0 | 0 | 28 | 1500 to 3400 |
| | 0 | 0 | 0 | 33 | 1500 to 3350 |
| | 0 | 0 | 0 | 34 | 1500 to 3400 |
| | 0 | 0 | 0 | 38 | 1500 to 3350 |
| | 0 | 0 | 0 | 43 | 1500 to 3400 |
| | 138 | 0 | 0 | 28 | 1500 to 3400 |
| | 138 | 0 | 0 | 38 | 1500 to 3400 |
| | 140 | 0 | 4 to 12 | 33 | 3350 |
| | 190 | 0 | -4 to 16 | 28 | 1500 to 3350 |
| | 190 | 0 | -4 to 16 | 33 | 1500 to 3400 |
| | 190 | 20 | 0 to 16 | 33 | 2000 to 3350 |
| | 190 | 30 | 0 to 16 | 33 | 2000 to 3350 |
| | 190 | 0 | -4 to 18 | 33 | Windmill |
| | 190 | 0 | -4 to 18 | 38 | 1500 to 3400 |
| | 264 | 0 | 0 | 38 | 1500 to 2000 |

TABLE III (CONTD)

| AIRCRAFT CONFIGURATION | TUNNEL SPEED m/s, (ft/sec) | ANGLE OF ATTACK, (DEG.) | Q-FAN BLADE ANGLE, (DEG.) | Q-FAN RPM RANGE |
|---|---|---|---|---|
| WINGS OFF | 0 | 0 | 28 | 1000 to 3350 |
| | 0 | 0 | 33 | 1000 to 3350 |
| | 0 | 0 | 28 | 1000 to 3350 |
| | 50→140 | 0 | 28 | 3350 |
| | 50→140 | 0 | 33 | 3350 |
| | 50→140 | 0 | 28 | 3350 |
| | 100 | 4 to 12 | 33 | 3000, 3350 |
| | 140 | 0 | 33 | 2000 to 3350 |
| | 140 | 4 to 12 | 33 | 3000, 3350 |
| | 190 | 0 | 28 | 1500 to 3350 |
| | 190 | 0 | 33 | 1500 to 3350 |
| | 190 | 0 to 12 | 33 | 3000, 3350 |
| | 190 | 0 | 38 | 1500 to 3350 |
| WINGS OFF & FAN OFF | 140 | -4 to 18 | | |
| | 190 | -4 to 18 | | |

## TABLE IV

## MICROPHONE CORRECTIONS FOR 19' RADIUS

| Microphone | Actual Measuring Radius | Correction to Add For 19' Radius, dB |
|---|---|---|
| 1 | 34.2 | 5.1 |
| 2 | 33.1 | 4.8 |
| 3 | 31.8 | 4.5 |
| 4 | 30.1 | 4.0 |
| 5 | 28.2 | 3.4 |
| 6 | 26.8 | 3.0 |
| 7 | 25.4 | 2.5 |
| 8 | 24.0 | 2.0 |
| 9 | 22.1 | 1.3 |
| 10 | 20.5 | 0.6 |

## TABLE V

## COMPARATIVE PERFORMANCE

## 7500 FT. CRUISE @ 160 MPH

| Propulsor | Approximate Pressure Ratio | Shaft Horsepower Req'd. Kw (HP) | Propulsive Efficiency | |
|---|---|---|---|---|
| 1. Propeller | 1.00 + | 160 (215) | 90% | Test Data |
| 2. 5-Way Shrouded Propeller | 1.03 | 220 (295) | 65% | Test Data |
| 3. Q fan | 1.04 | 231 (310) | 62% | Test Data |
| 4. Turbofan | 1.50 | 414 (555) | 35% | Calculations |

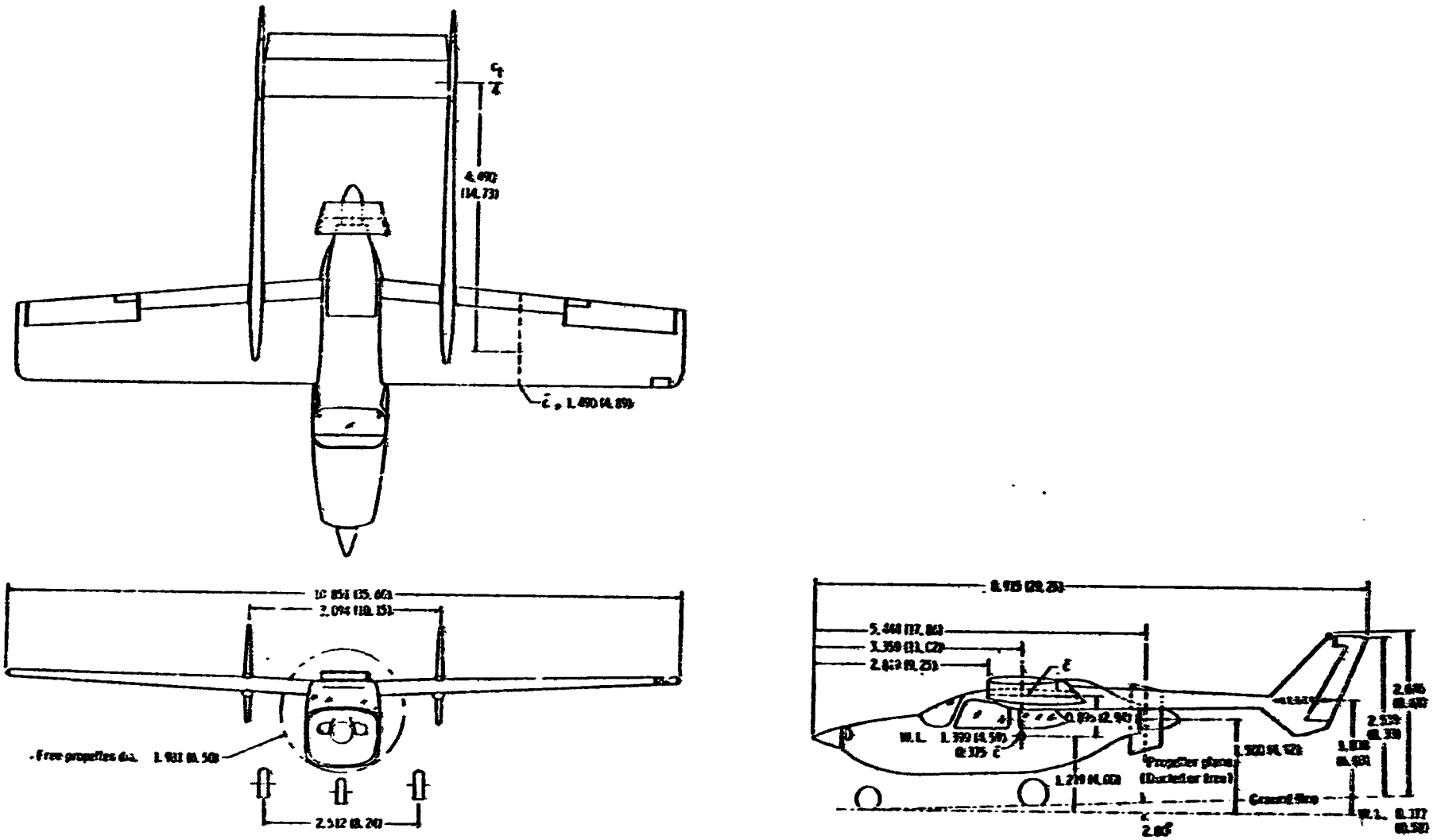

Figure 1 - Geometric characteristics of test airplane. All dimensions in meters (feet).
Measurements made in conventional units.

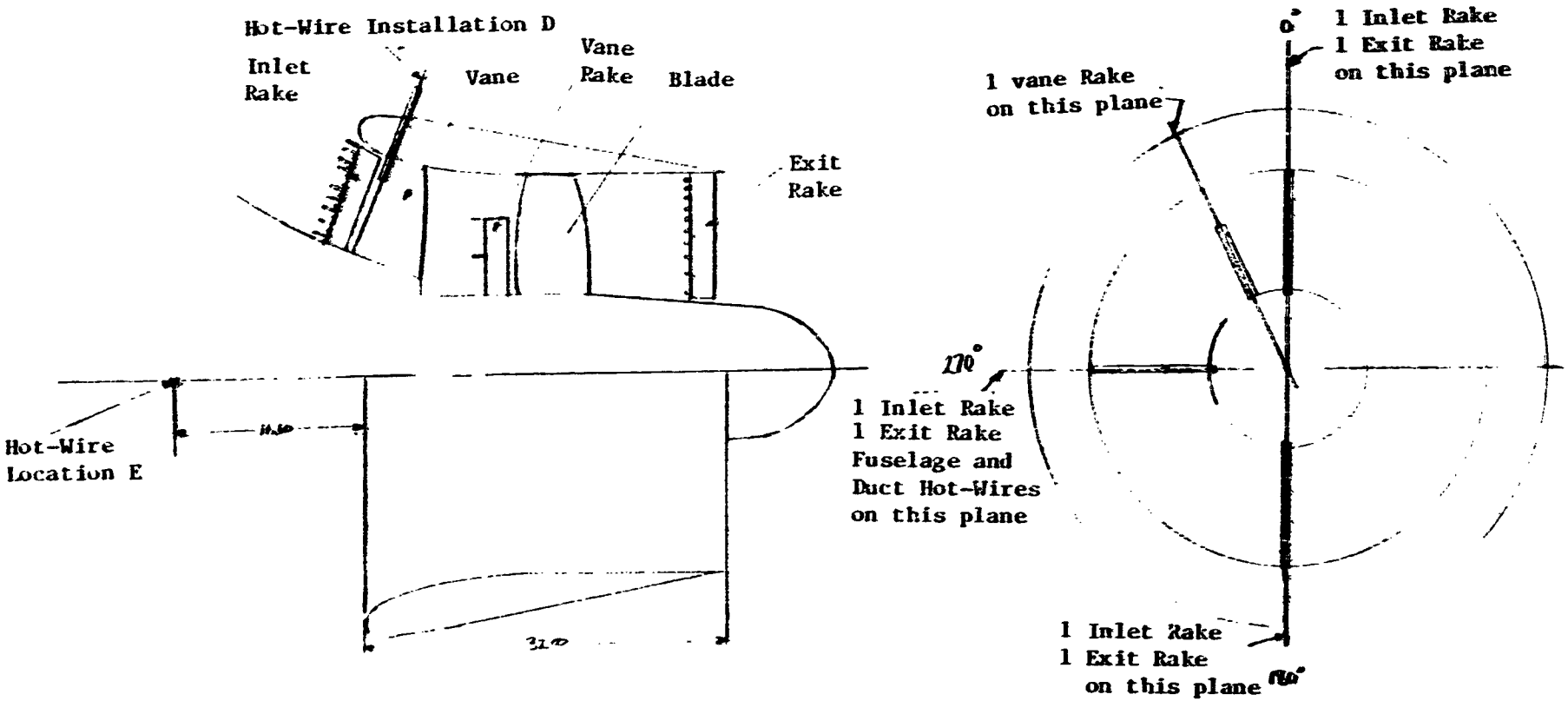


Figure 2. Q-Fan Schematic Showing Location of Instrumentation

# REAR HUB HALF AND BLADES

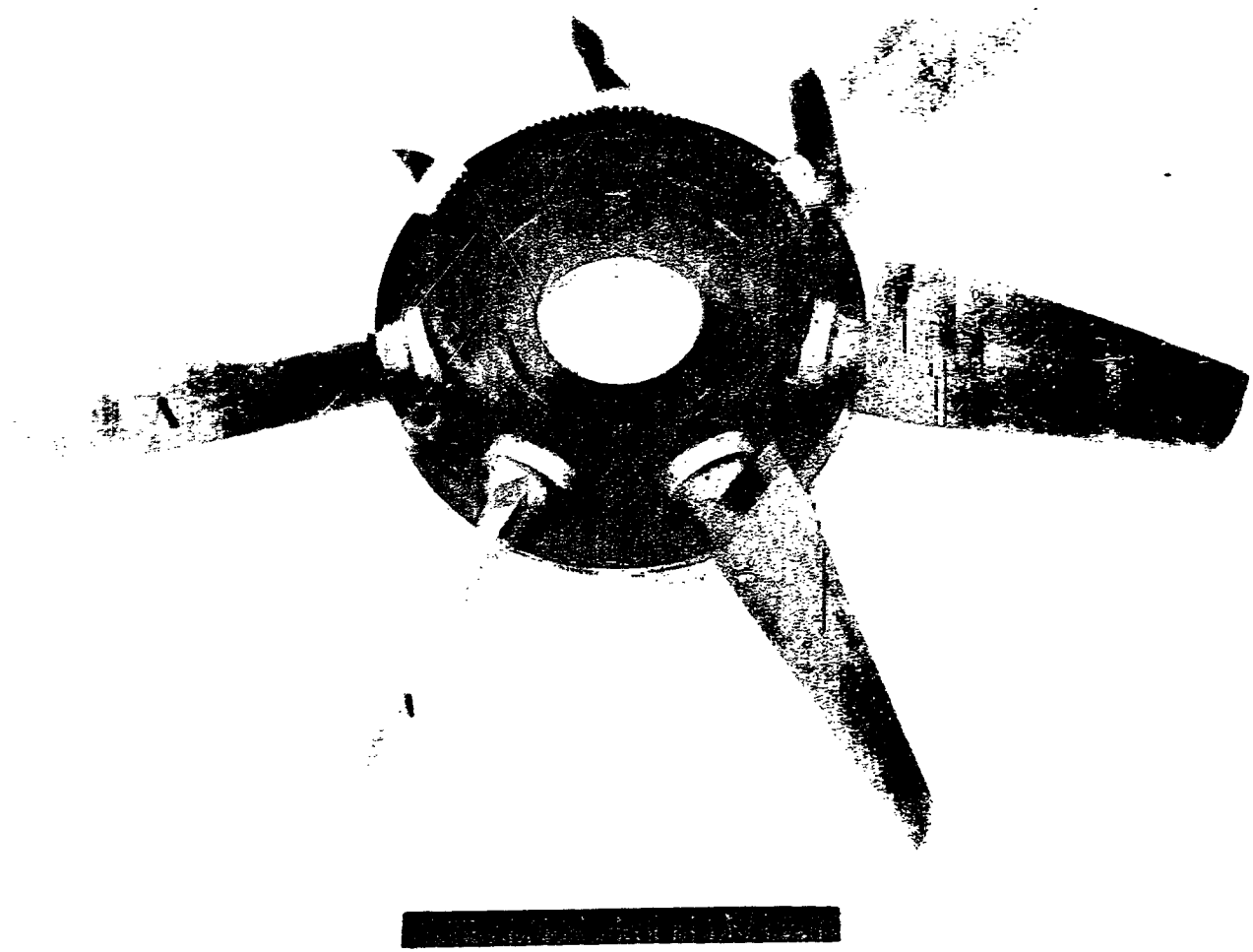

FIGURE 3.

# DUCT ACOUSTIC TAIL SECTION

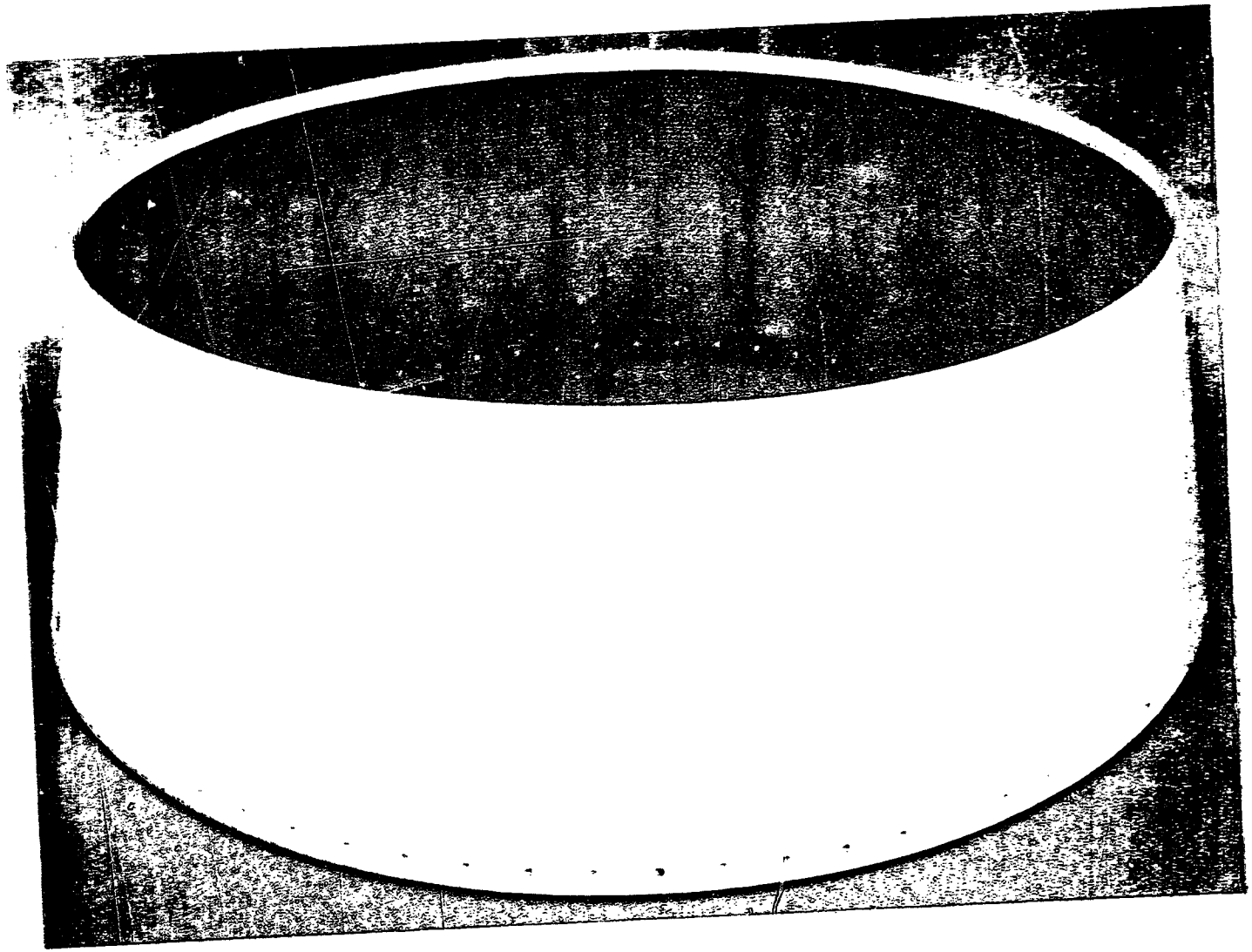

FIGURE 4

# ACOUSTICALLY TREATED CENTERBODY

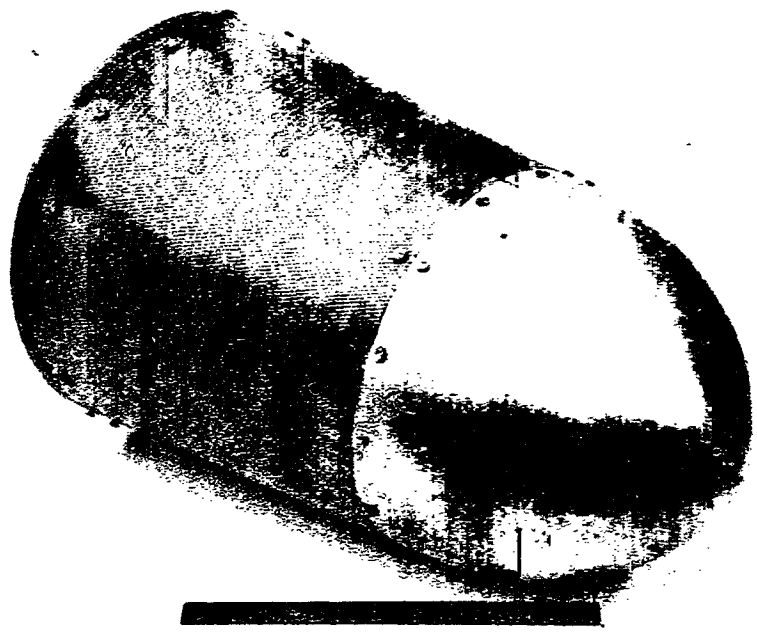

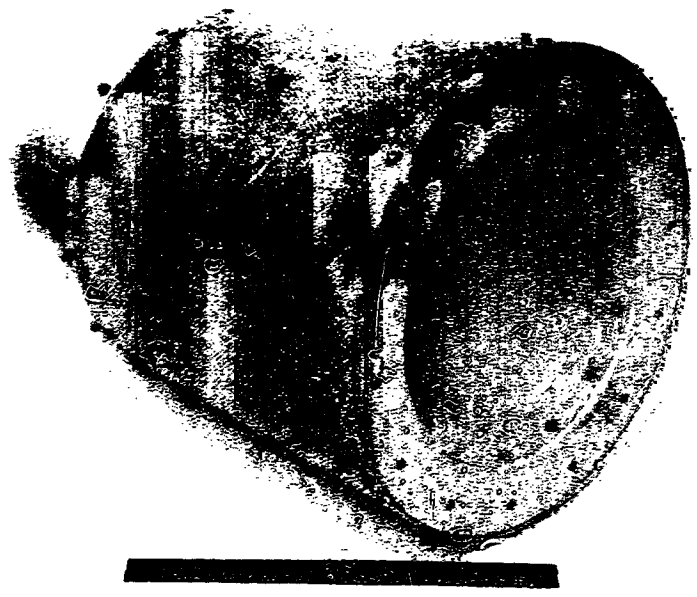

FIGURE 5

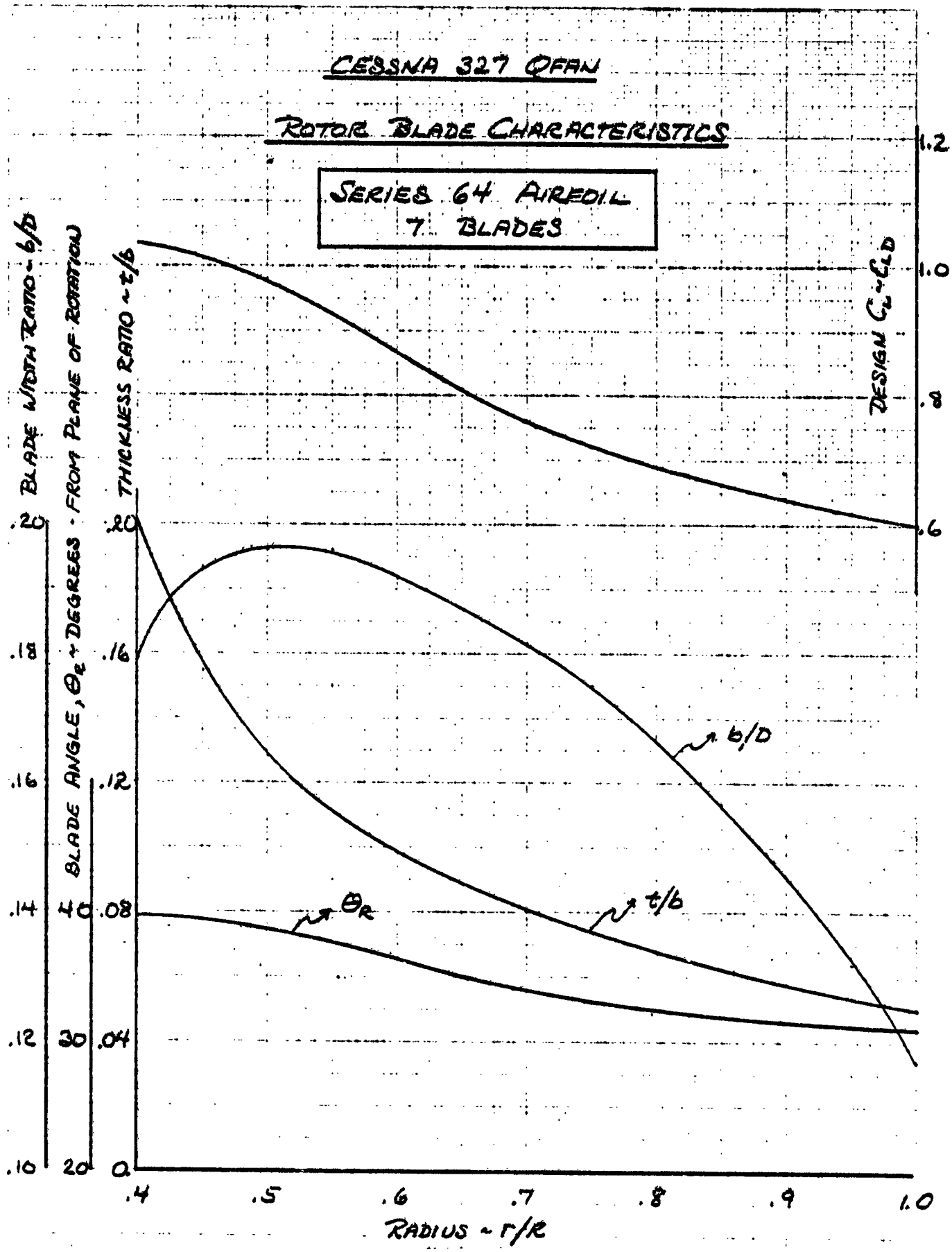


Figure 6

4/18/75

# CESSNA 327 QFAN

## INLET GUIDE VANE (IGV) CHARACTERISTICS

| | |
|---|---|
| AIRFOIL SERIES | 64 |
| NO IGV'S | 9 |
| THICKNESS RATIO | 10% |
| DESIGN $C_L$ | 1.50 |

ALL SECTIONS ARE NORMAL TO IGV L.E.

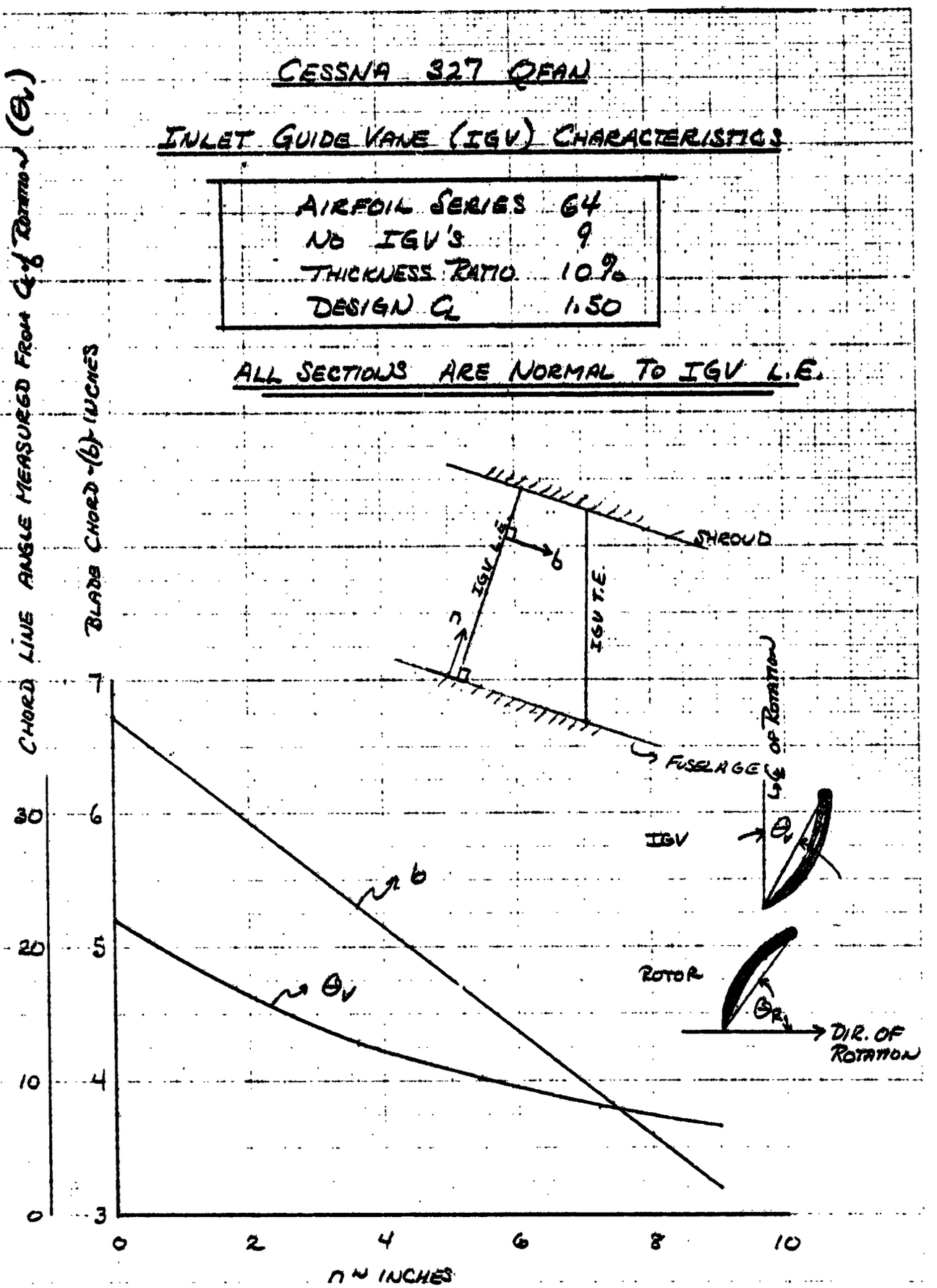


4/18/75

Figure 7

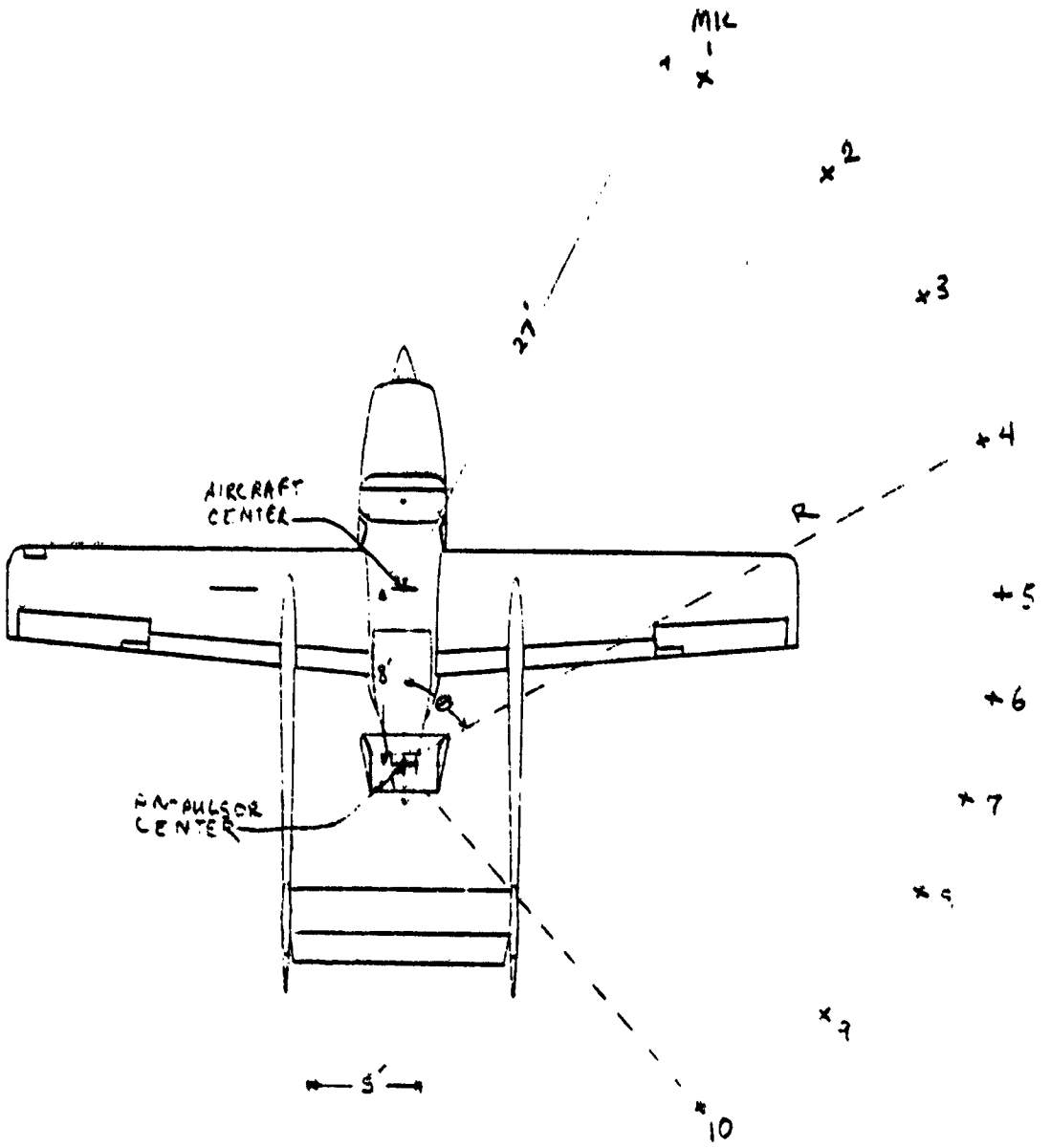


Figure 8. Schematic of Microphone Installation for Q-Fan Test

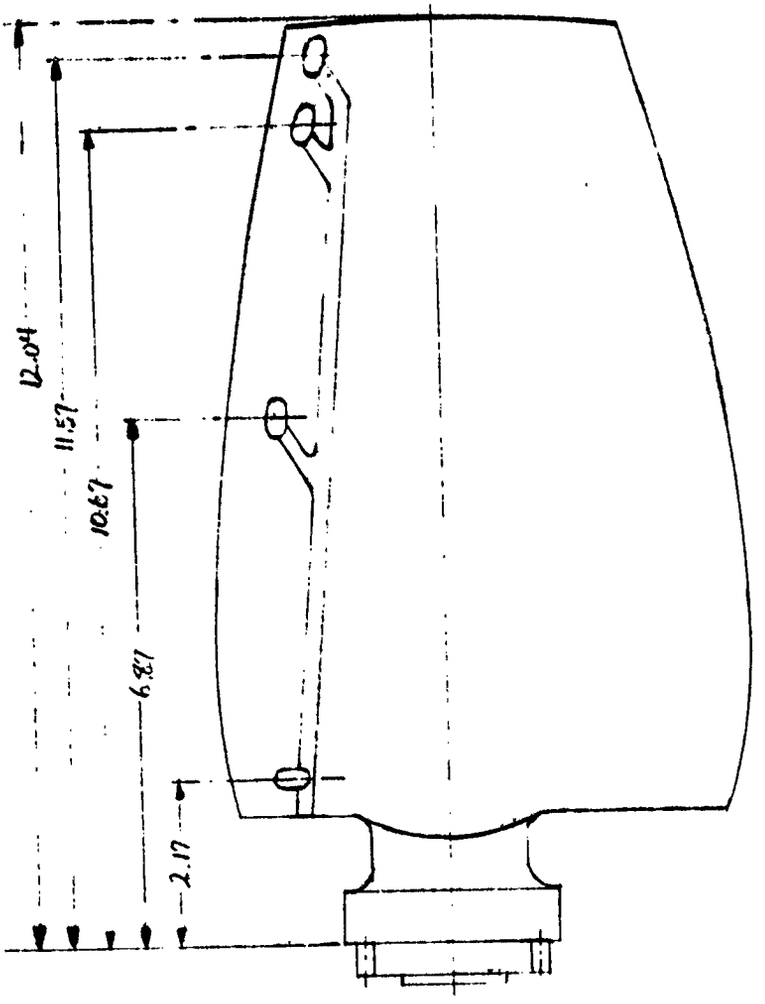


Figure 9. Schematic of Blade Pressure Transducer Installation

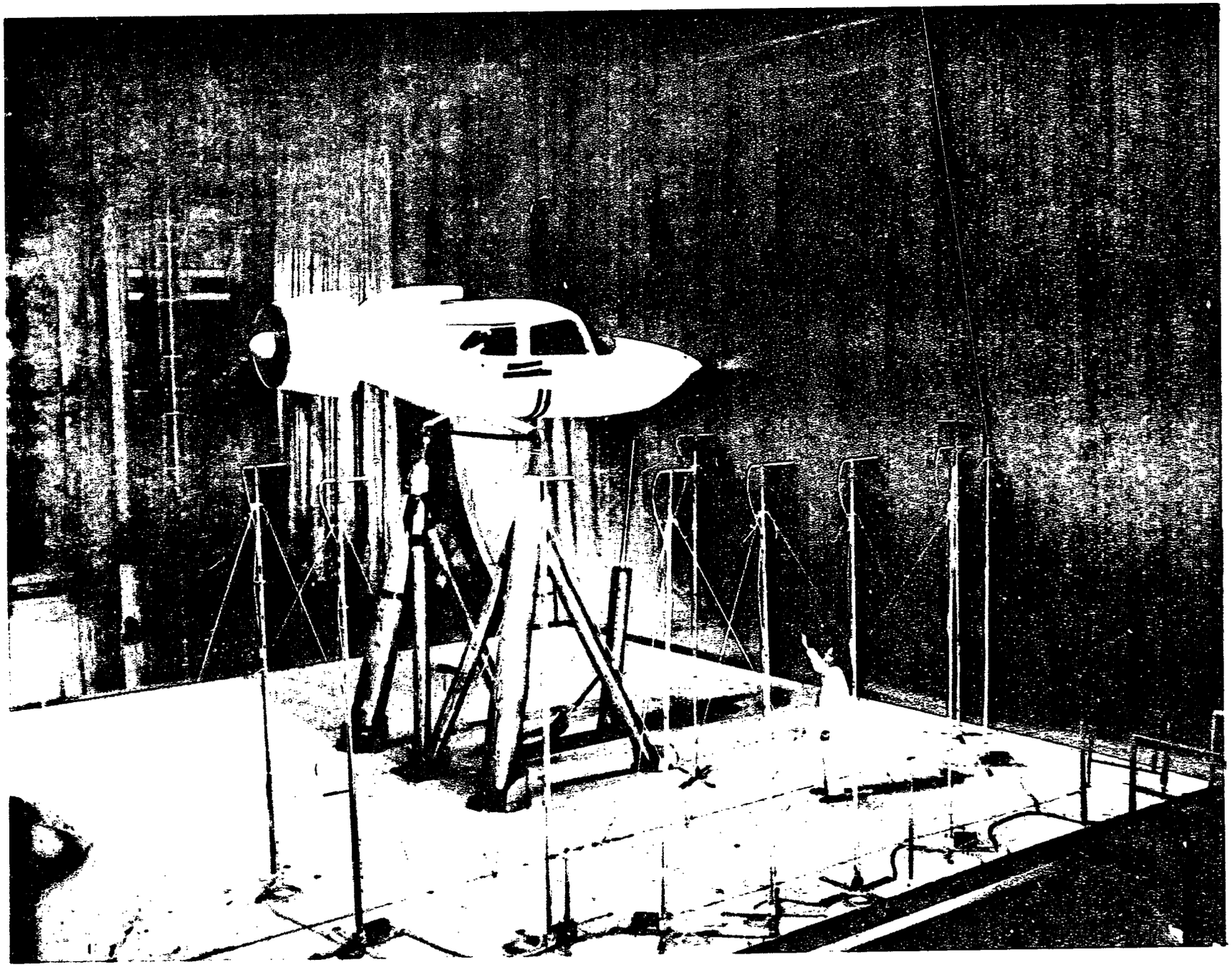

Figure 10

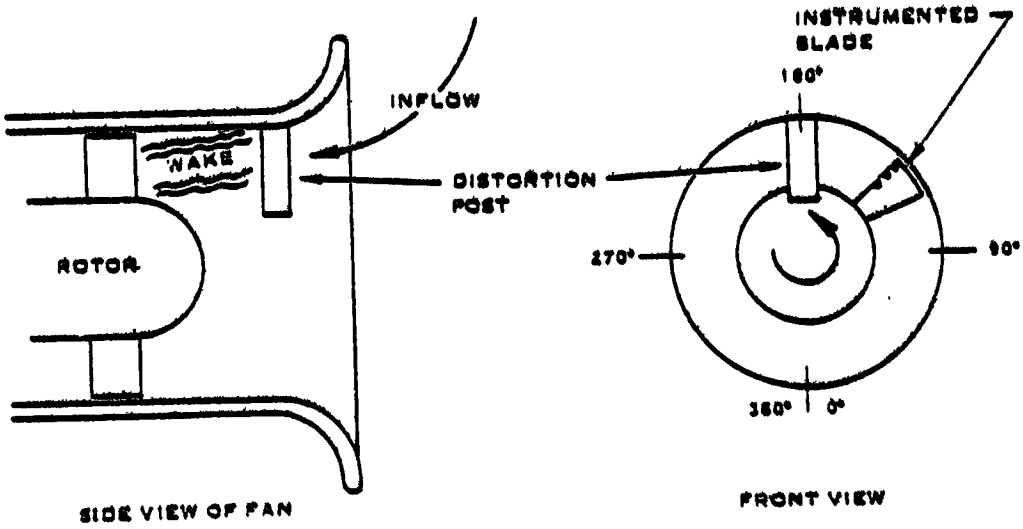


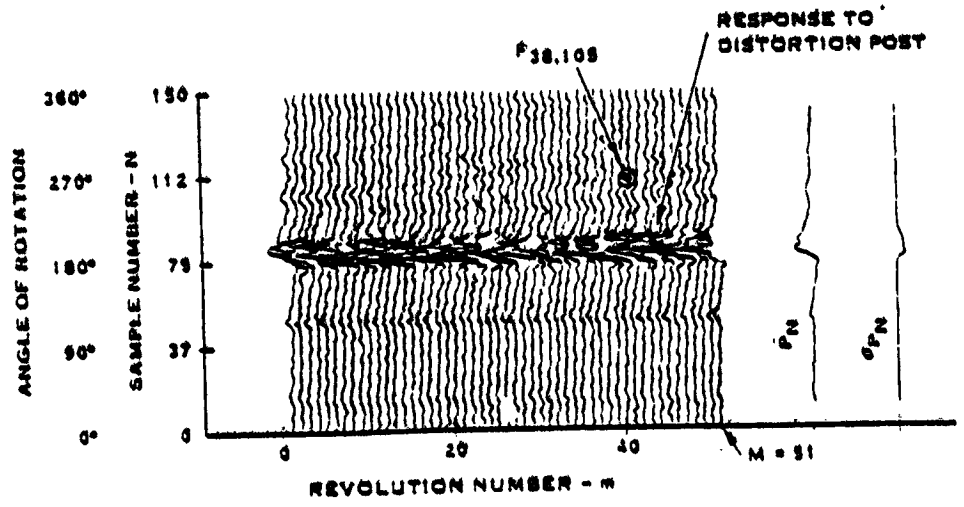


Figure 11. Key to Blade Pressure Waveform Plots

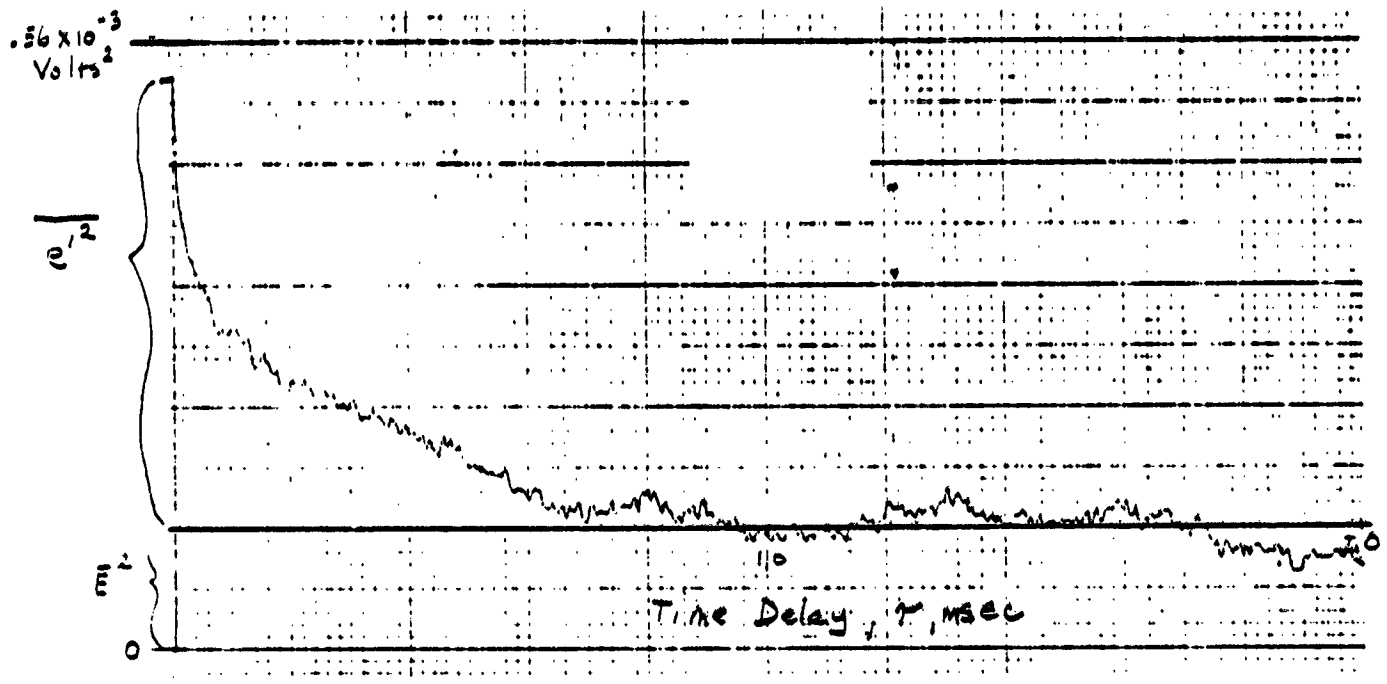


Figure 12. Sample Correlogram Plot, A-B Signal (Proportional to Transverse Velocity Component)

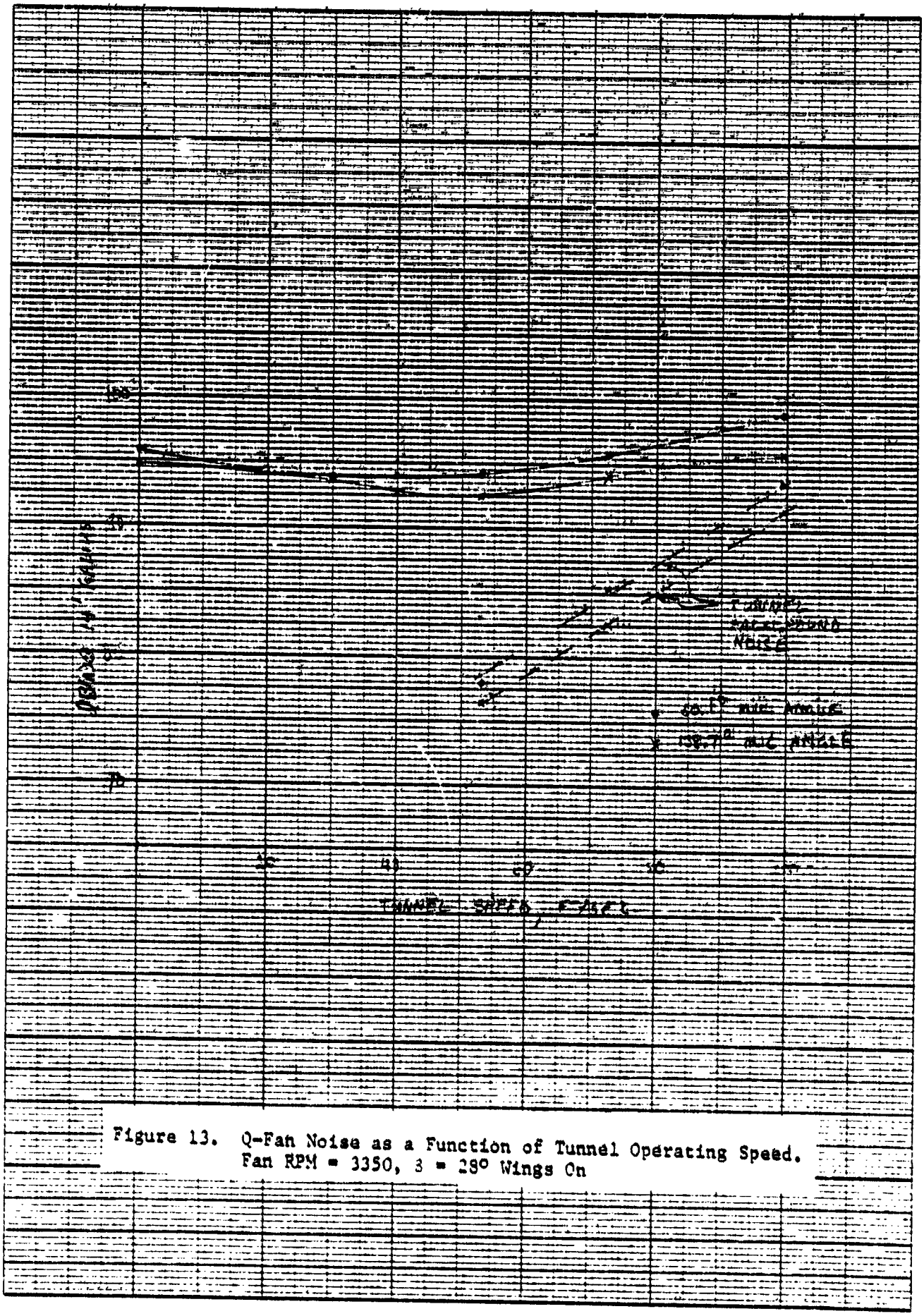

Figure 13. Q-Fan Noise as a Function of Tunnel Operating Speed. Fan RPM = 3350, $\beta$ = 28° Wings On

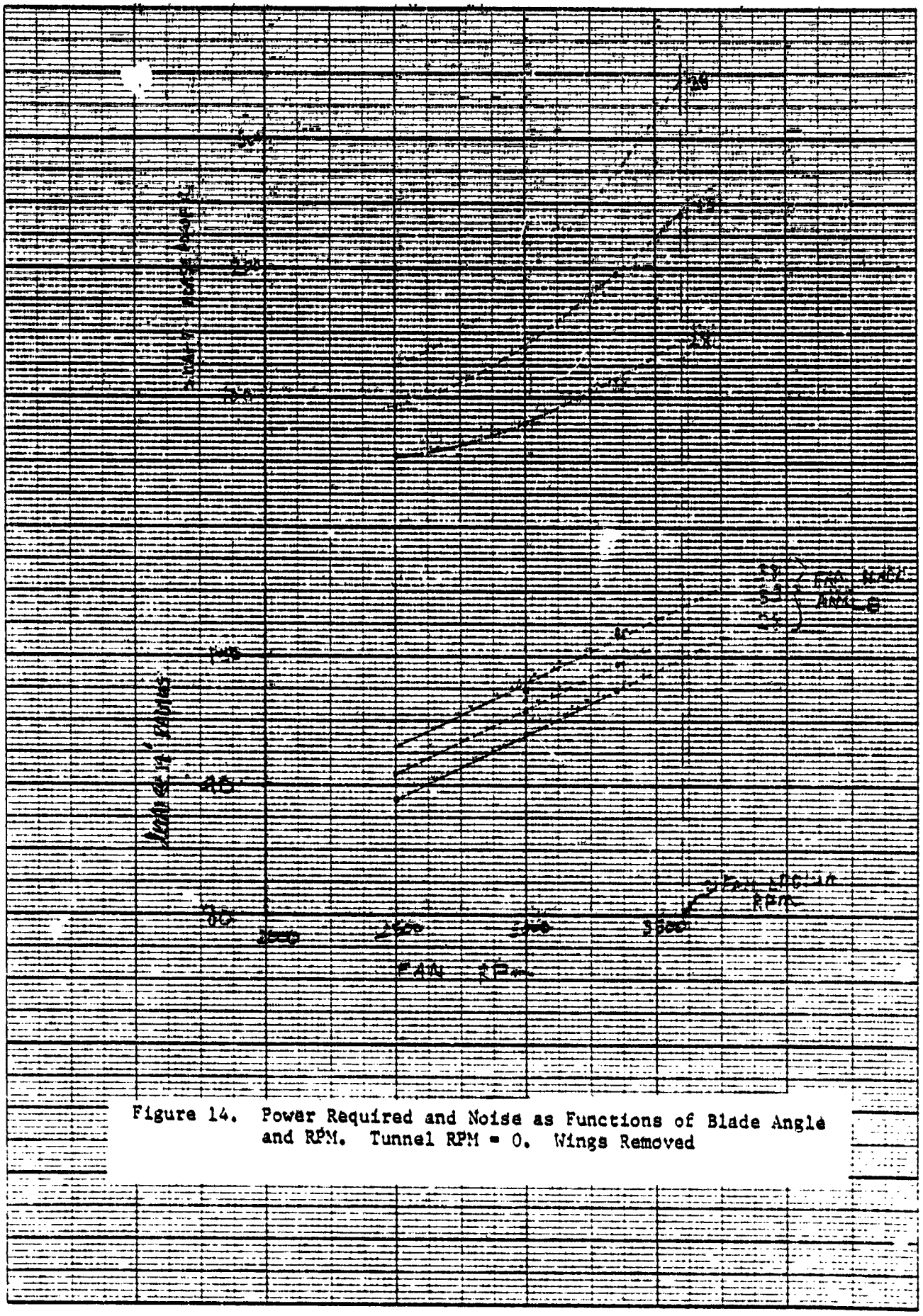

Figure 14. Power Required and Noise as Functions of Blade Angle and RPM. Tunnel RPM = 0. Wings Removed

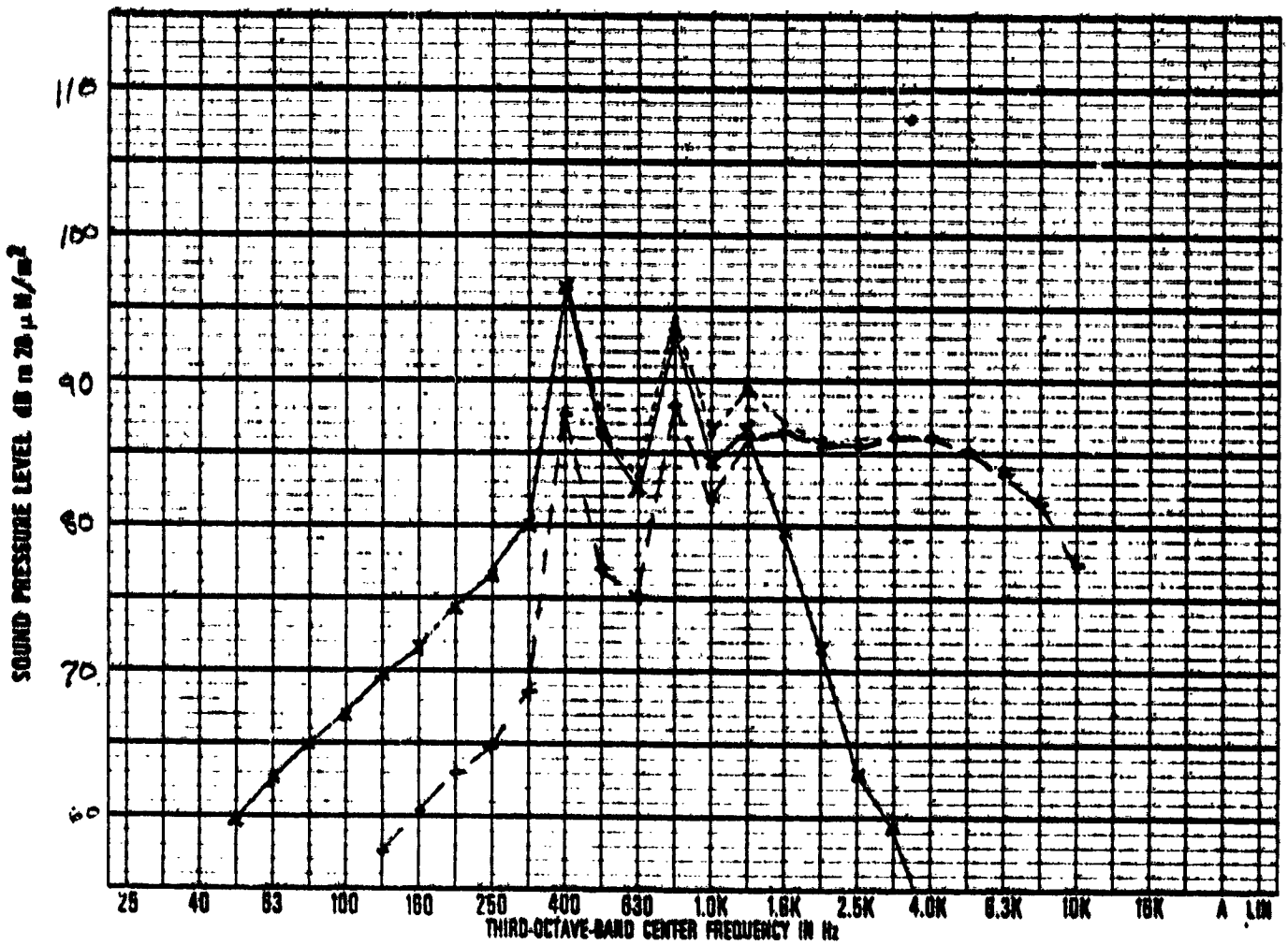


Figure 15a. Predicted Noise Spectra for Q-Fan at a 30.1 ft Measuring Radius (3600 Fan RPM, Design Condition)

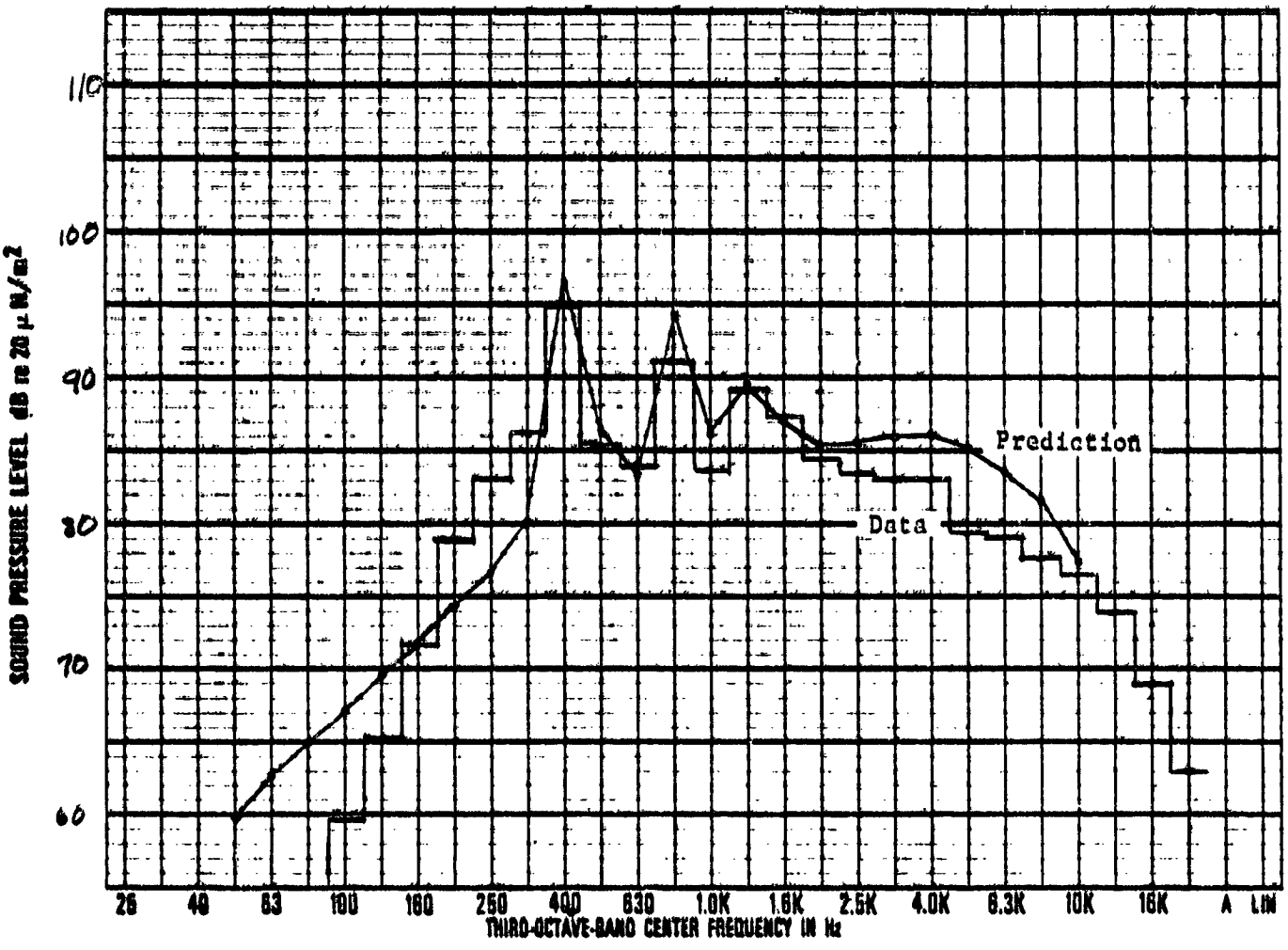


Figure 15b. Comparison of Measured and Predicted Noise Levels for Wings on Configuration (Data is Corrected to 3600 Fan RPM, Design Condition). 30.1 ft Measuring Radius.

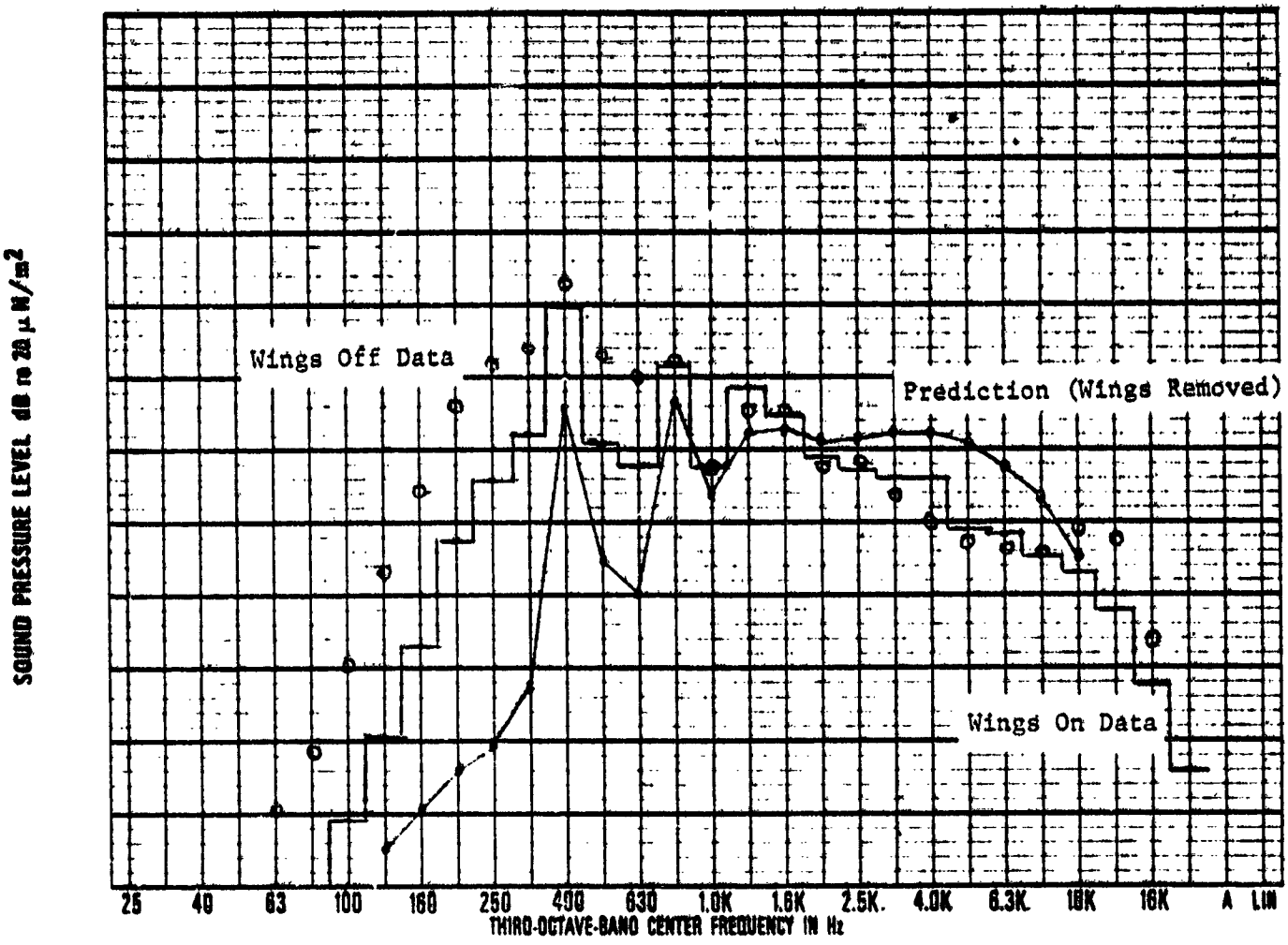


Figure 15c. Comparison of Measured & Predicted Wings Off Noise Levels for Q-Fan Design Condition. Measured Wings on Data is Included. 30.1 ft Measuring Radius.

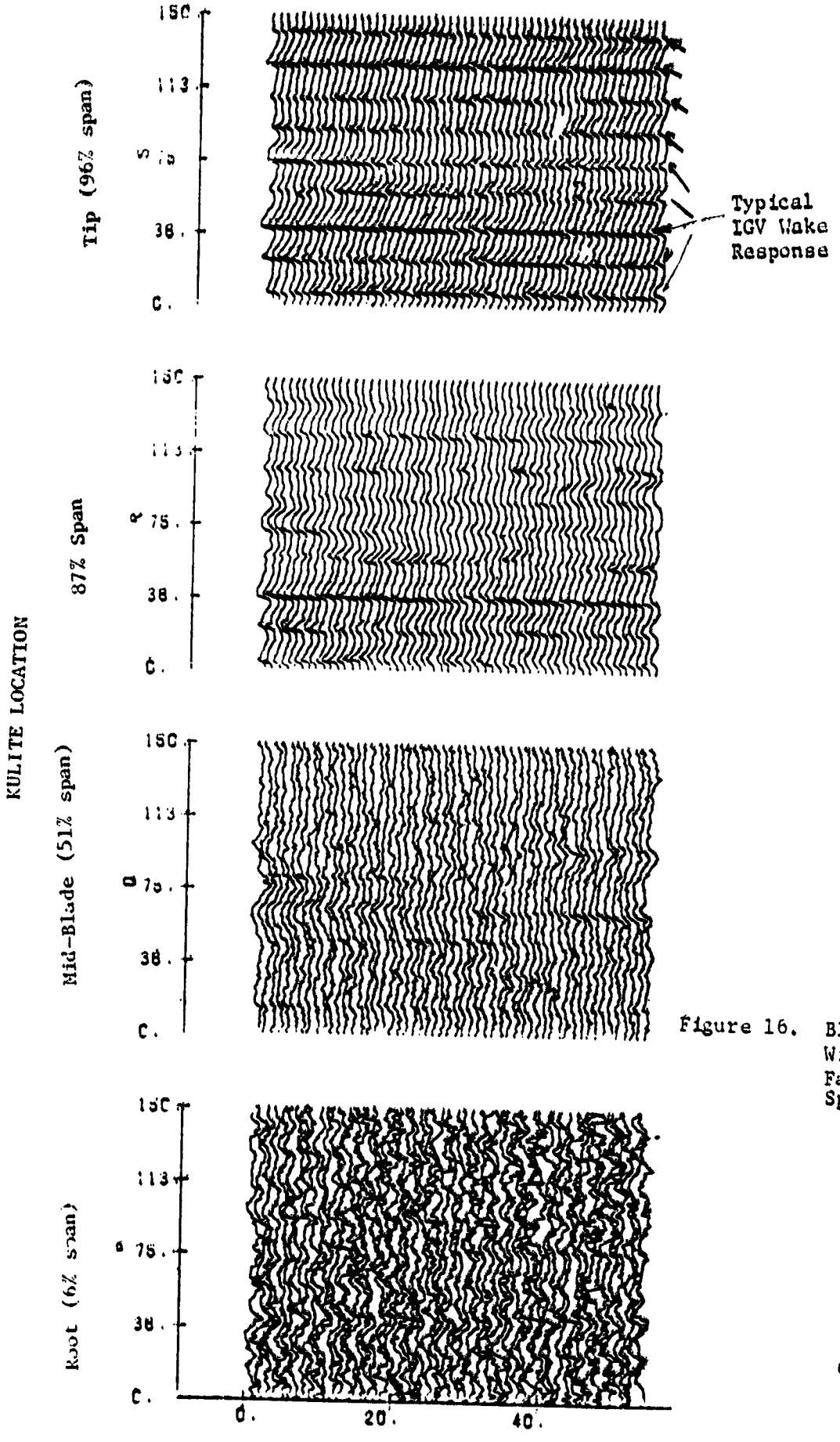


Figure 16. Blade Pressure Signals, Wings on $\beta = 28^{0}$, 3350 Fan RPM 0 FPS Tunnel Speed

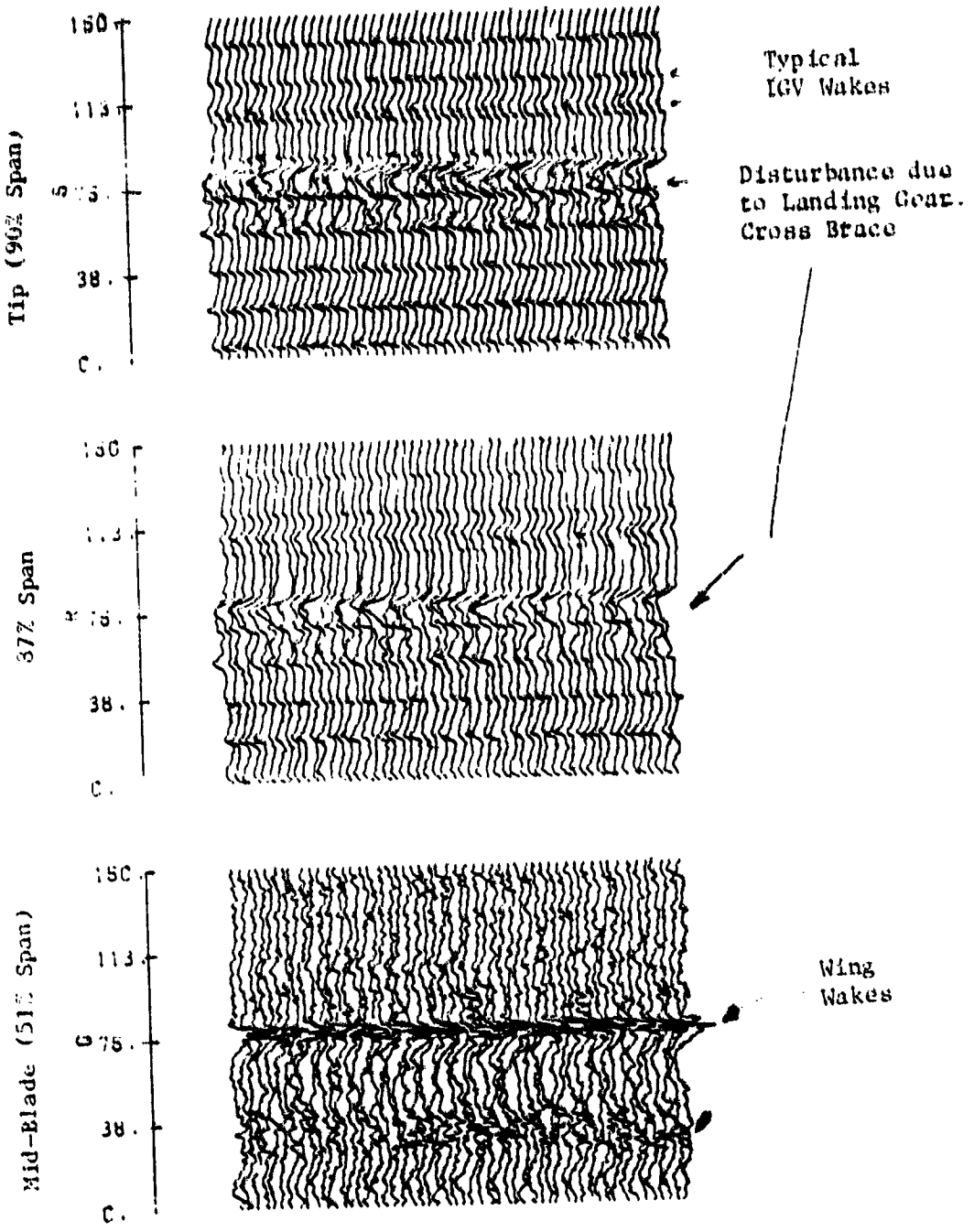


Figure 17. Blade Pressure Signals, Wings On $\delta = 28^{\circ}$, 3350 Fan RPM 99 FPS Tunnel Speed.

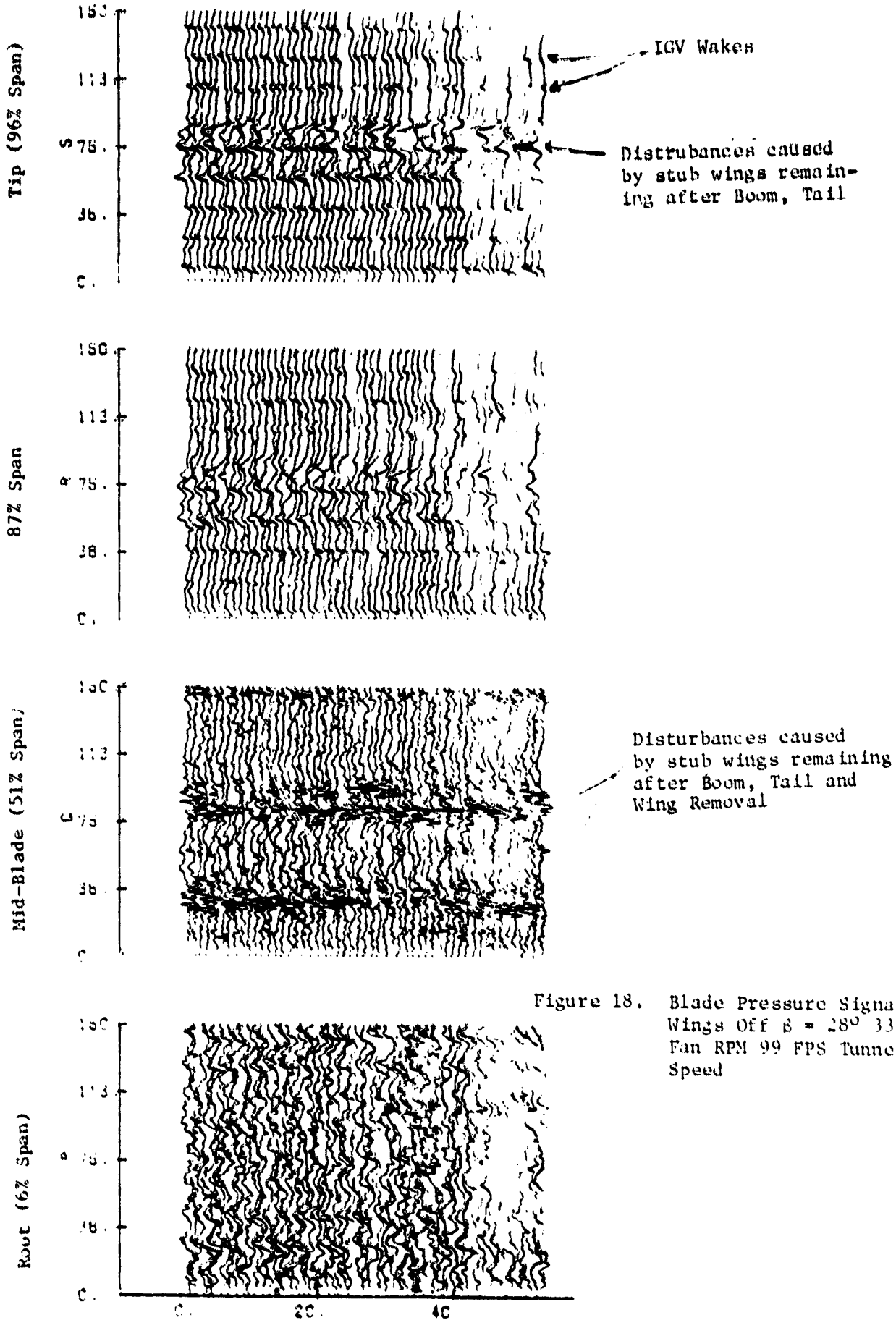


Figure 18. Blade Pressure Signals, Wings Off $\beta = 28^{0}$ 3350 Fan RPM 99 FPS Tunnel Speed

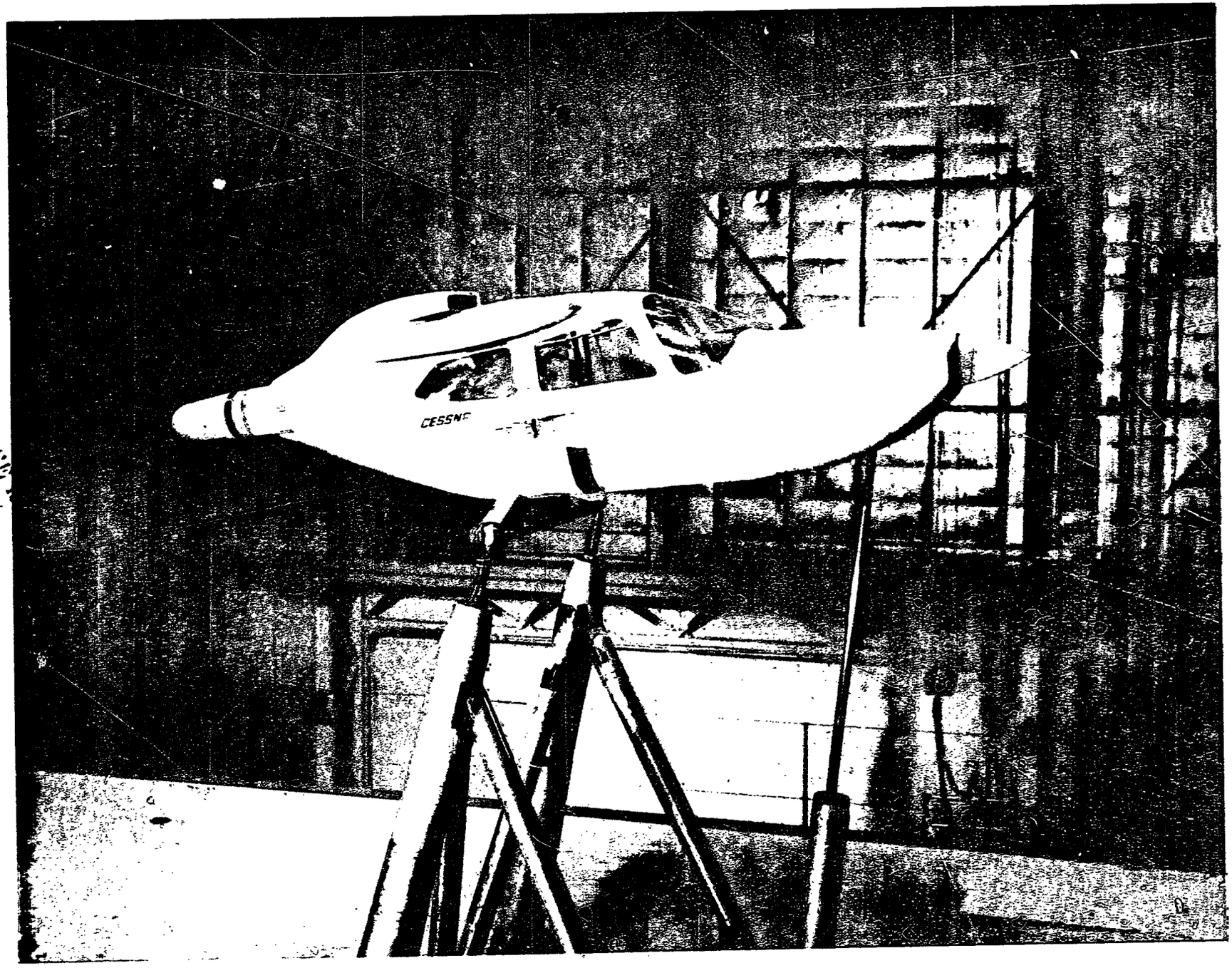


Figure 19. Wings Off Configuration

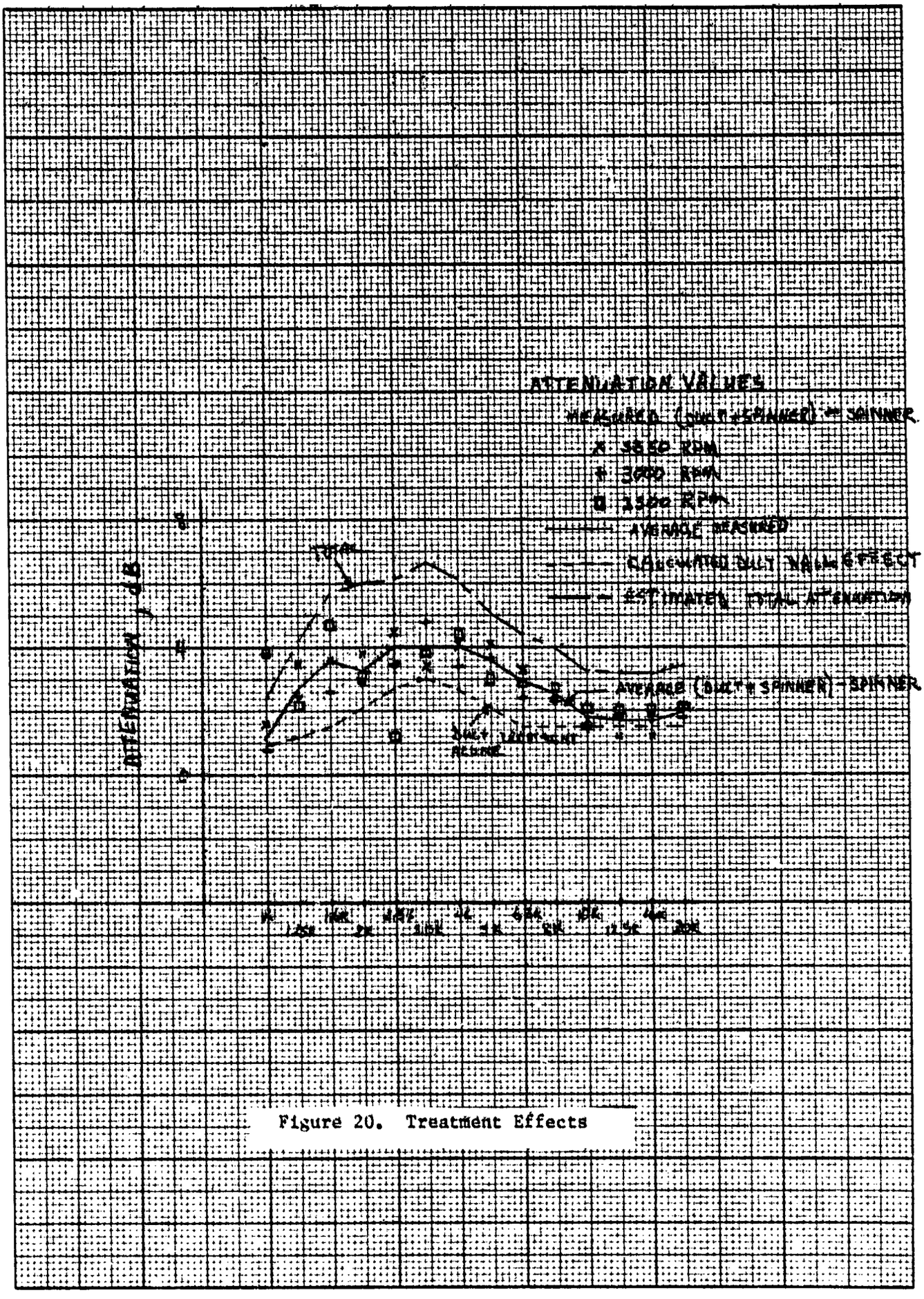


Figure 20. Treatment Effects

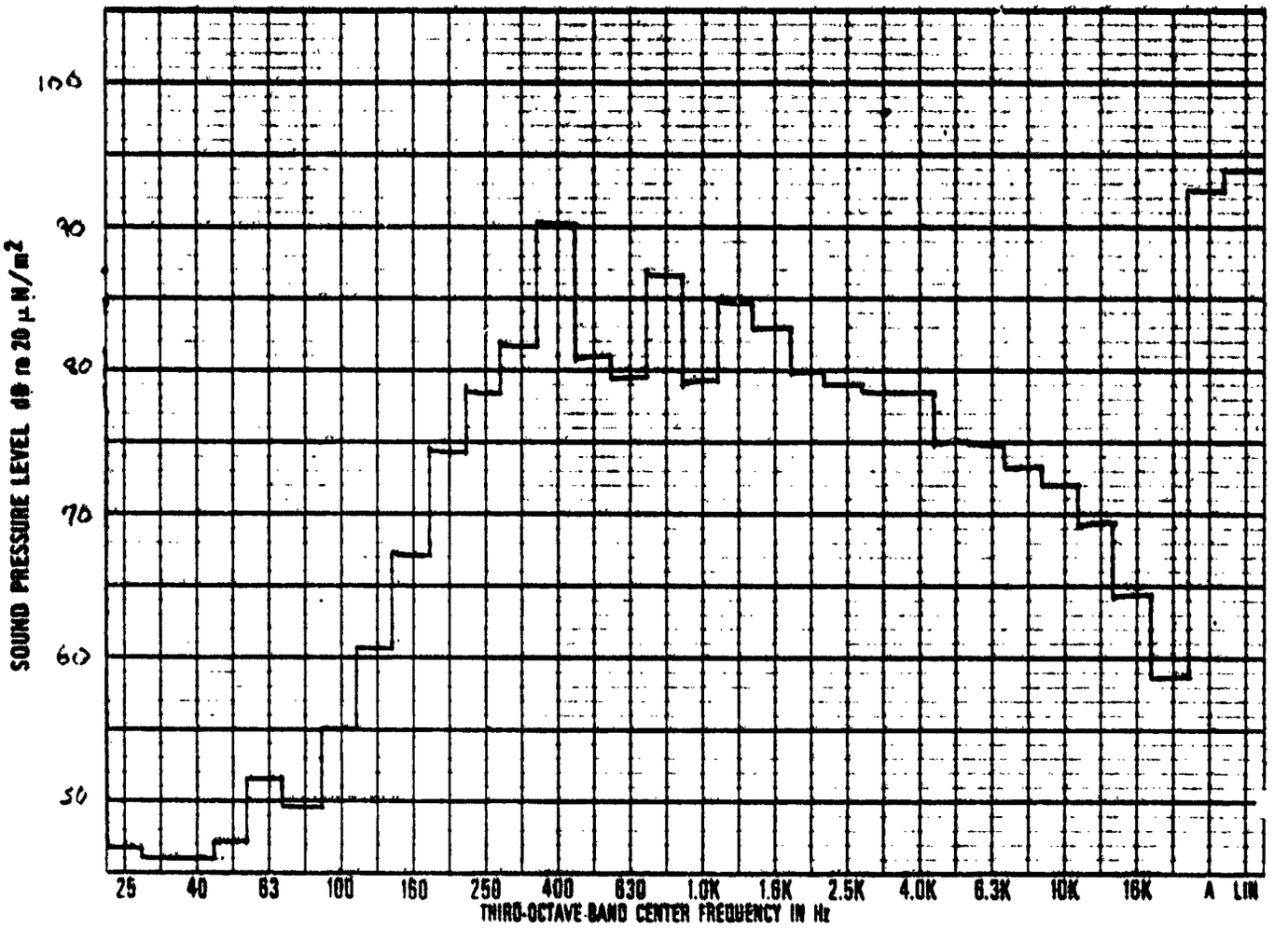


Figure 21. 1/3 Octave Band Spectrum for Mic #4, Wings On,
73 FPS Tunnel Speed,
3350 Fan RPM, 28° Blade Angle

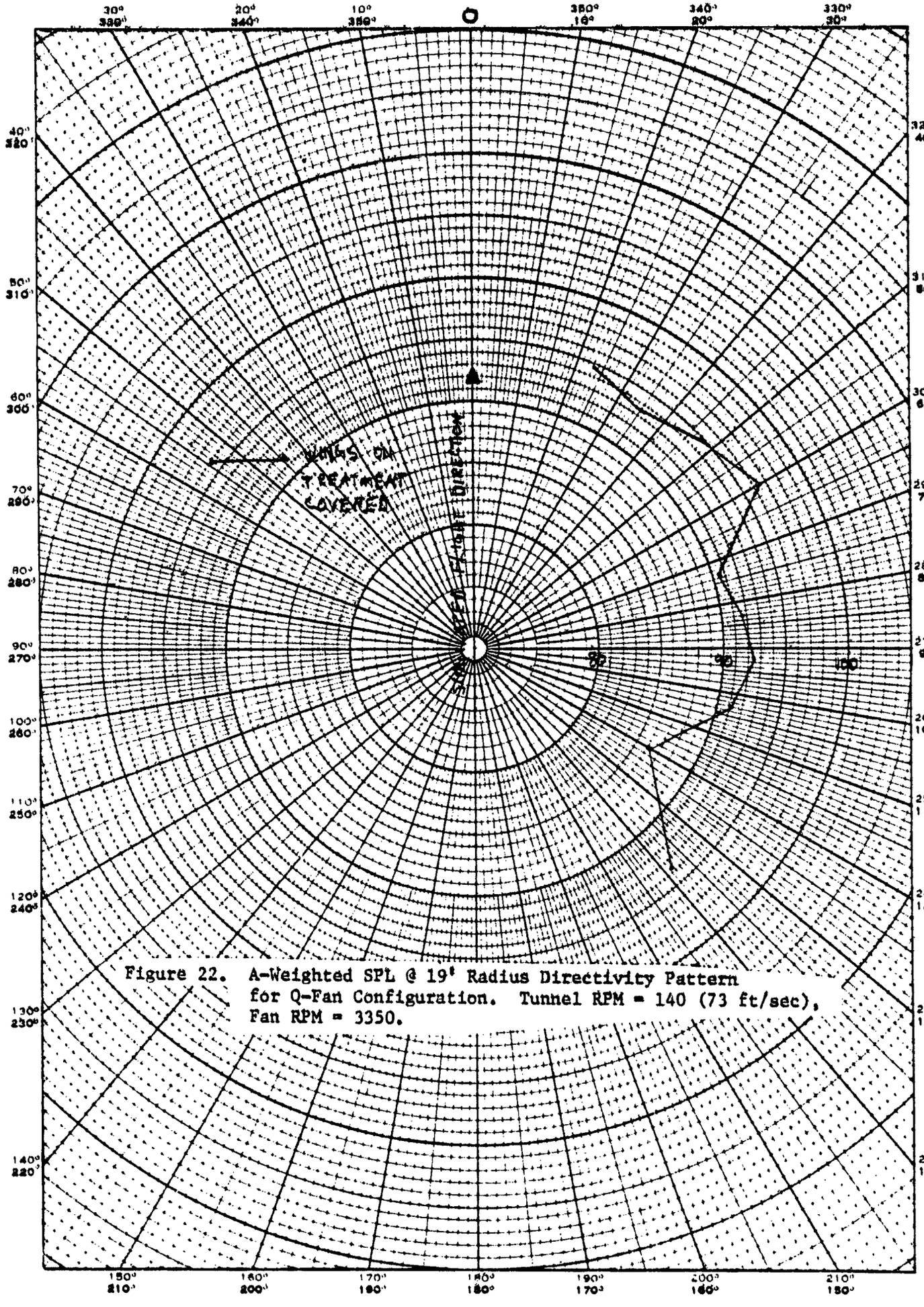


Figure 22. A-Weighted SPL @ 19' Radius Directivity Pattern for Q-Fan Configuration. Tunnel RPM = 140 (73 ft/sec), Fan RPM = 3350.

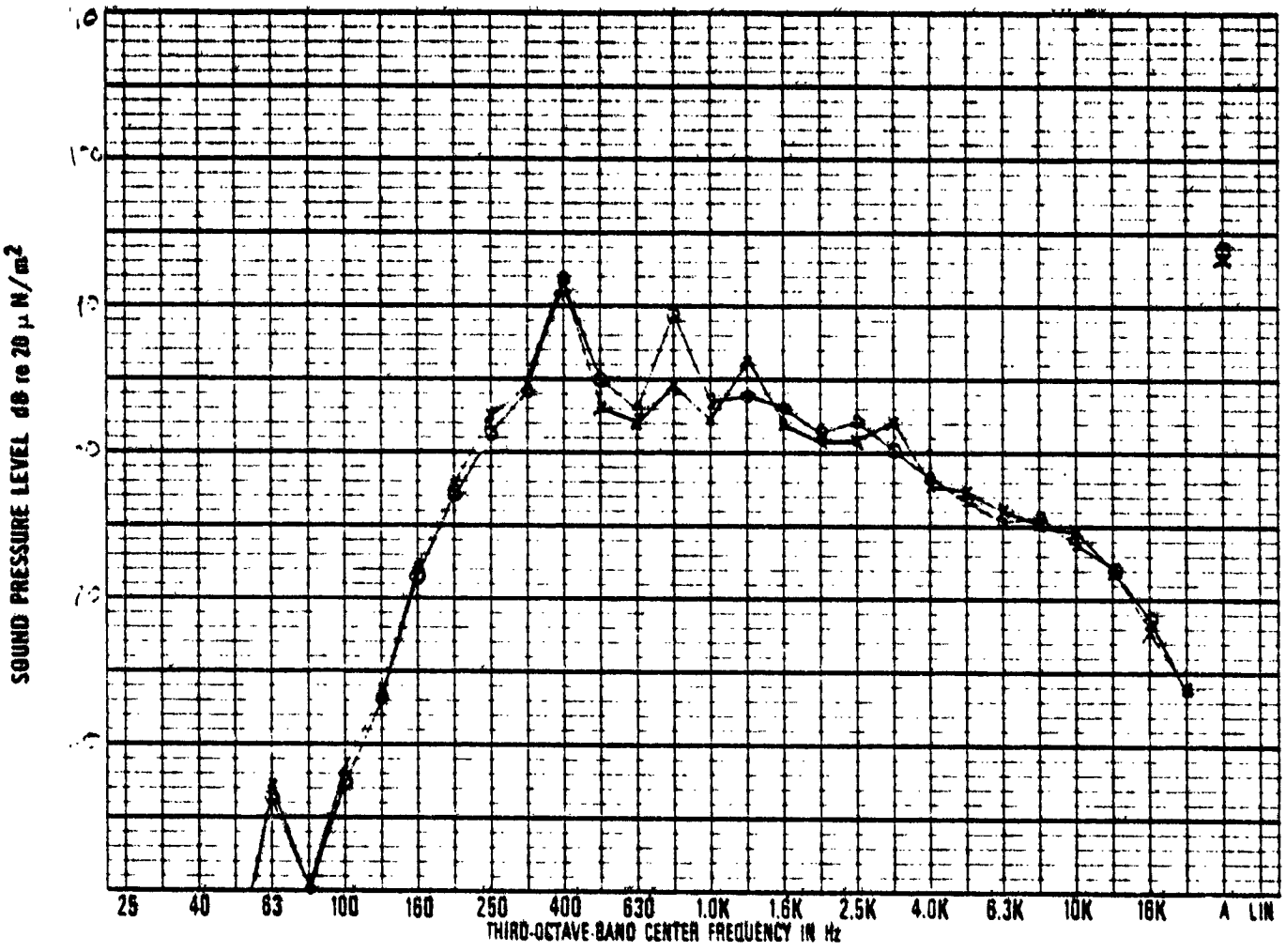


X - X $0^{o}$ Angle of Attack

0 - 0 $4^{o}$ Angle of Attack

Figure 23. Angle of Attack Effect for mic #10
73 FPS Tunnel Speed
3350 Fan RPM

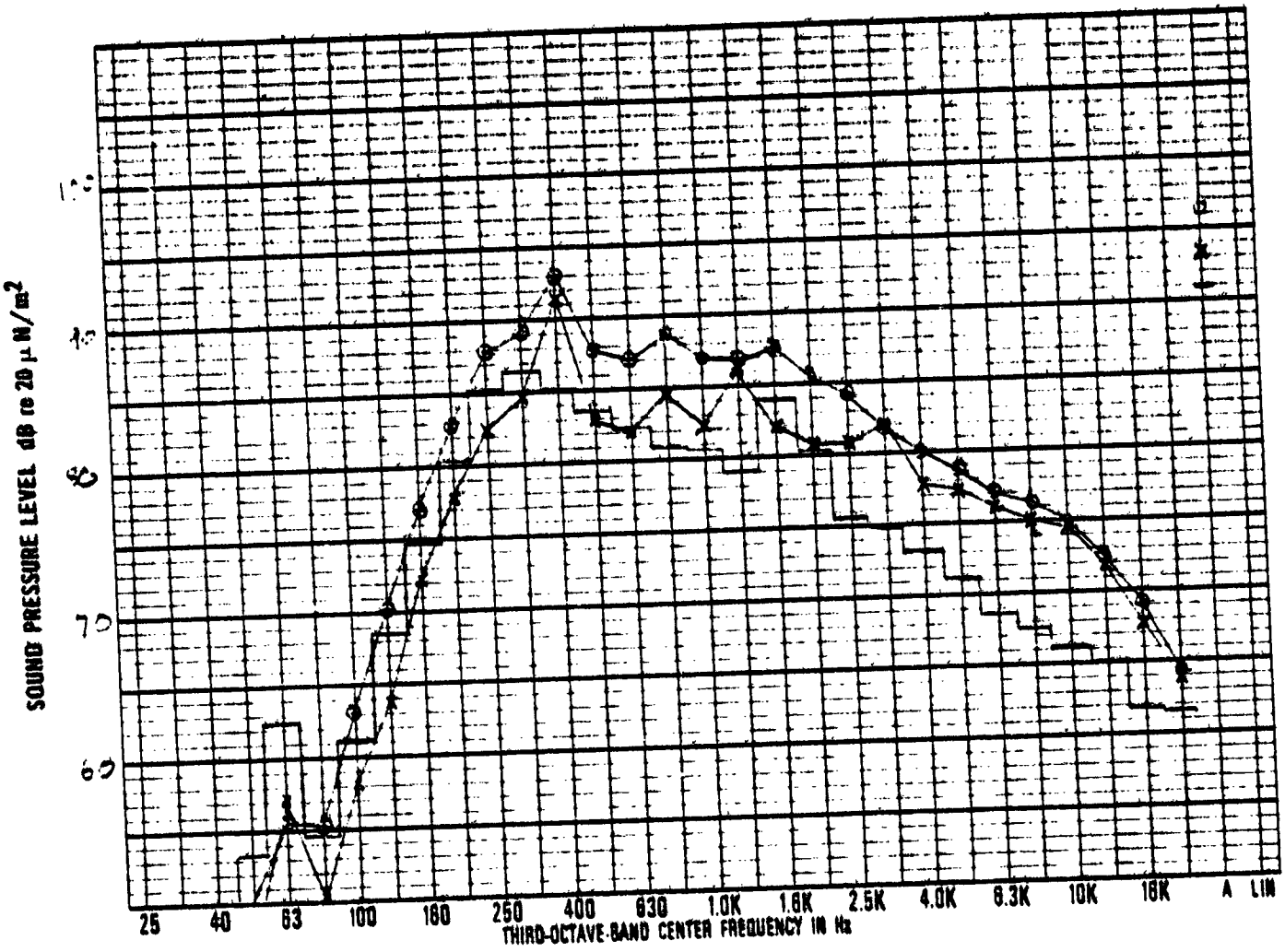


X - X 73 FPS Tunnel, 3350 Fan, 0° AOA

0 - 0 99 FPS Tunnel, 3350 Fan, 6° AOA, 20° Flaps

—— Background Noise @ 99 FPS Tunnel Speed

Figure 24. Angle of Attack & Flap Effect for mic #10

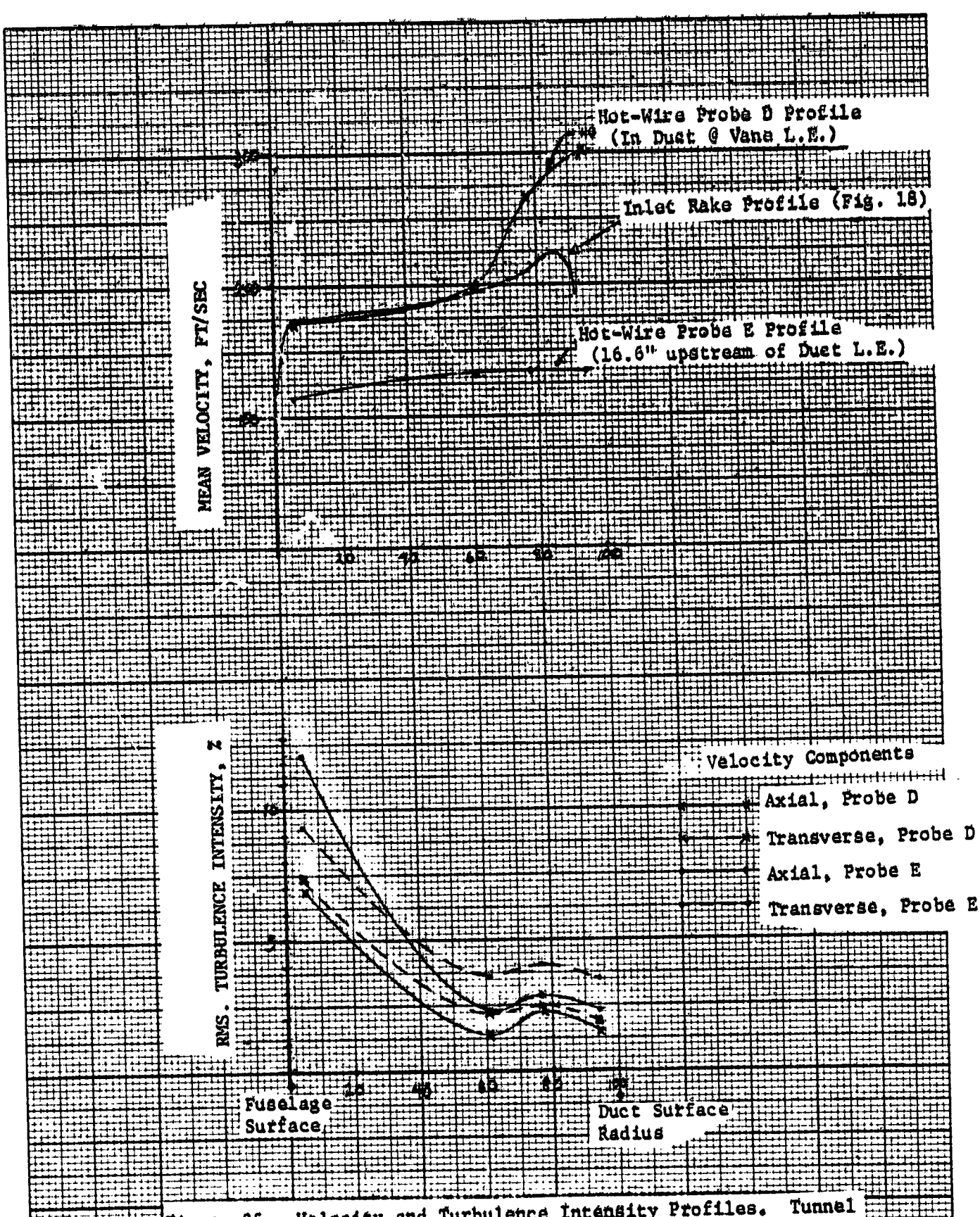


Figure 25. Velocity and Turbulence Intensity Profiles. Tunnel Speed = 99 FPS, 3350 Fan RPM. Wings Removed.

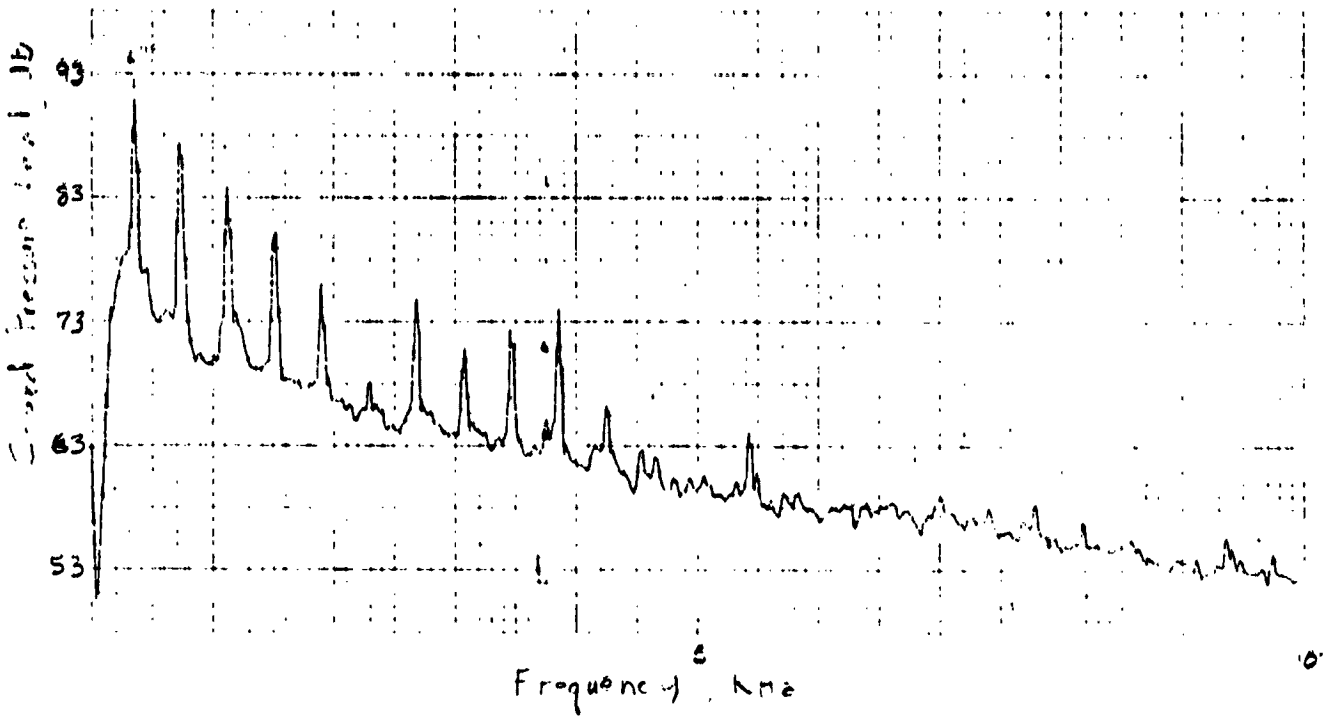


Figure 26. Narrow-band Spectrum for mic #4, Wings On, 73 fps Tunnel Speed, 3350 Fan RPM, 28° Blade Angle

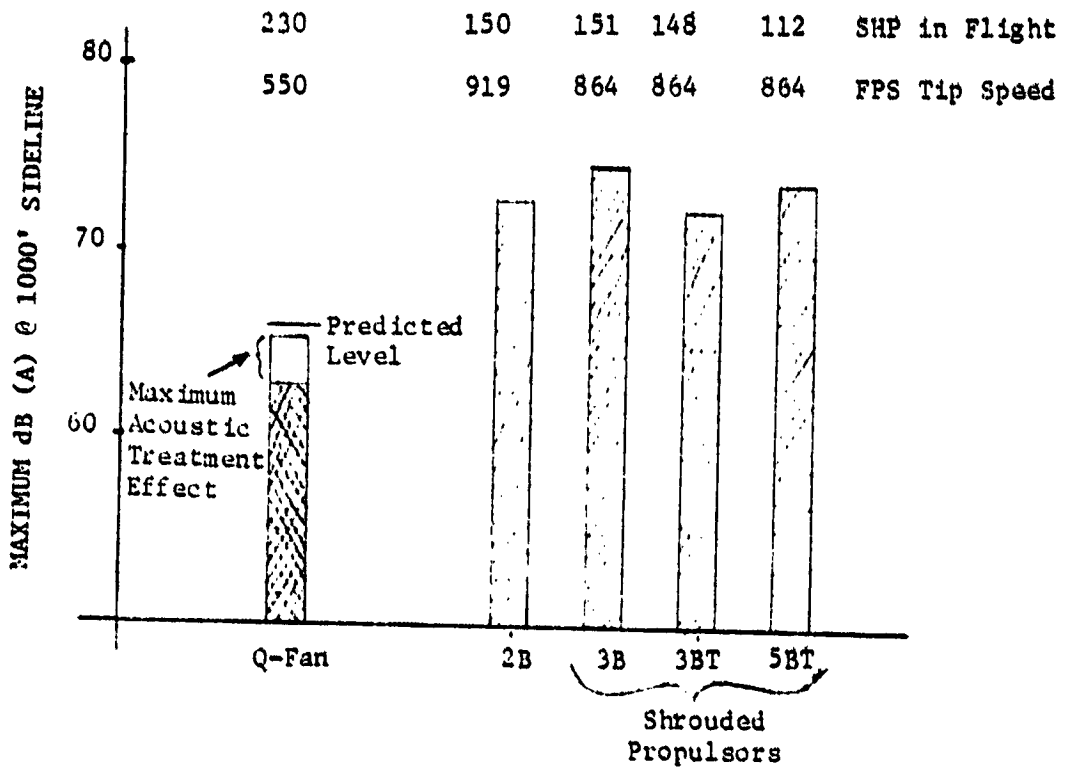


Figure 27. Noise Levels at Flight Condition for Cessna 327 Configurations Tested in the 30X60 Wind Tunnel

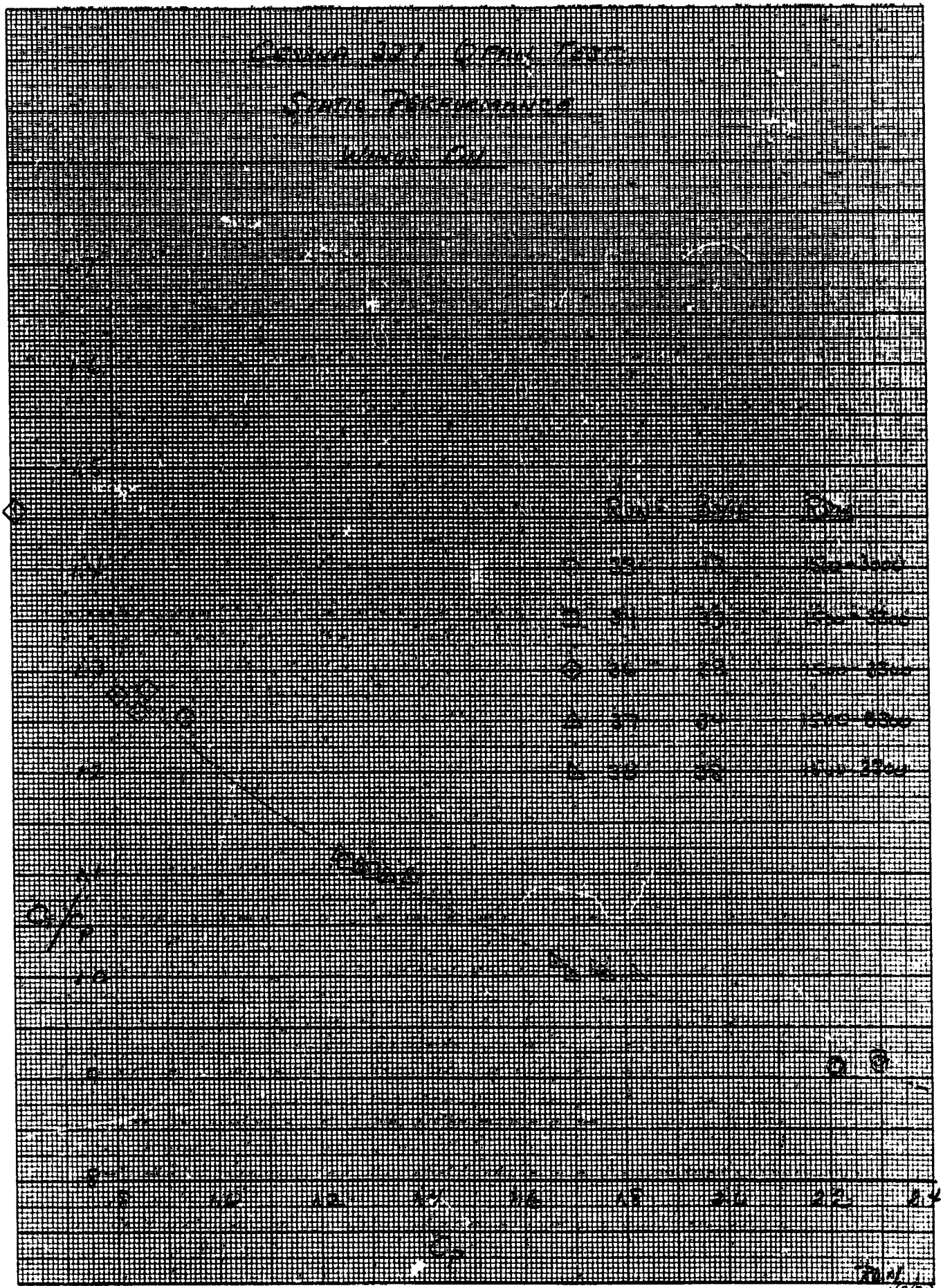

Figure 28

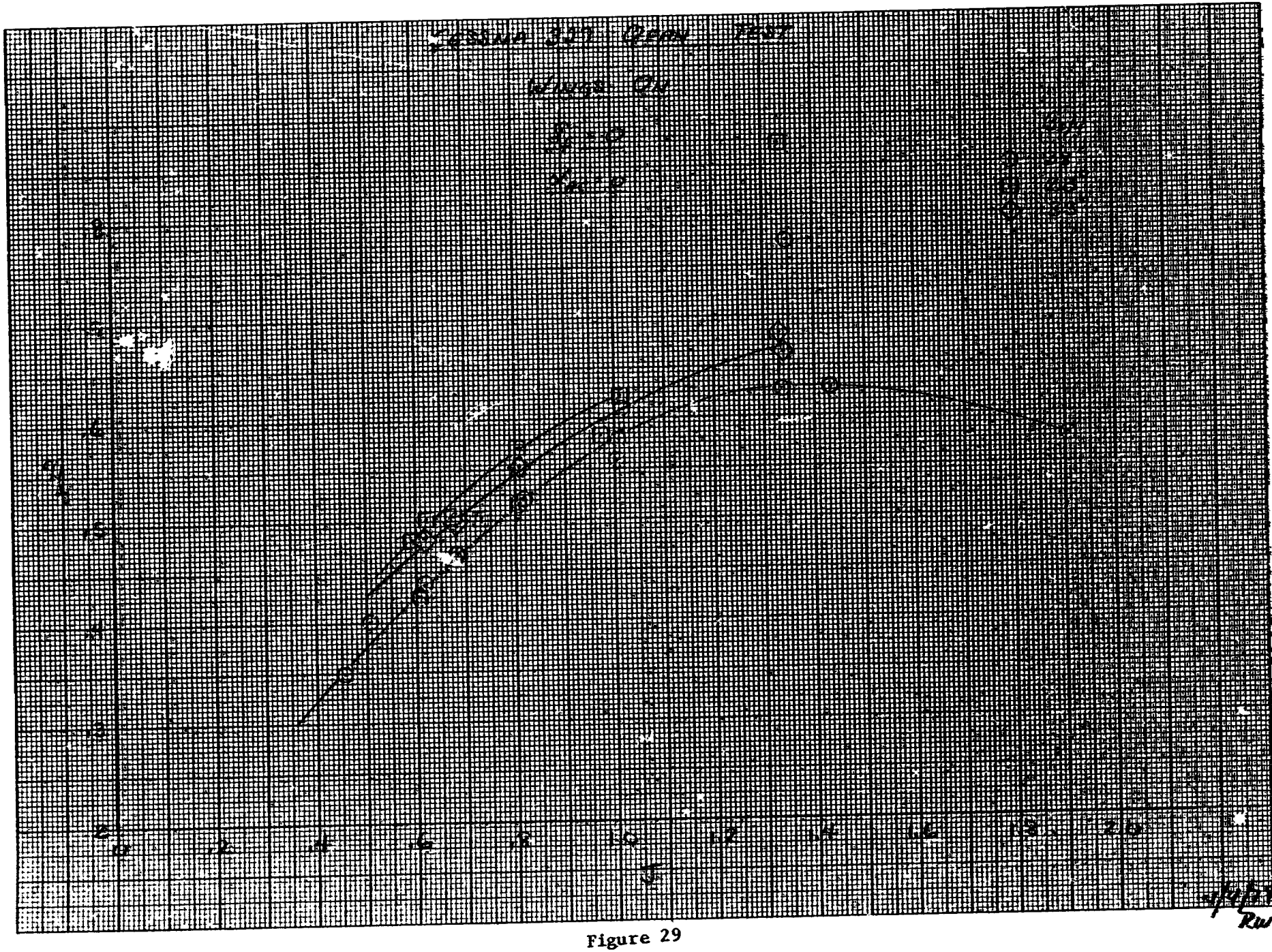

Figure 29

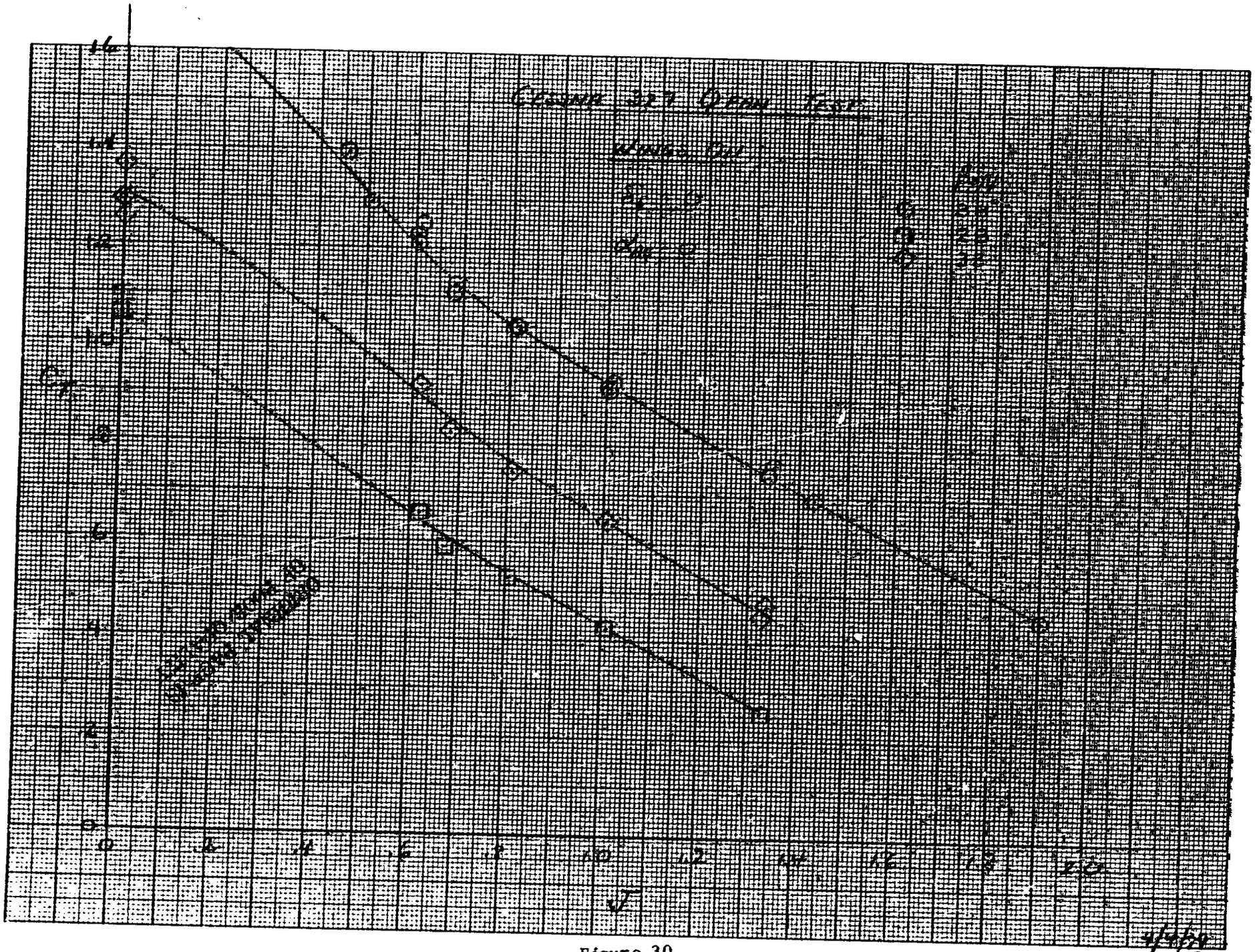

Figure 30

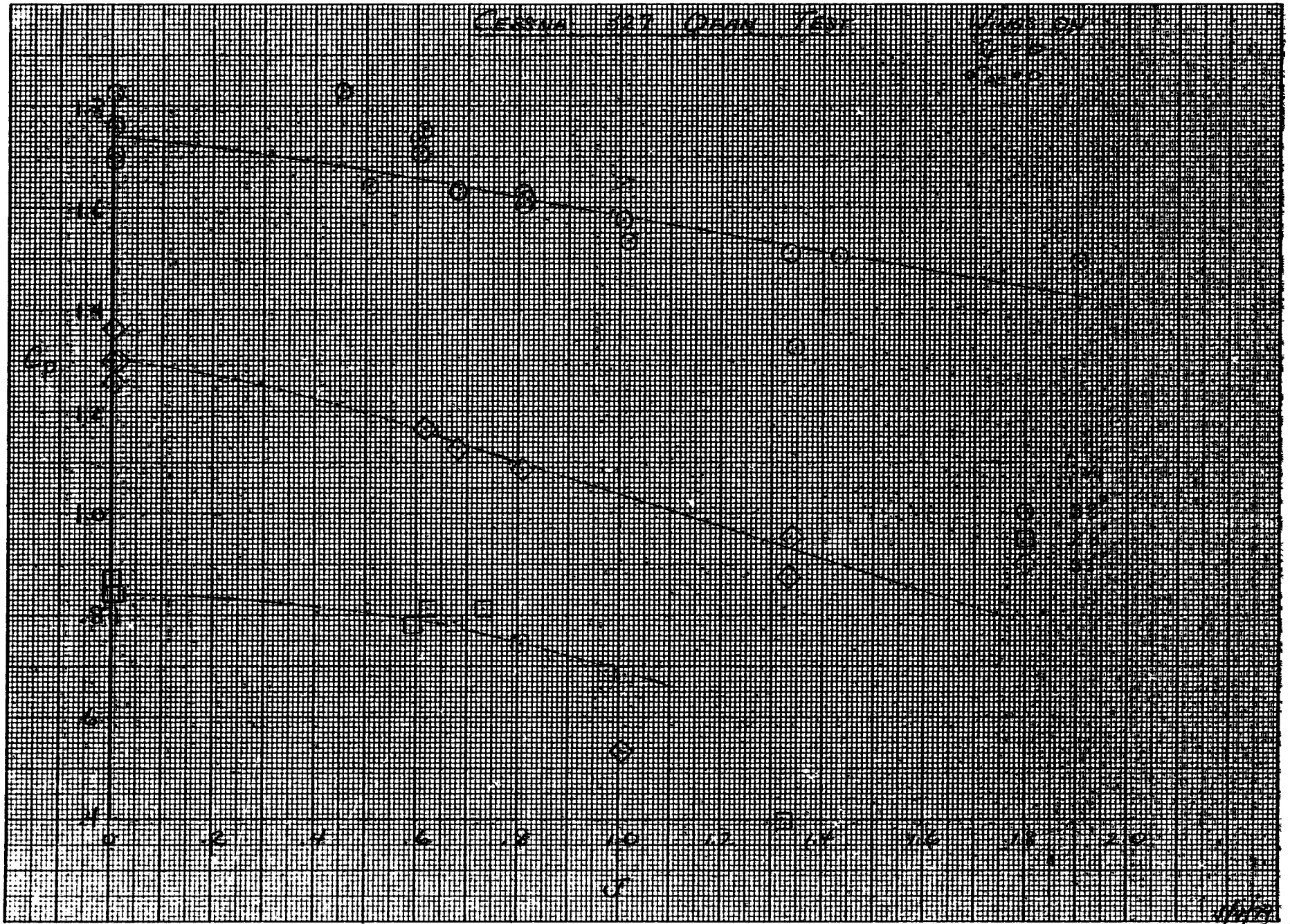

Figure 31

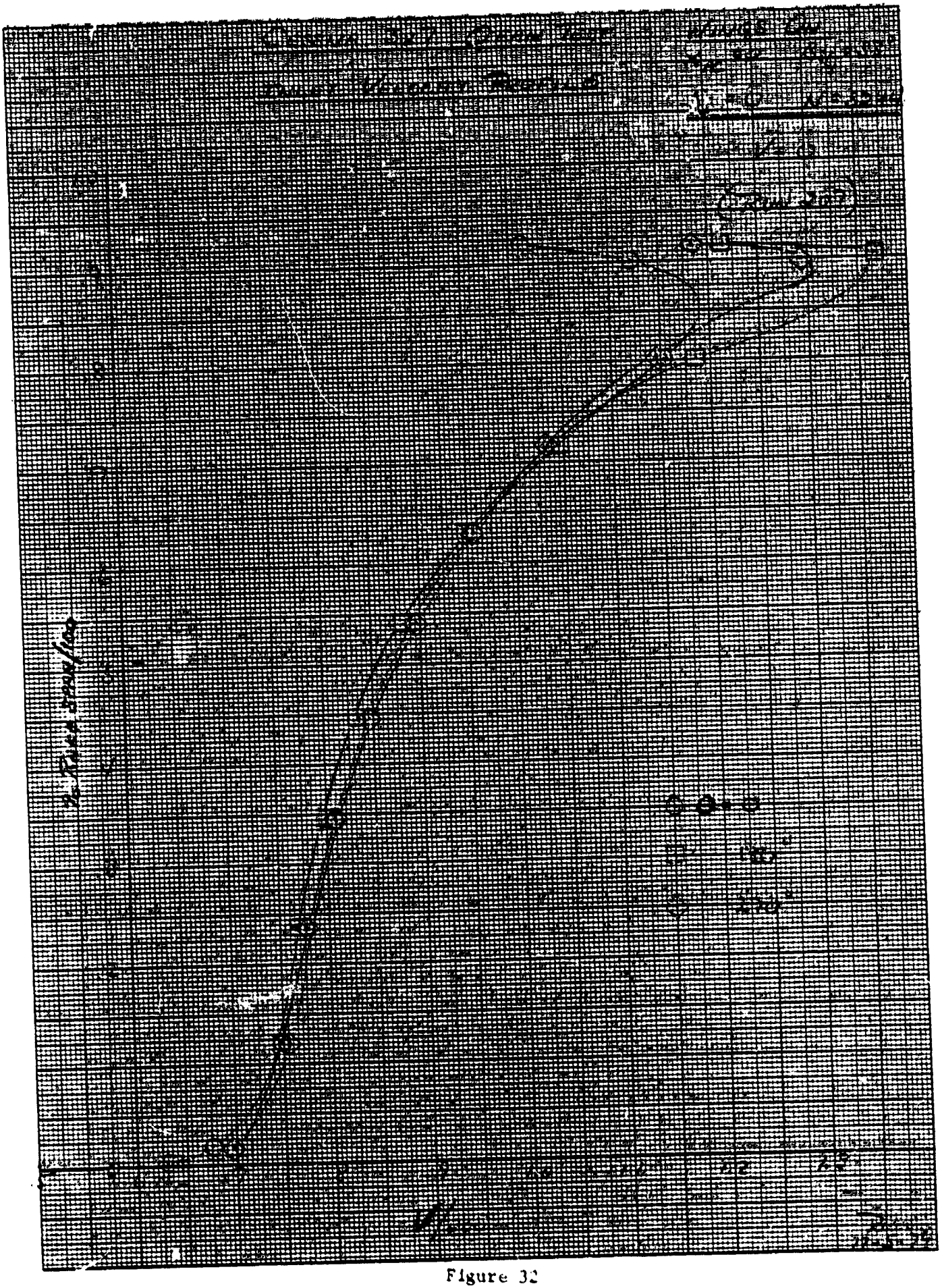

Figure 32

Figure 33

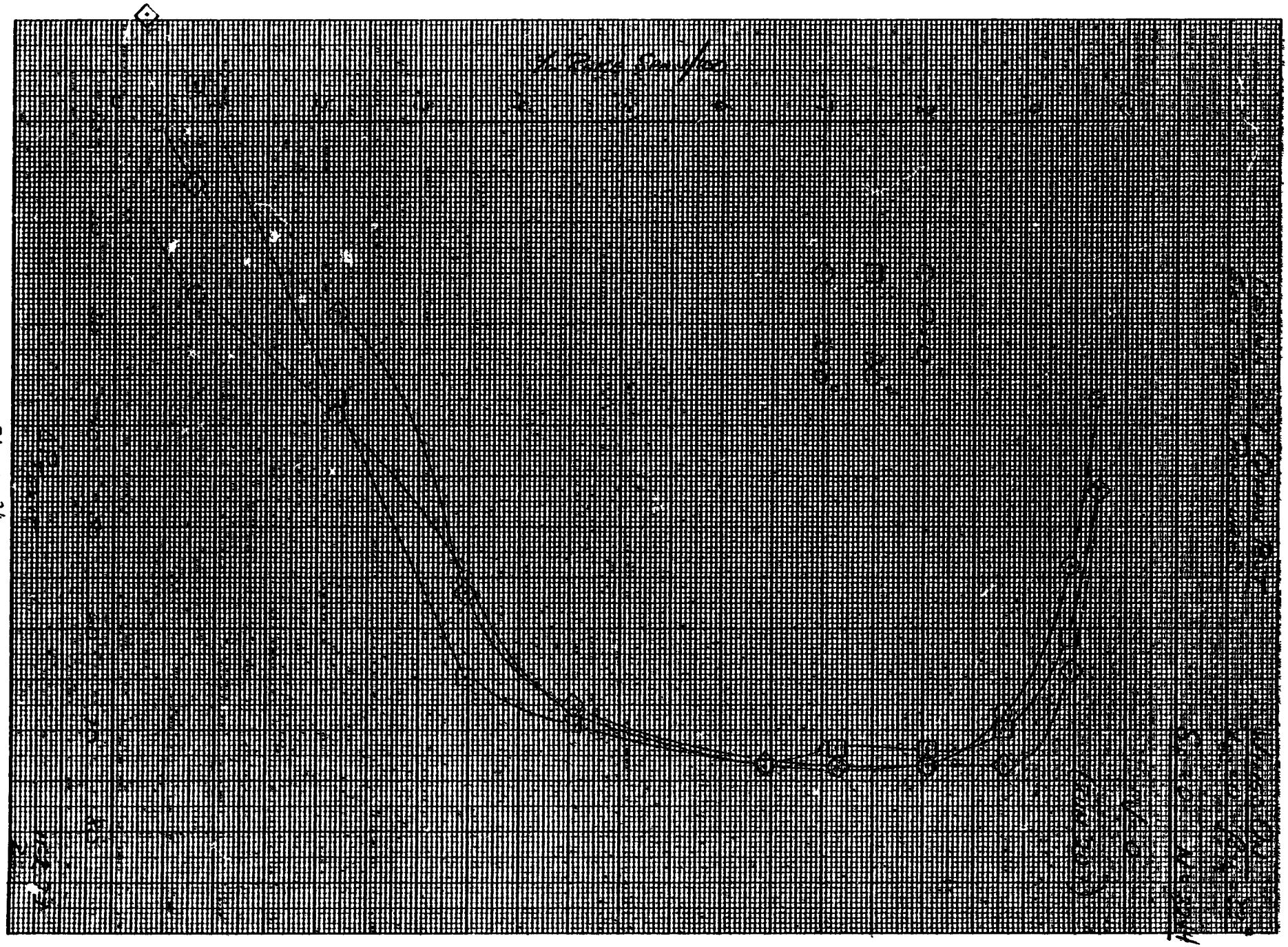

Figure 34

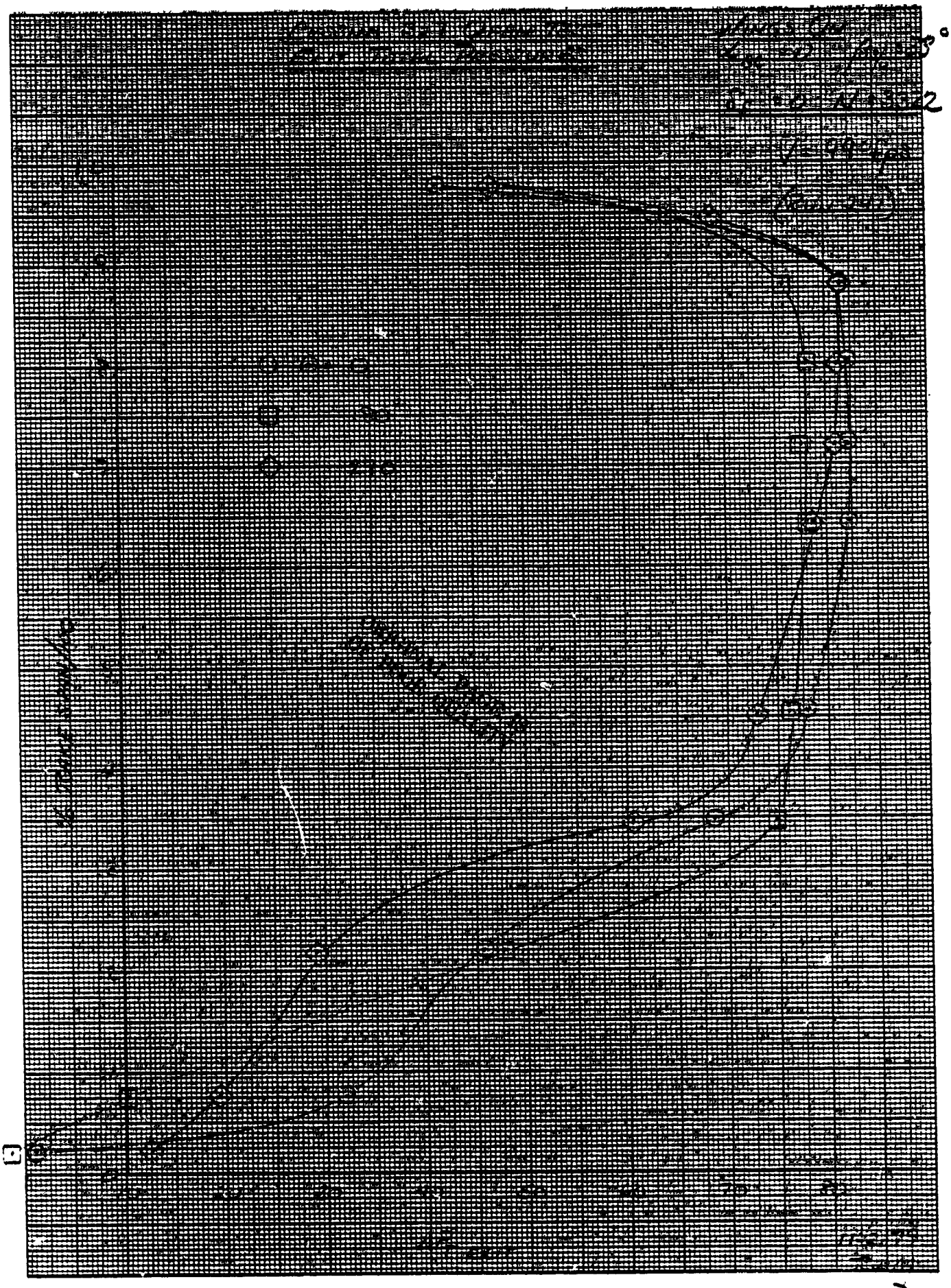

Figure 35

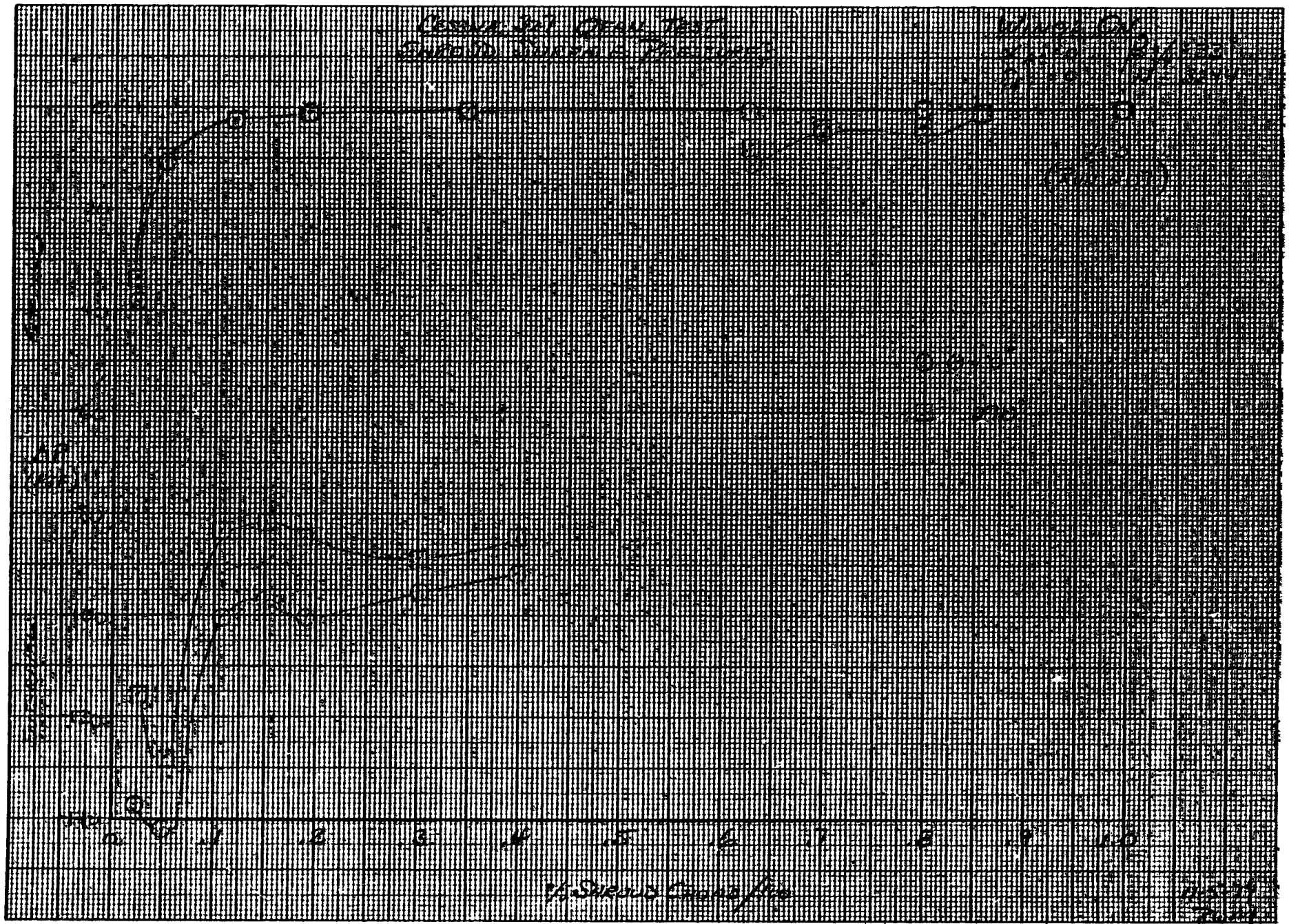

Figure 36

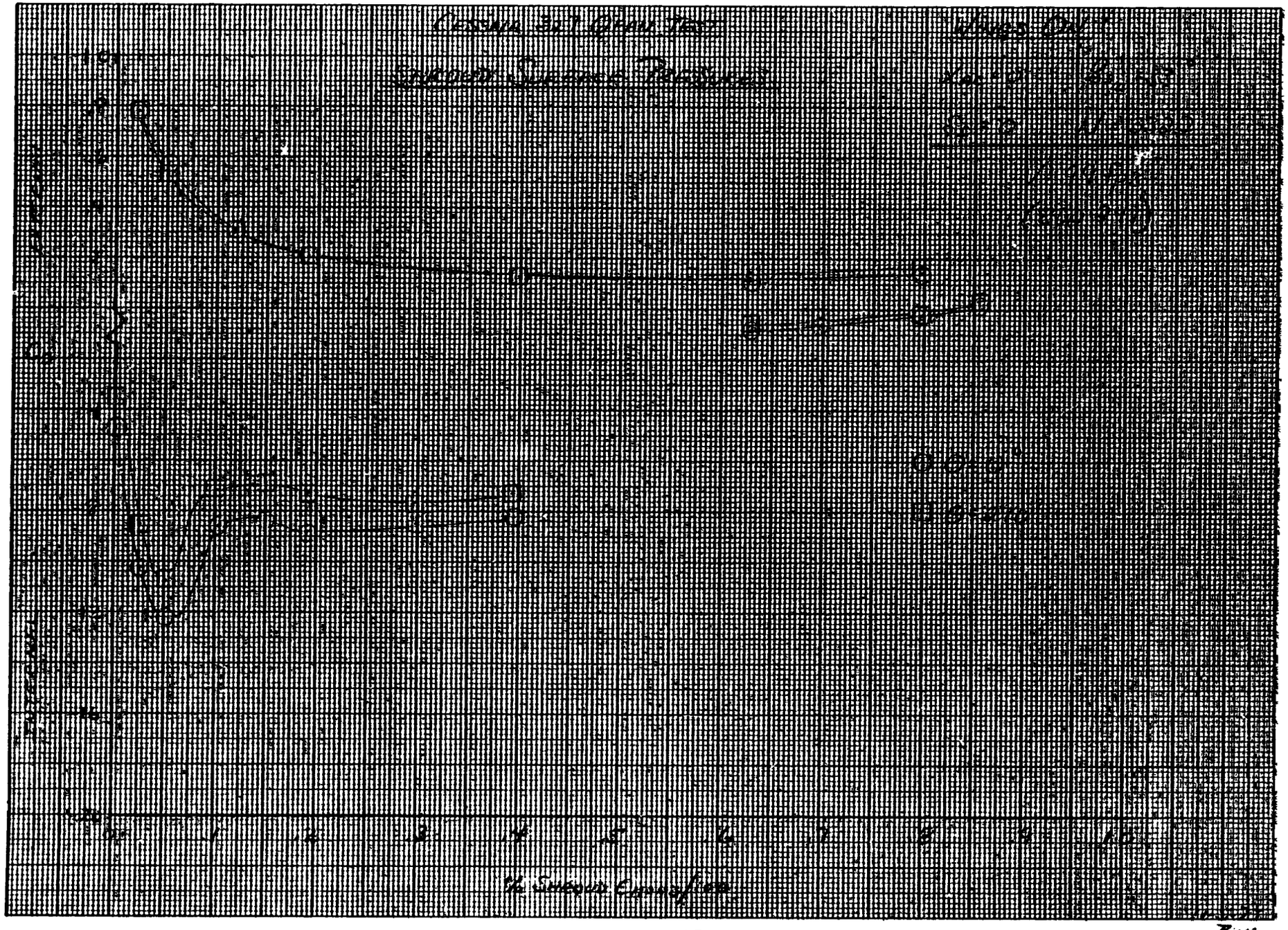

Figure 37

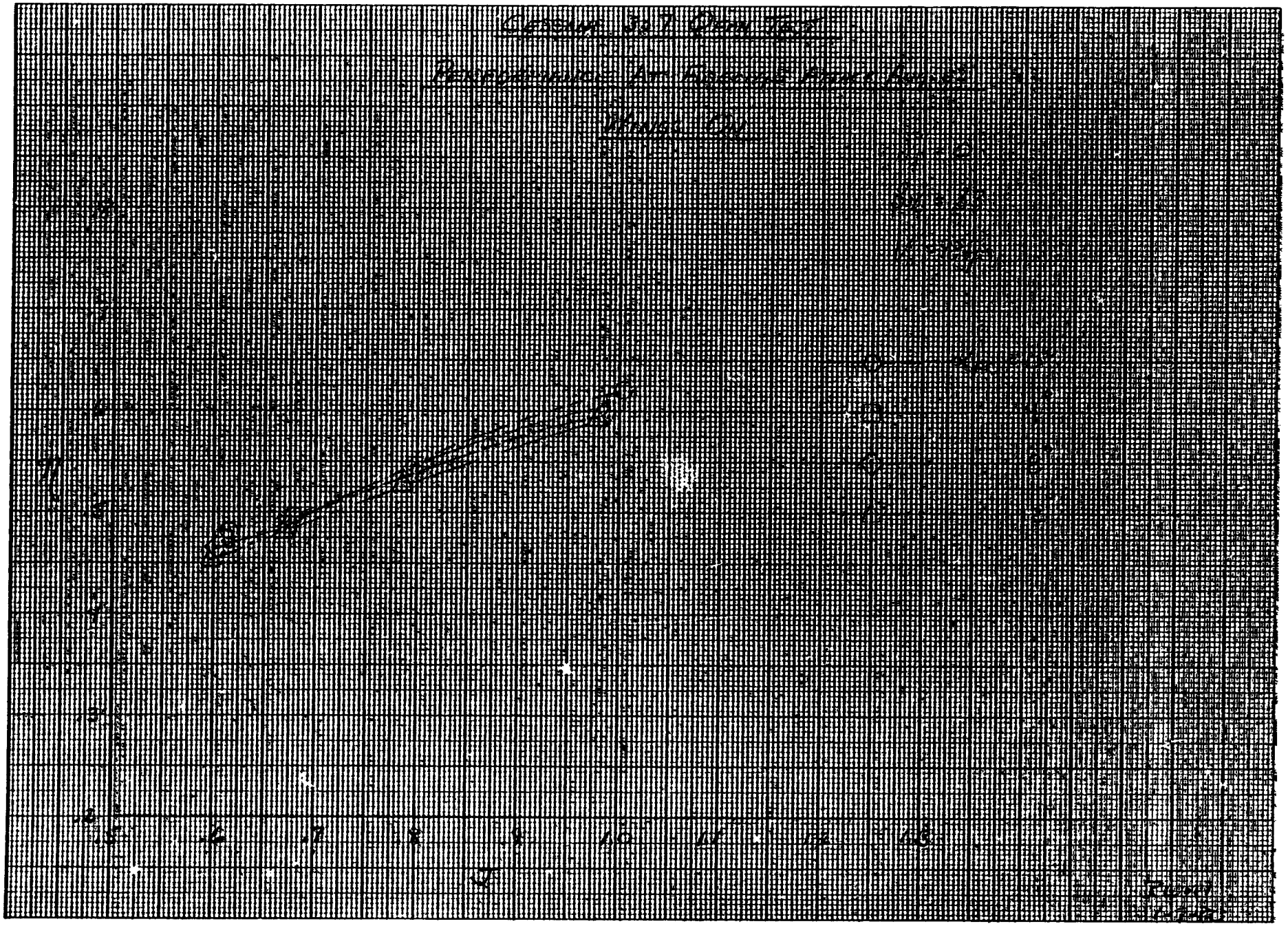

Figure 38

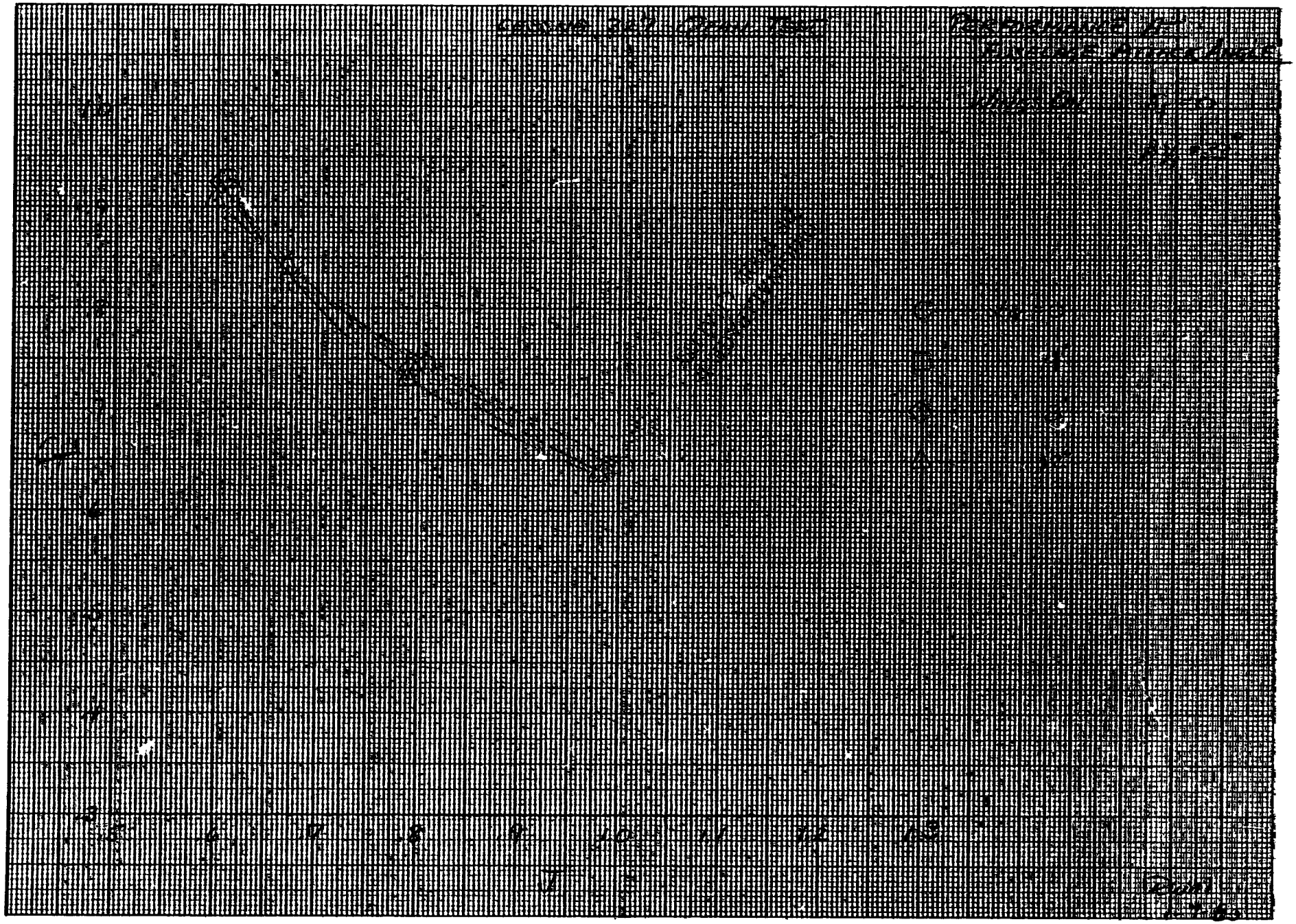

Figure 39

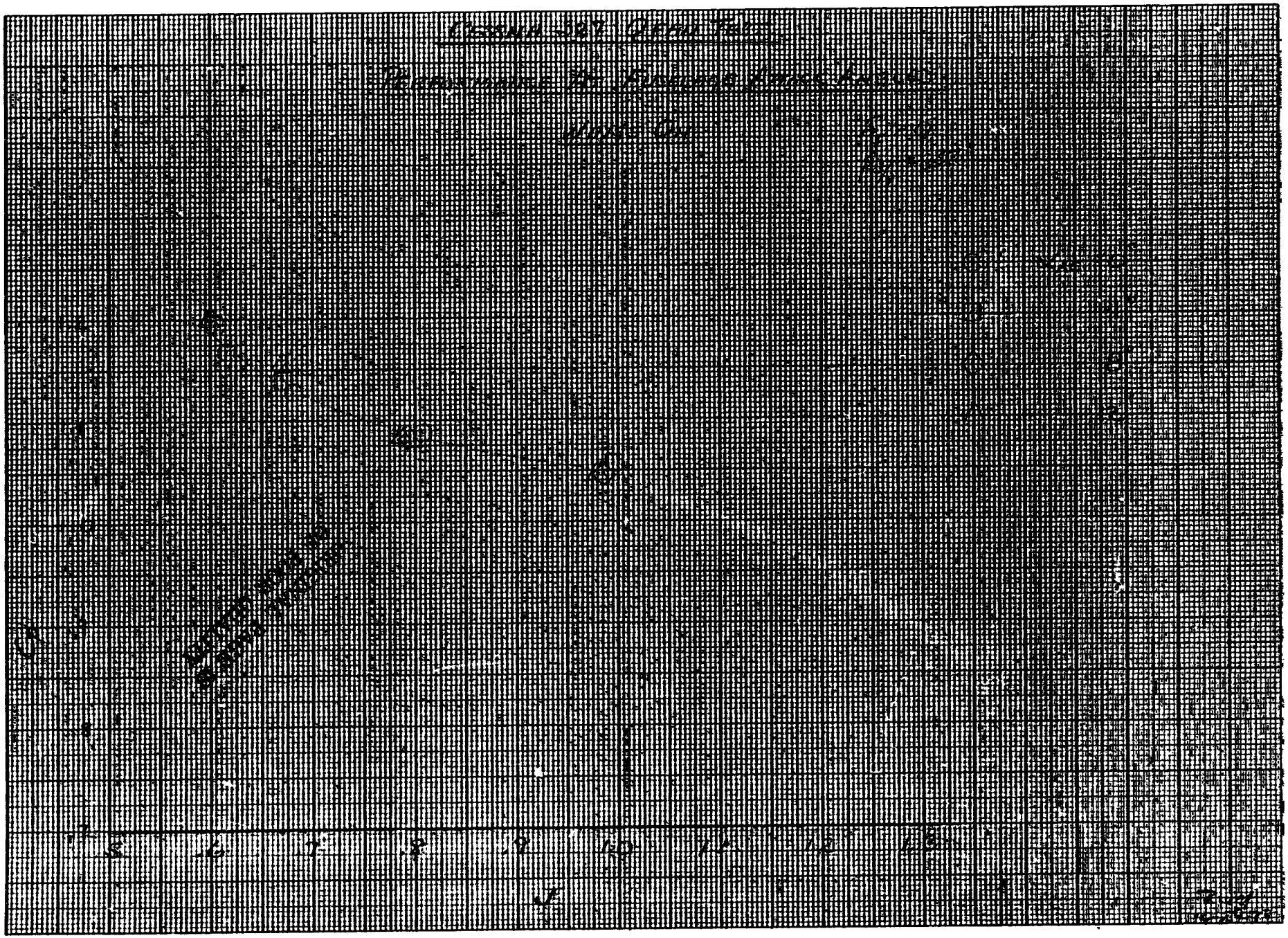

Figure 40

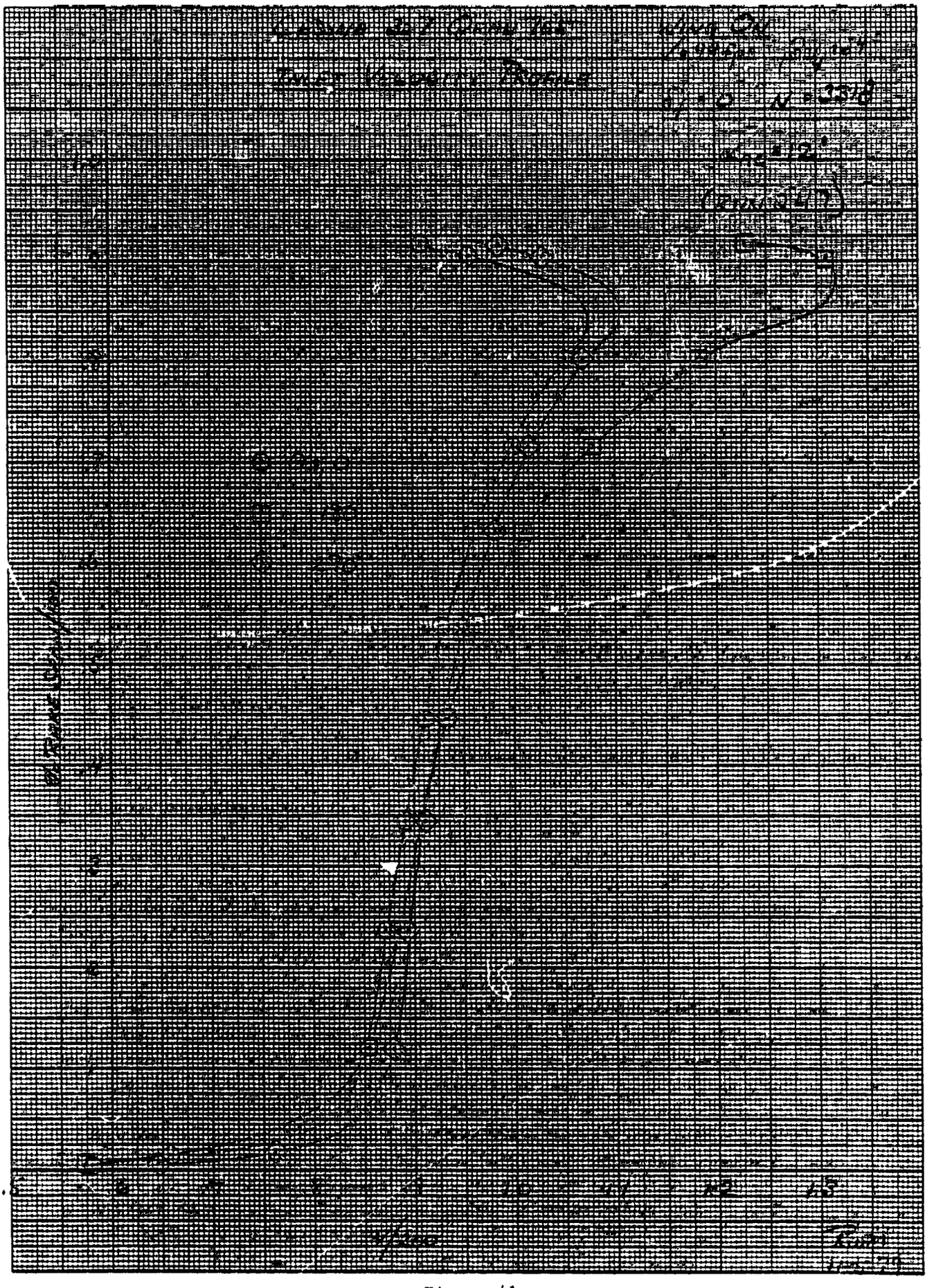

Figure 41

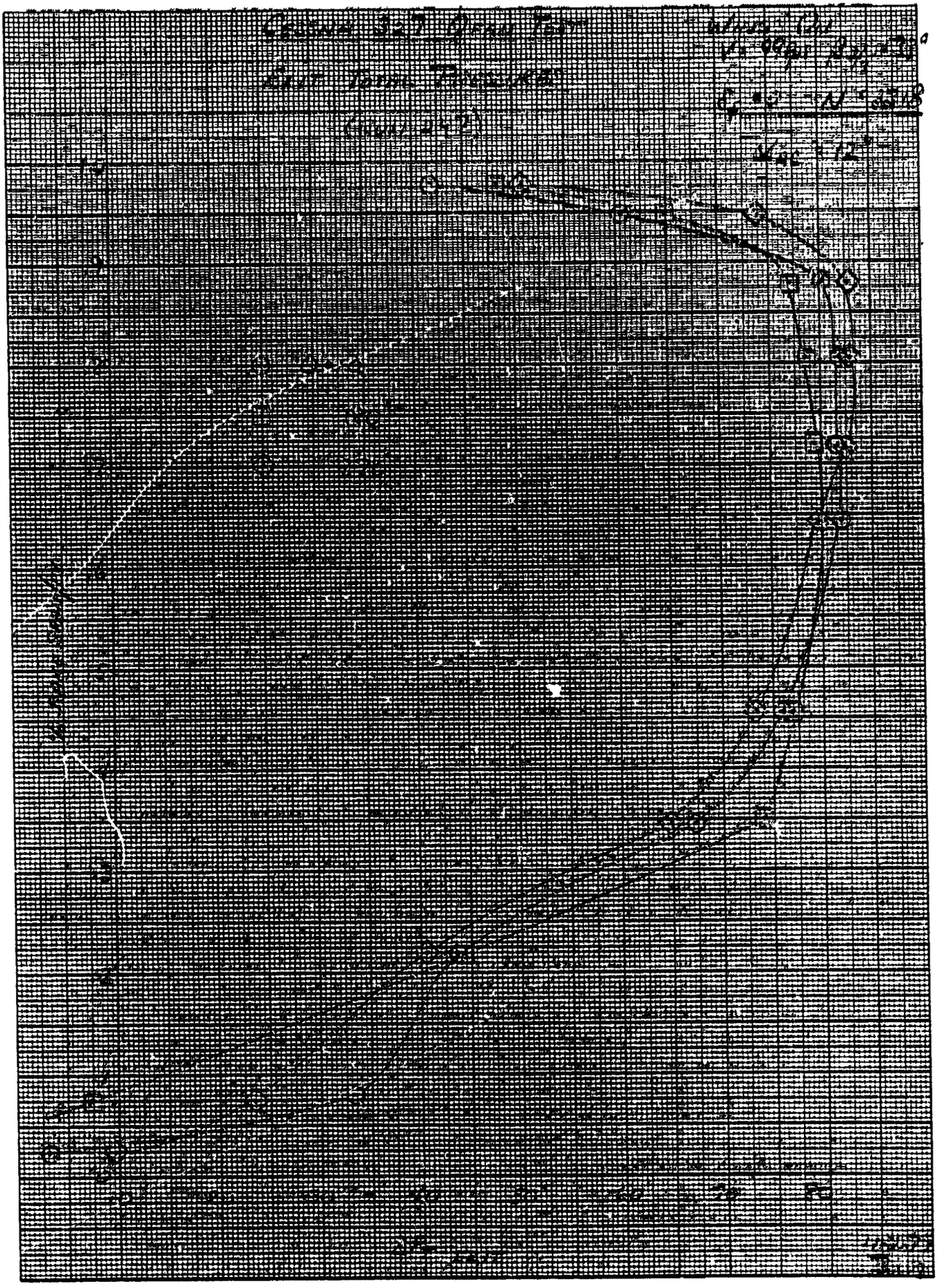

Figure 42

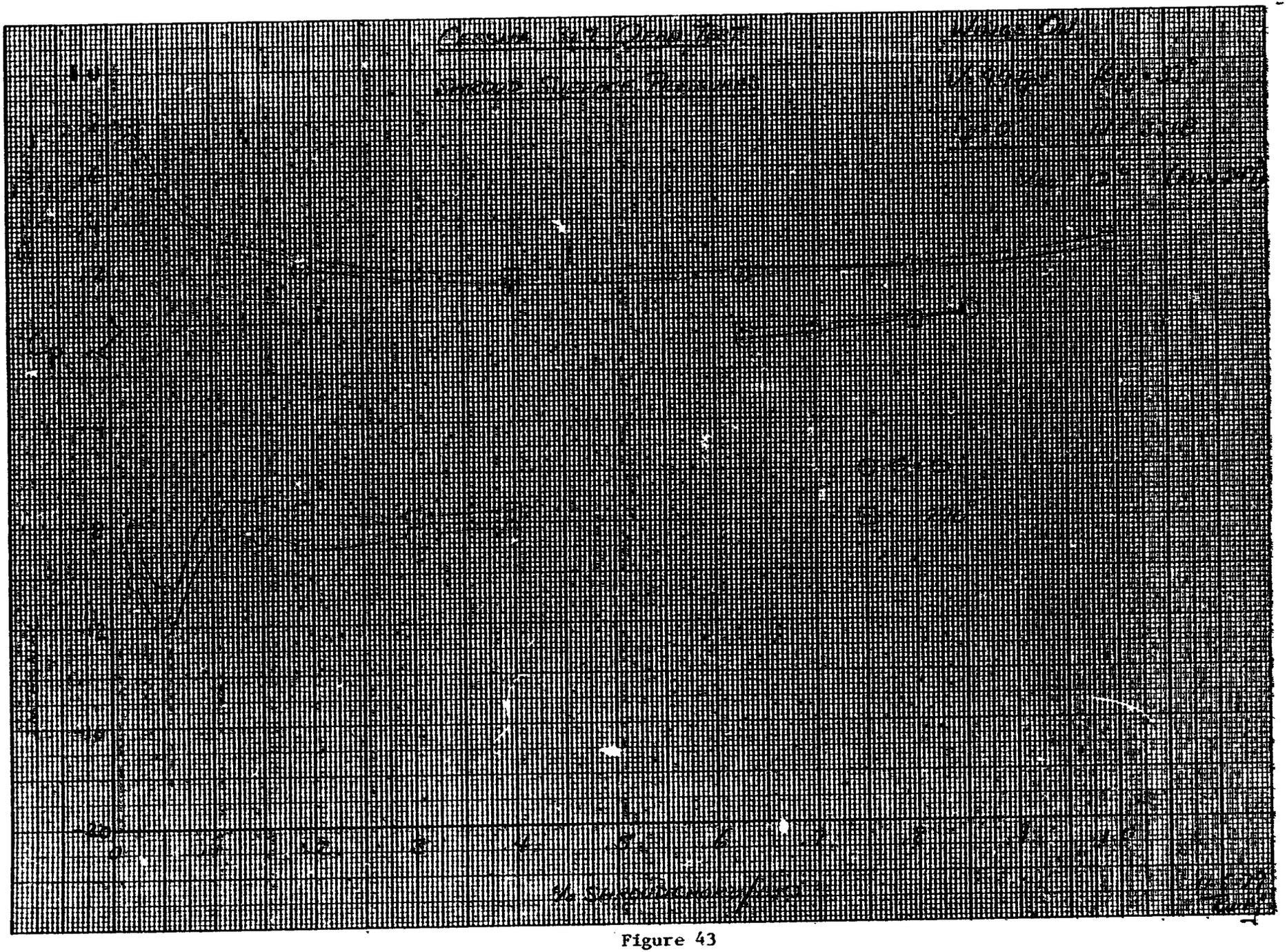

Figure 43

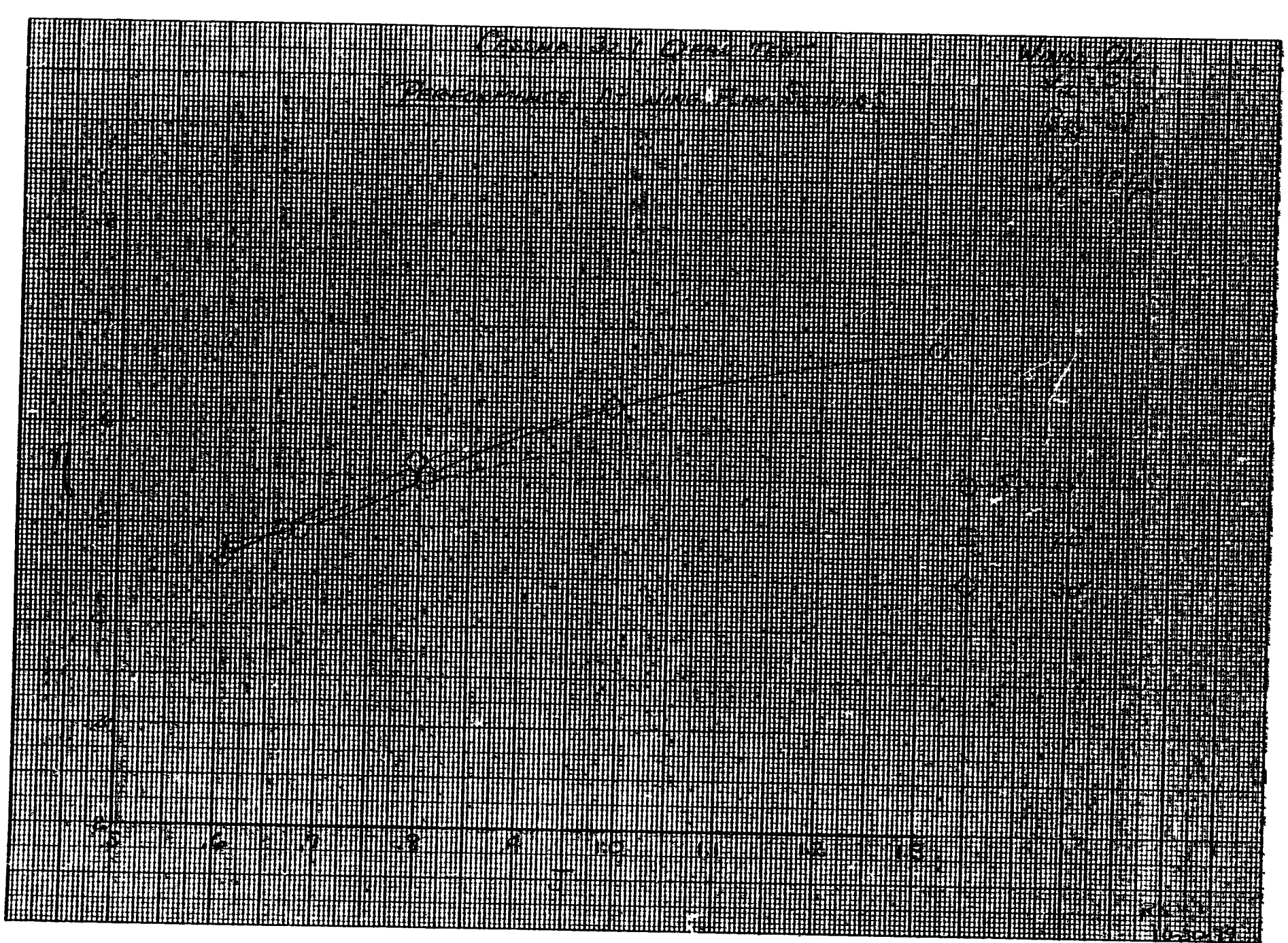

Figure 44

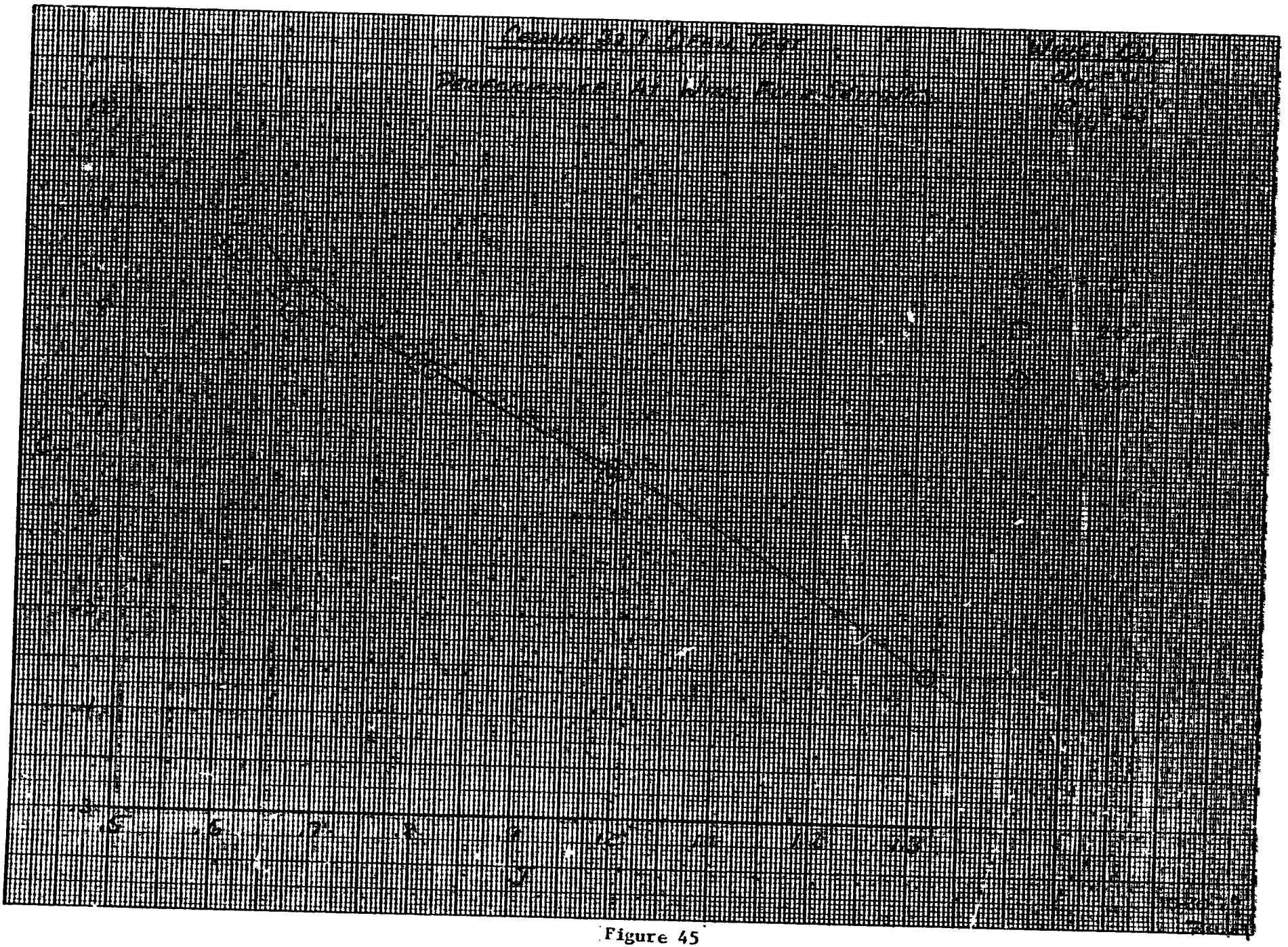

Figure 45

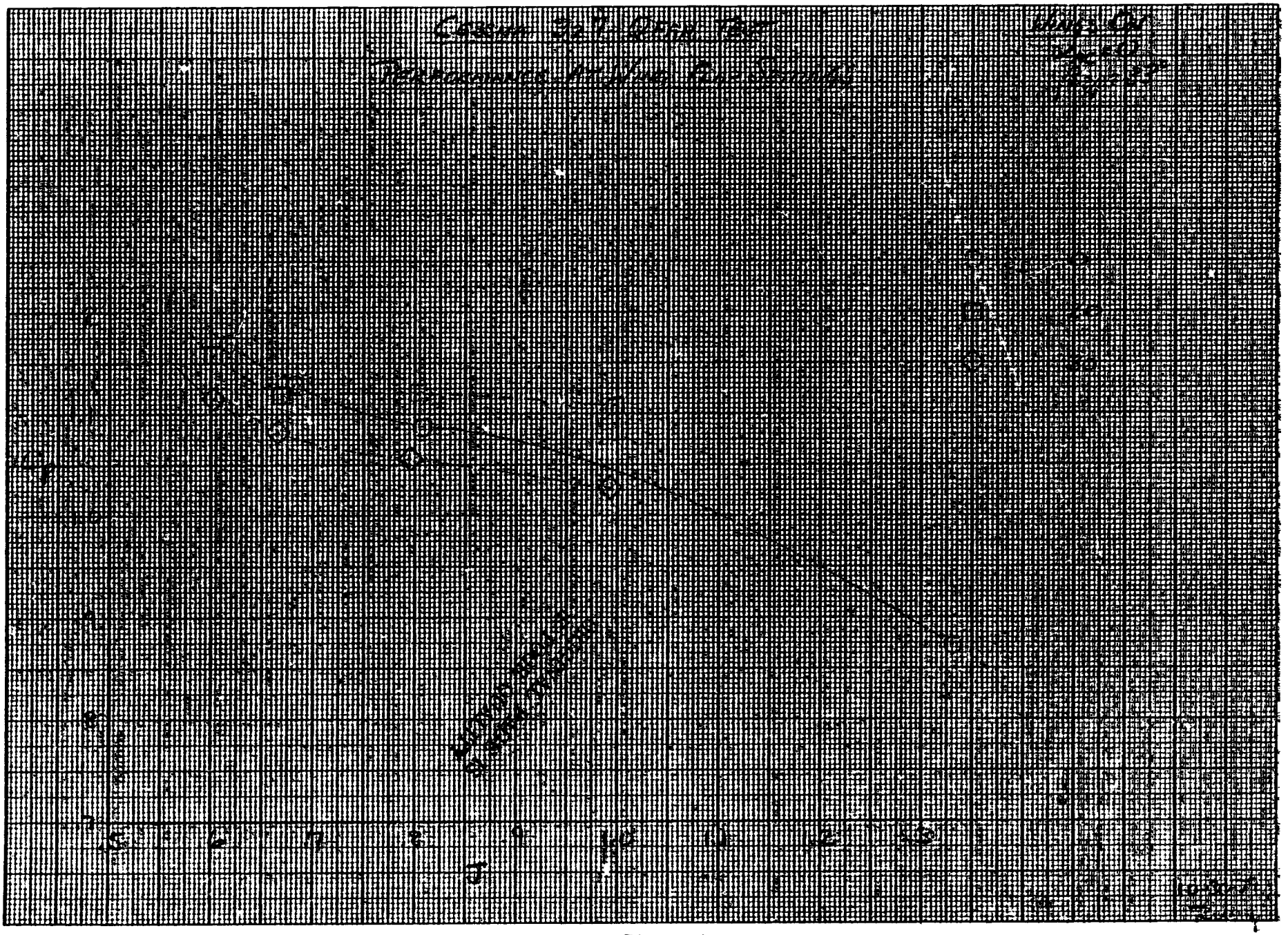

Figure 46

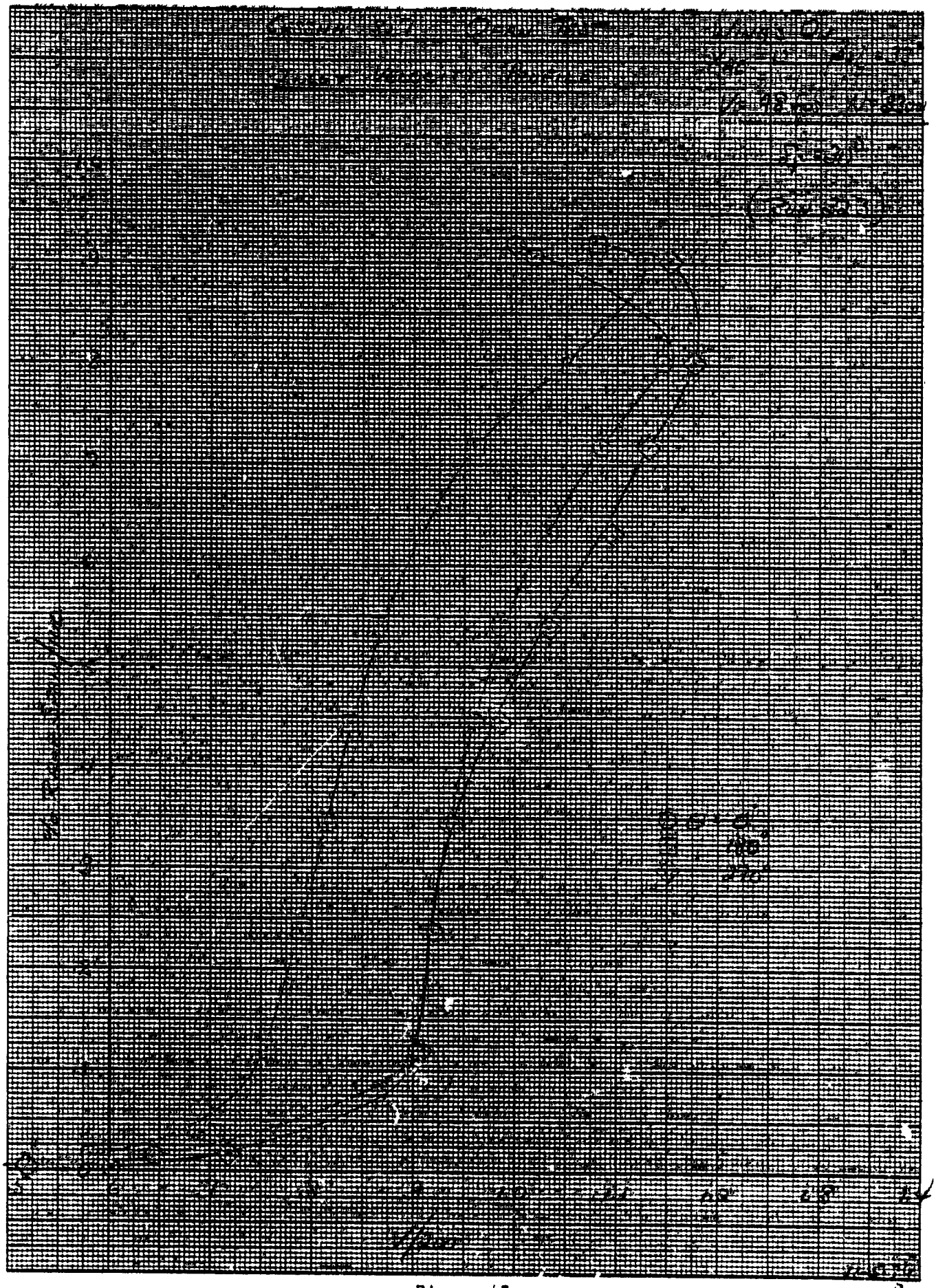

Figure 47

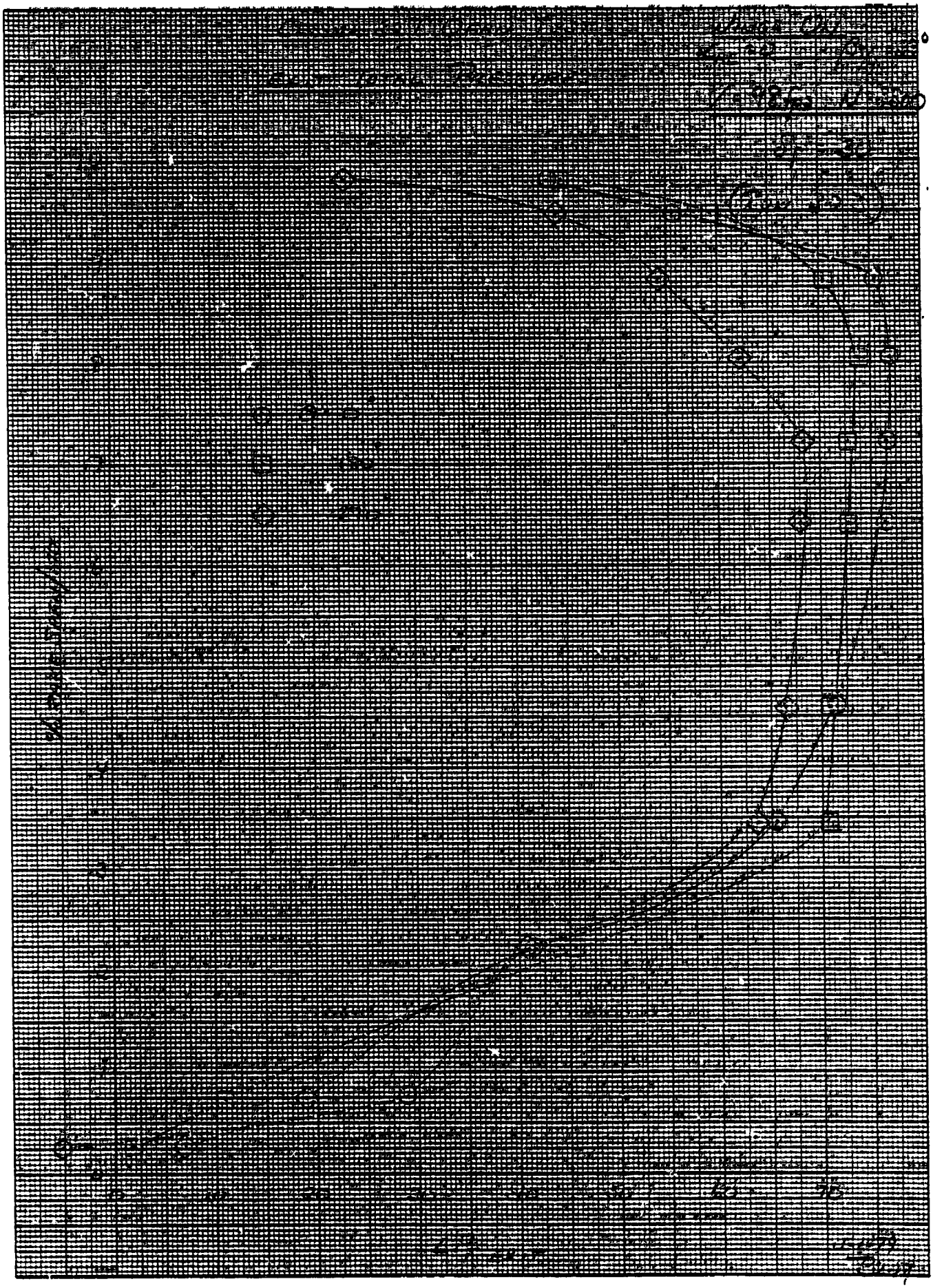

Figure 48

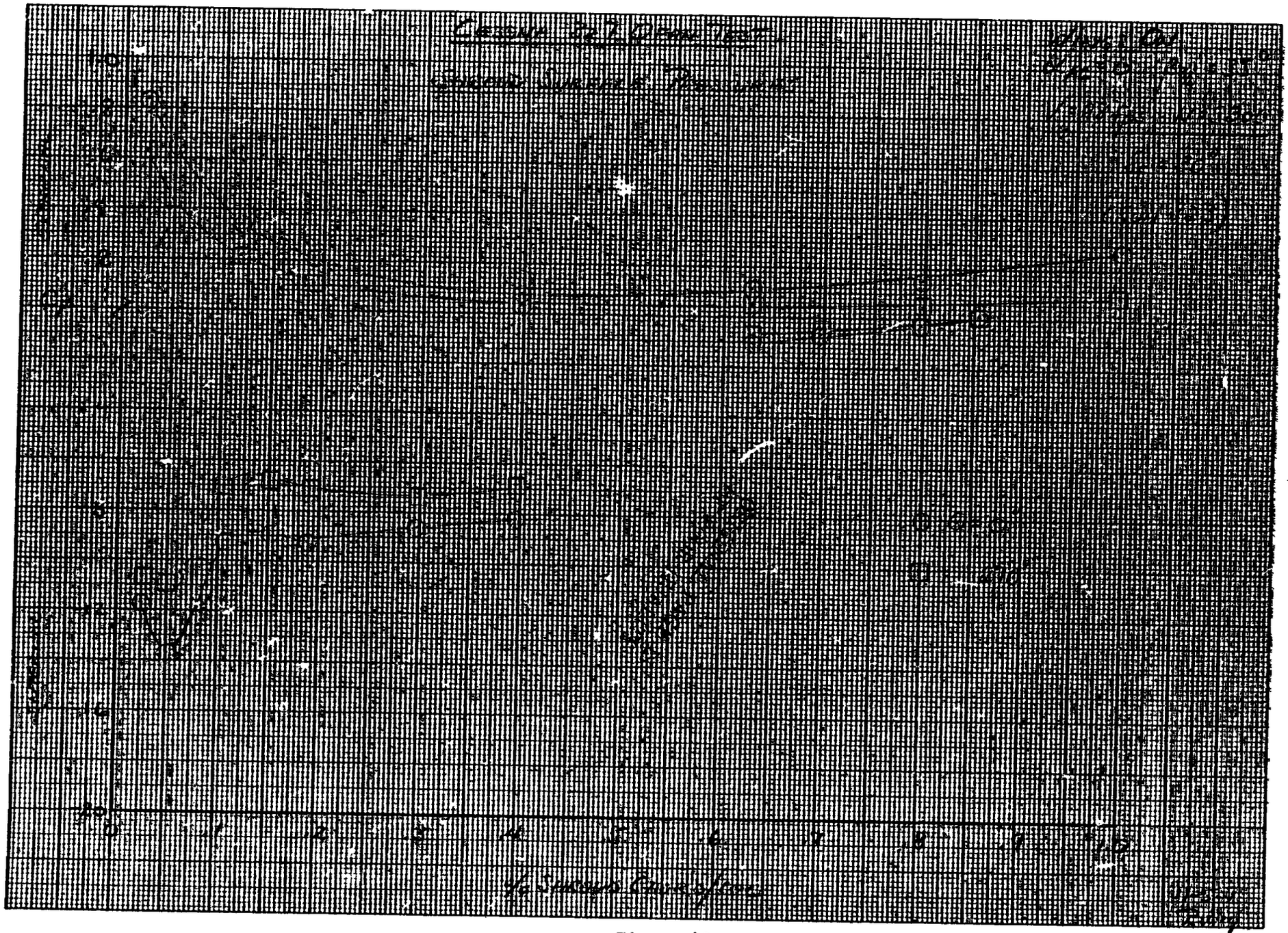

Figure 49

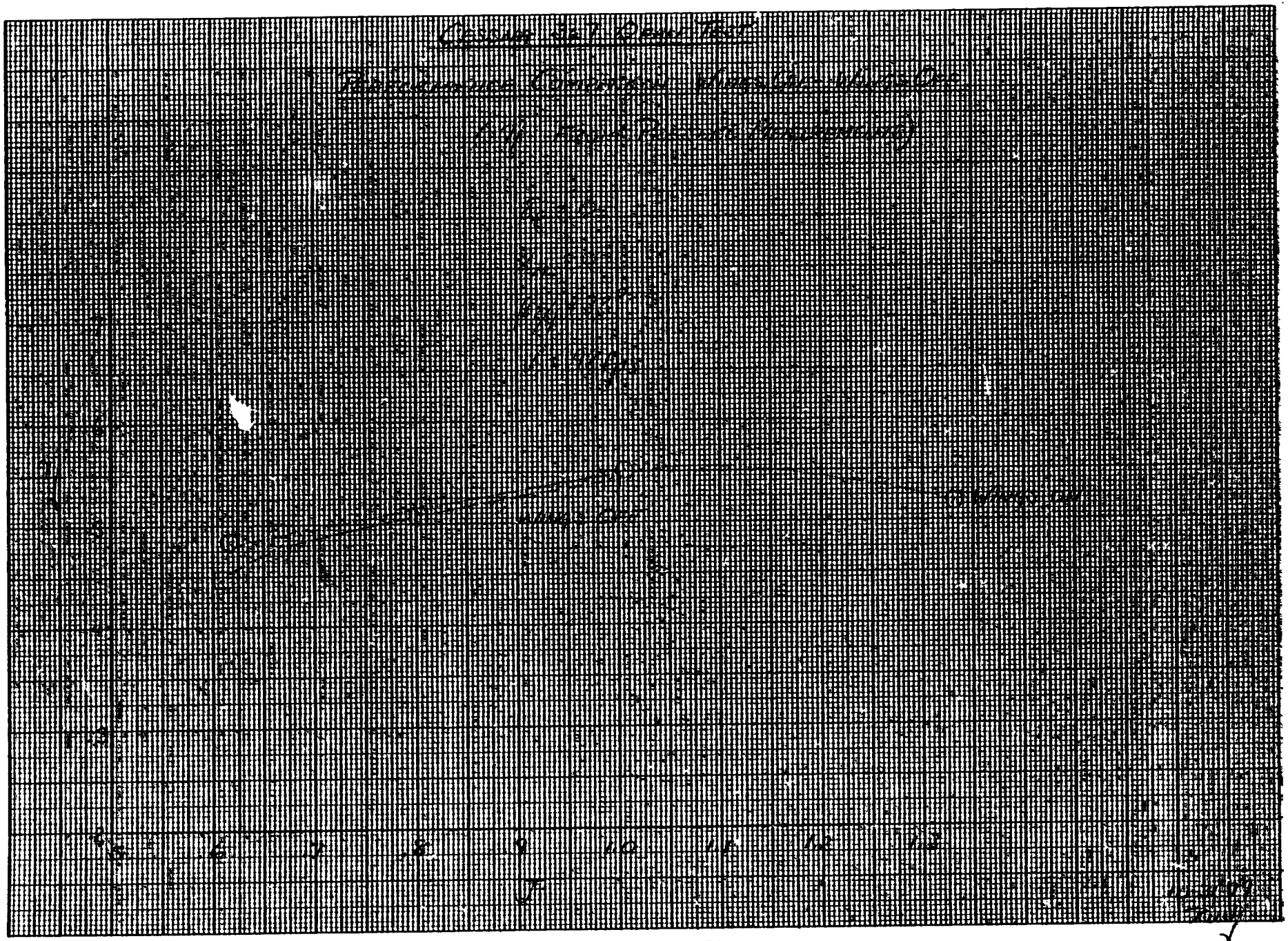

Figure 50

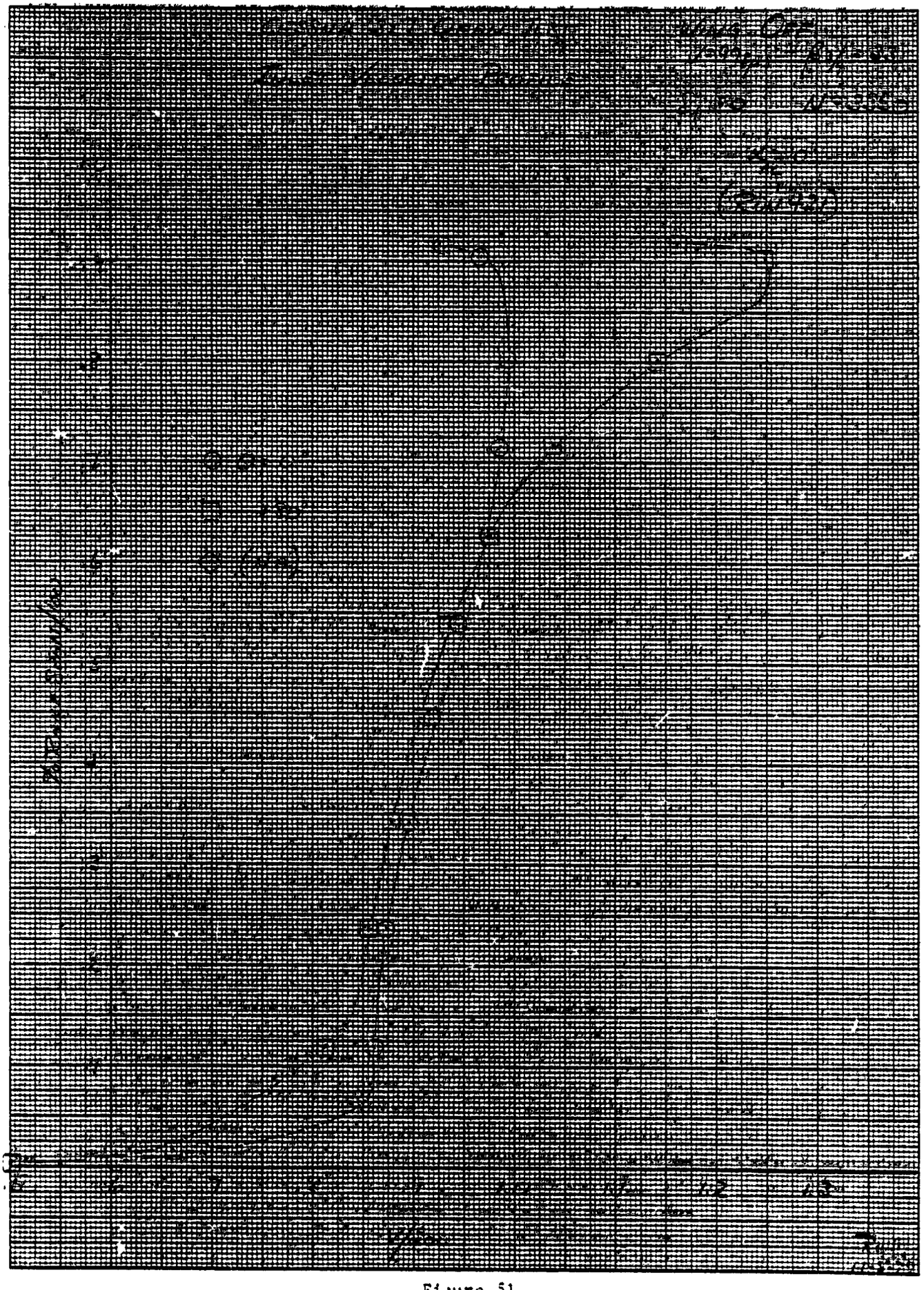

Figure 51

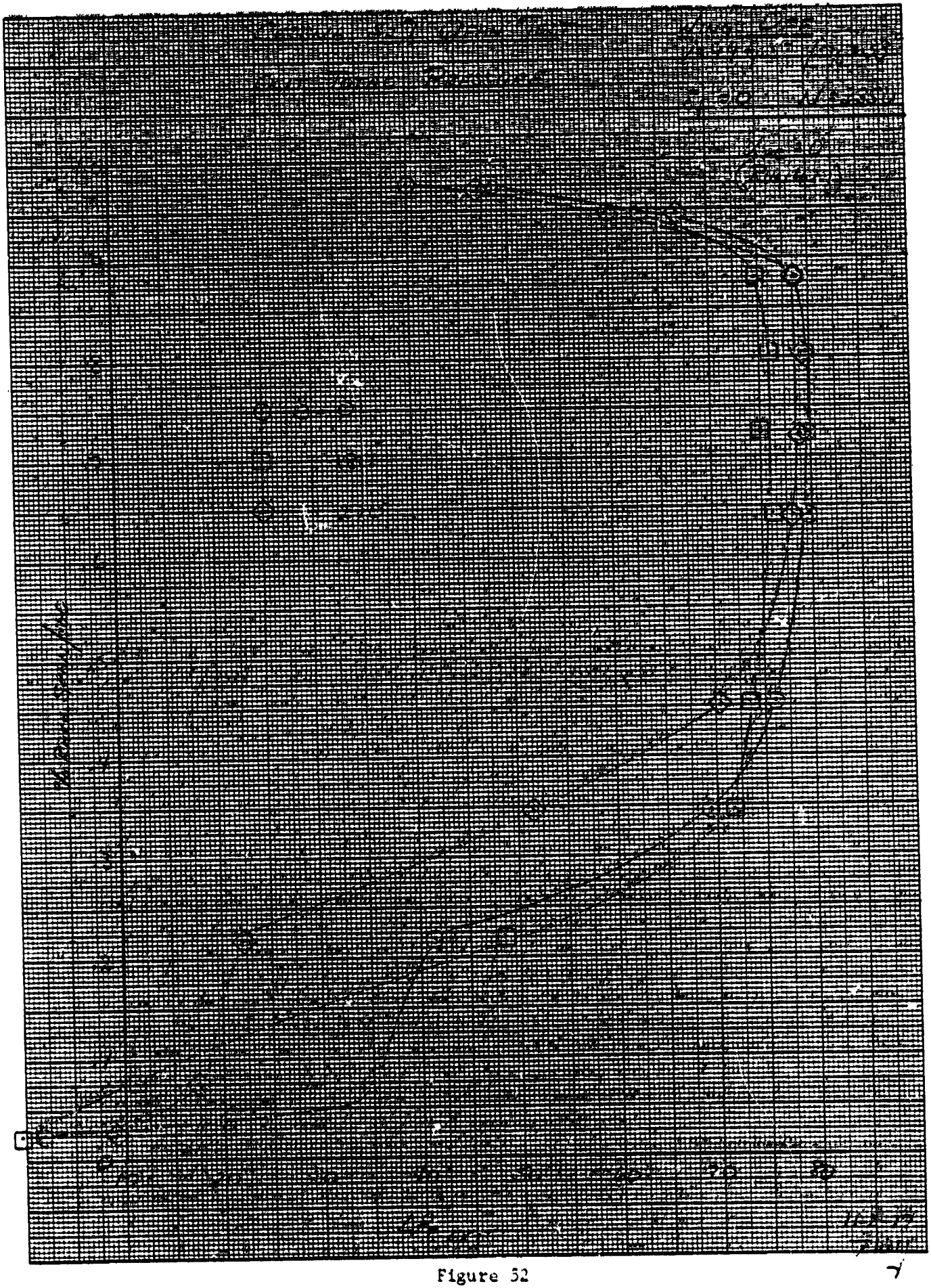

Figure 52

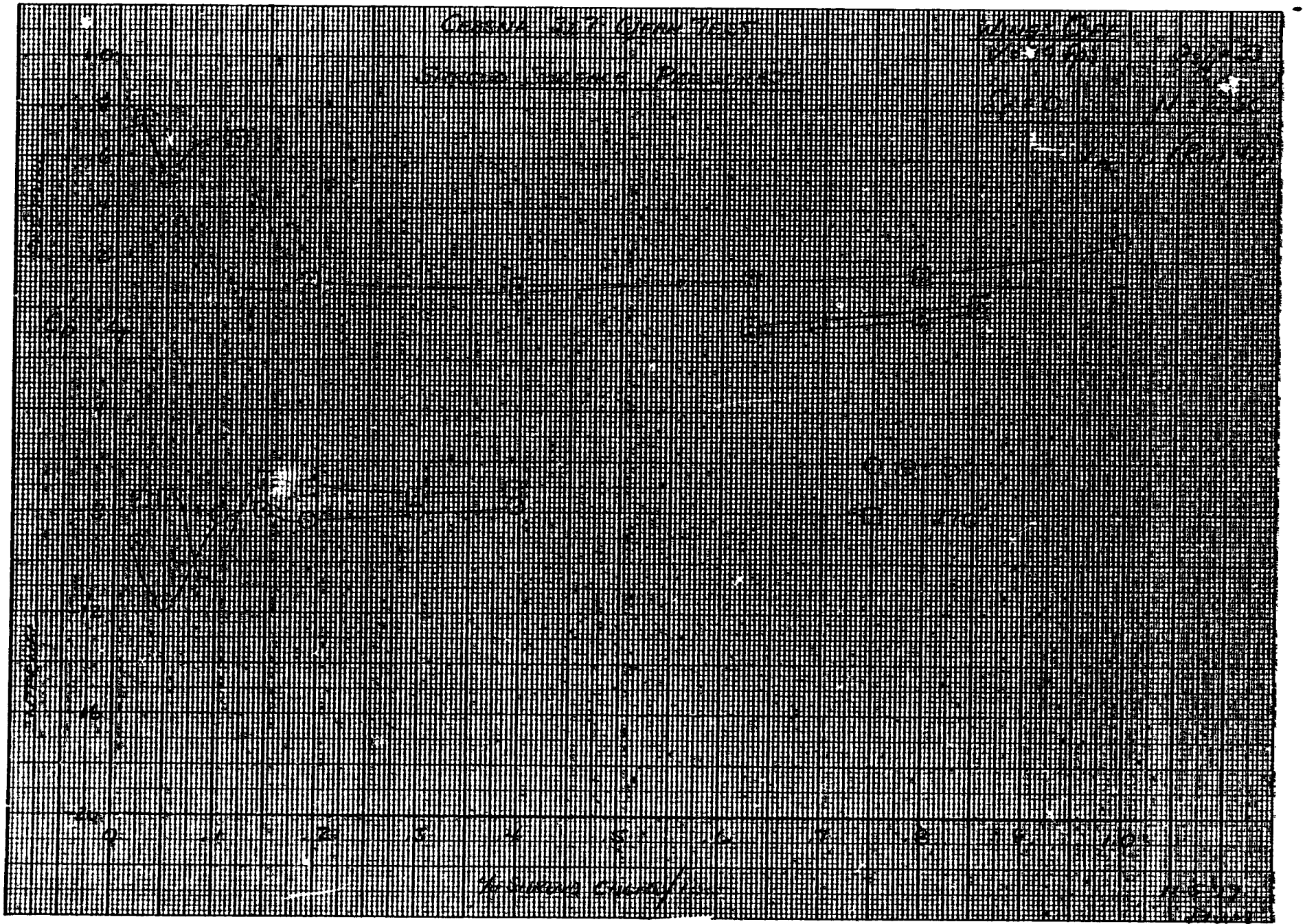

Figure 53

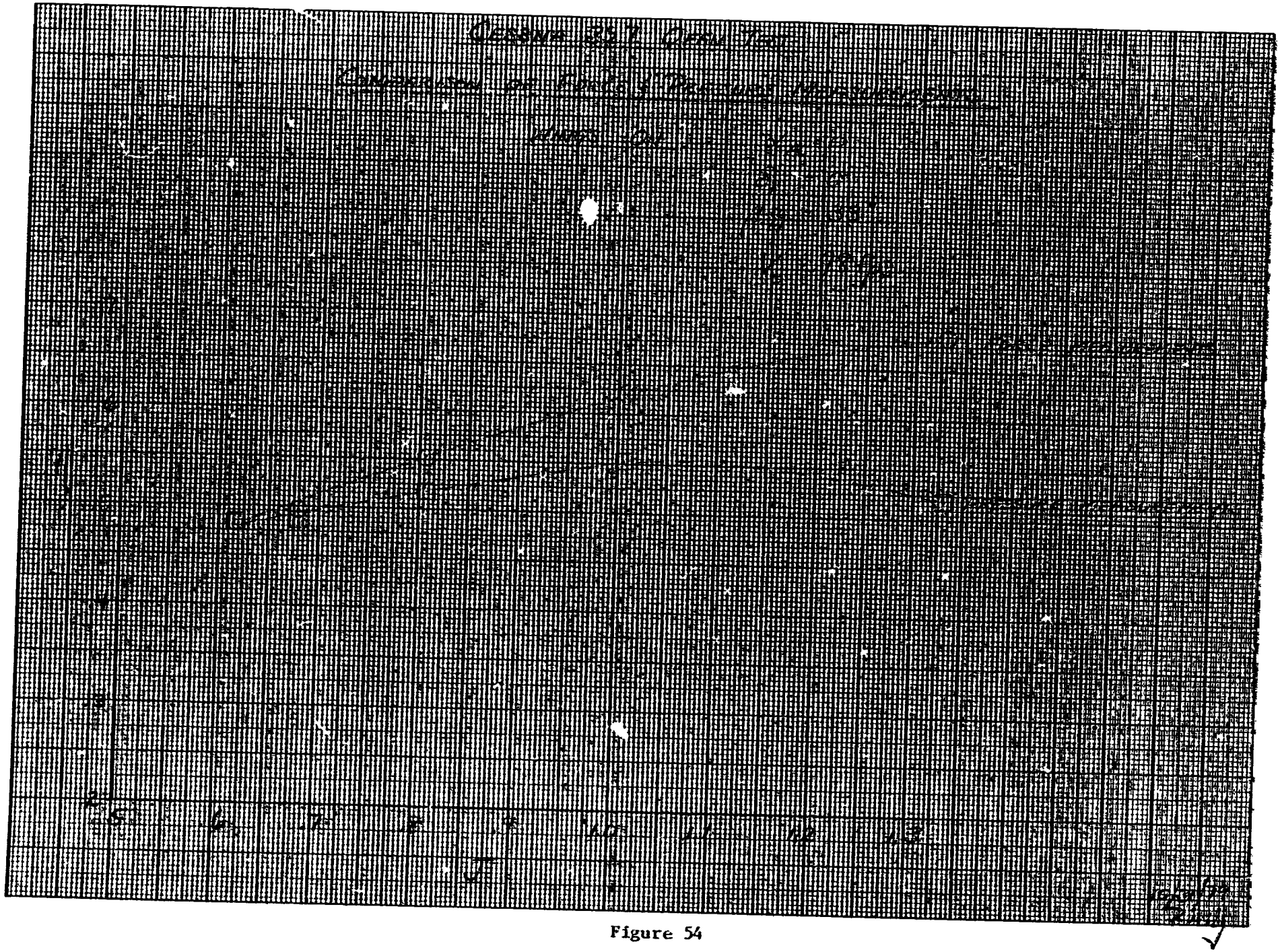

Figure 54

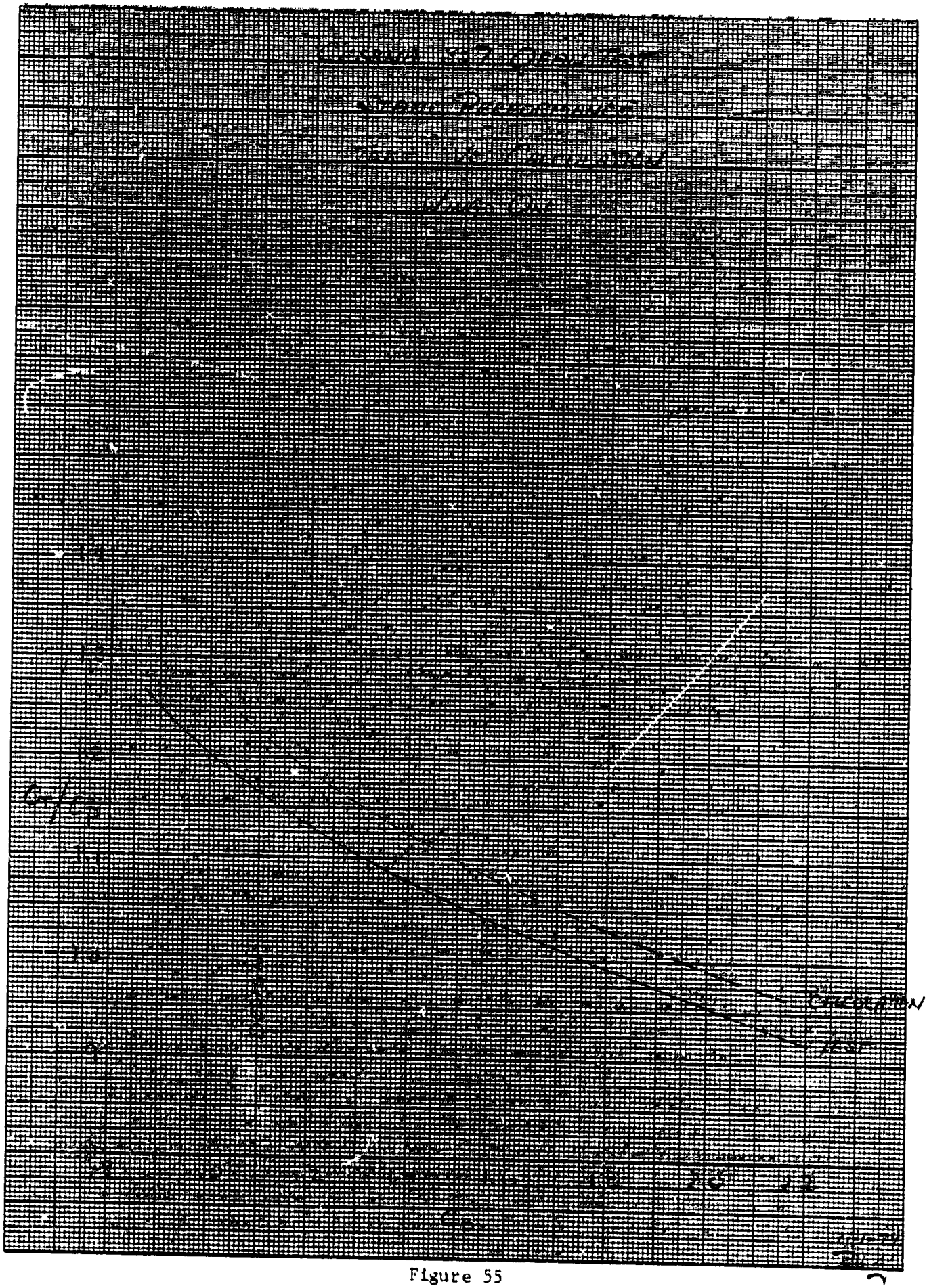

Figure 55

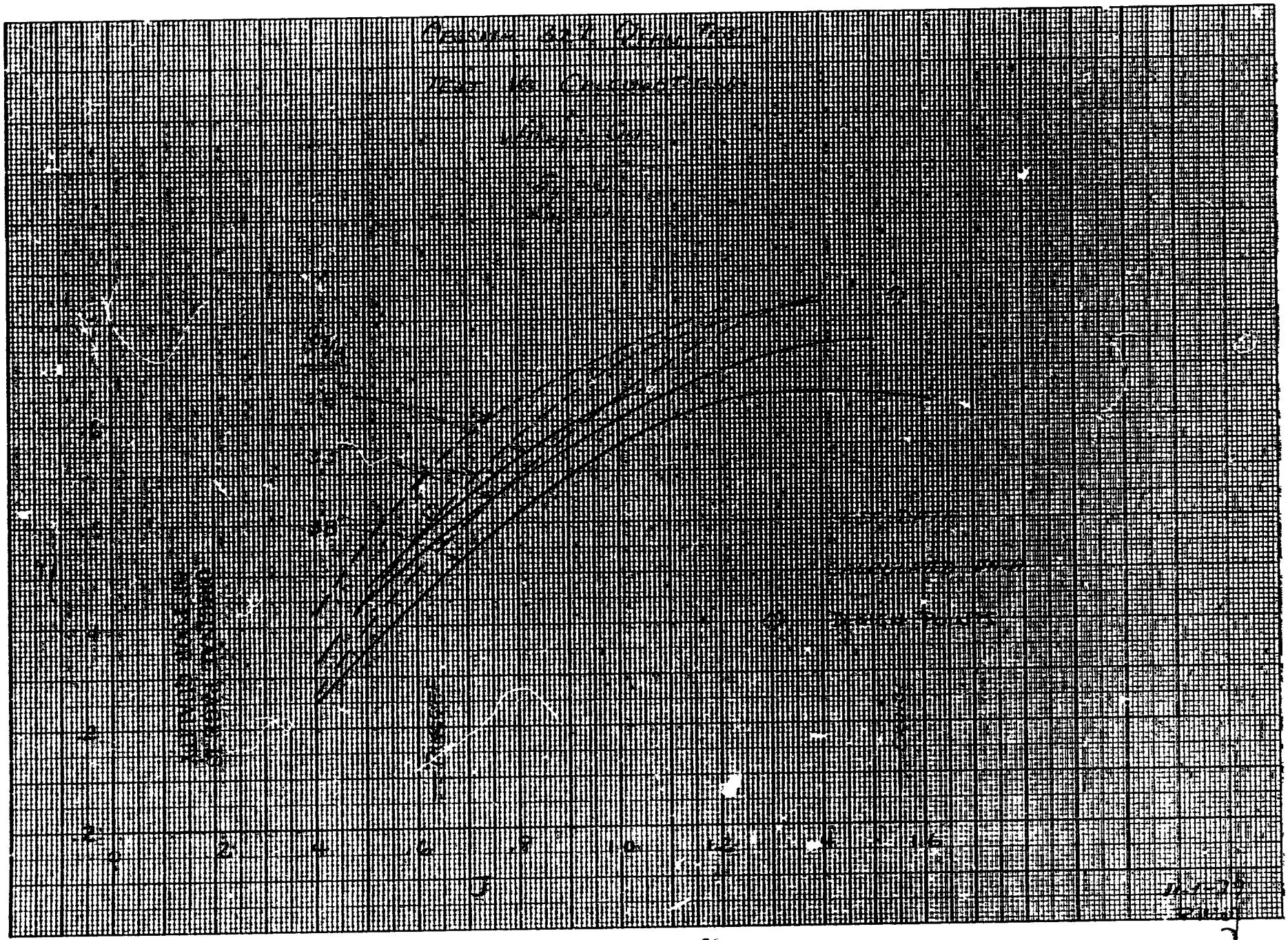

Figure 56

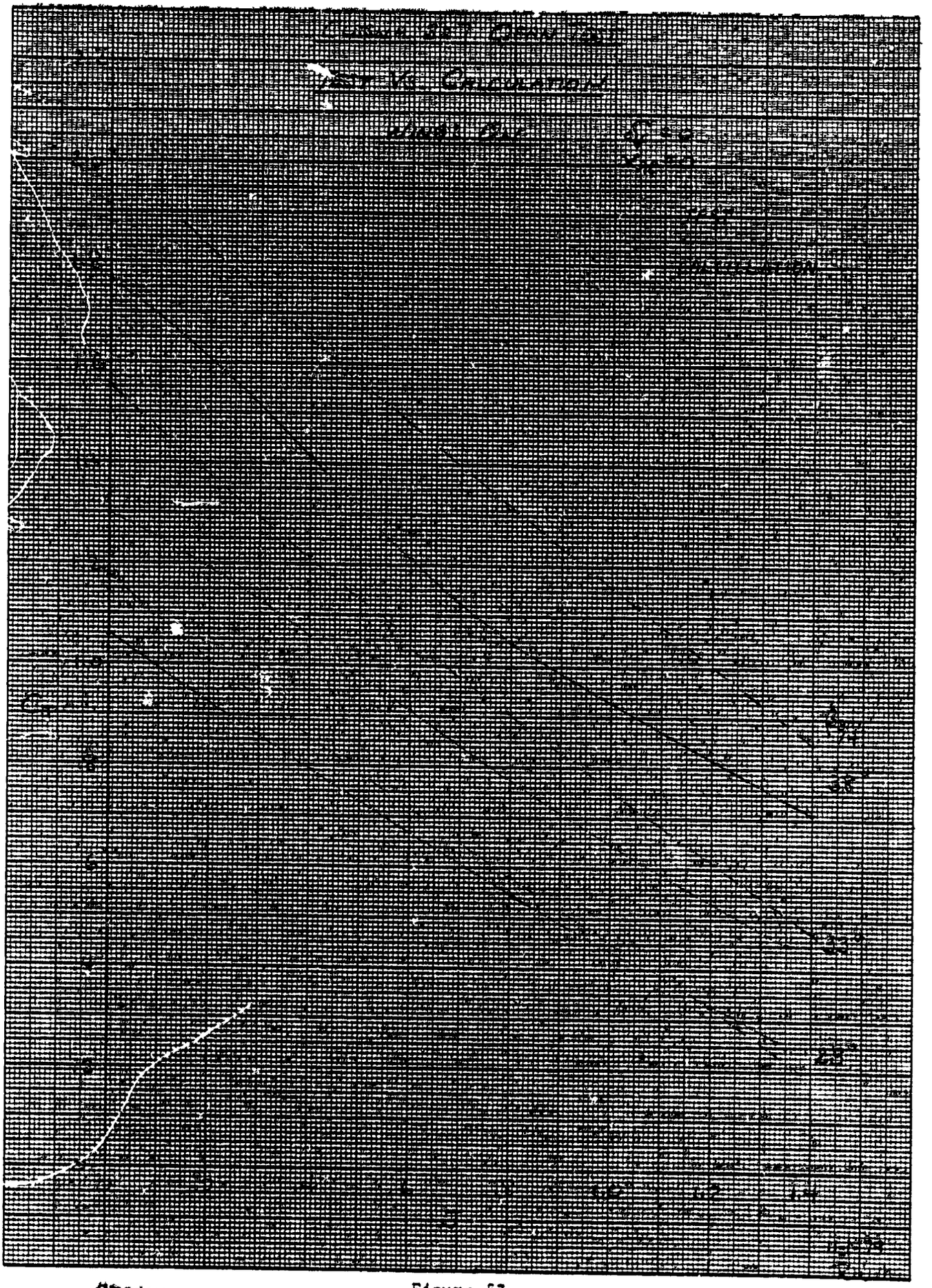

ORIGINAL PAGE IS
OF POOR QUALITY

Figure 57

C-2

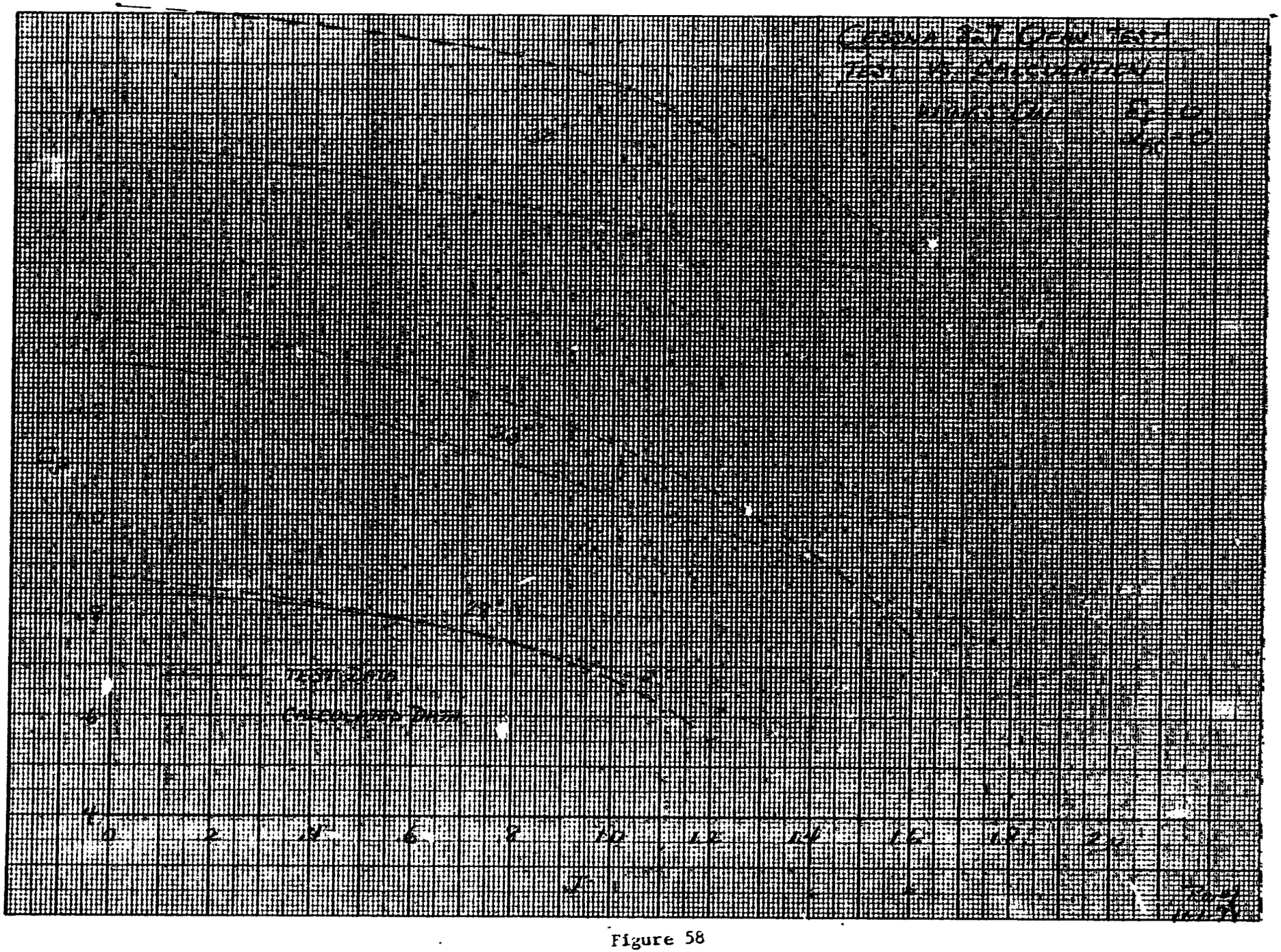

Figure 58

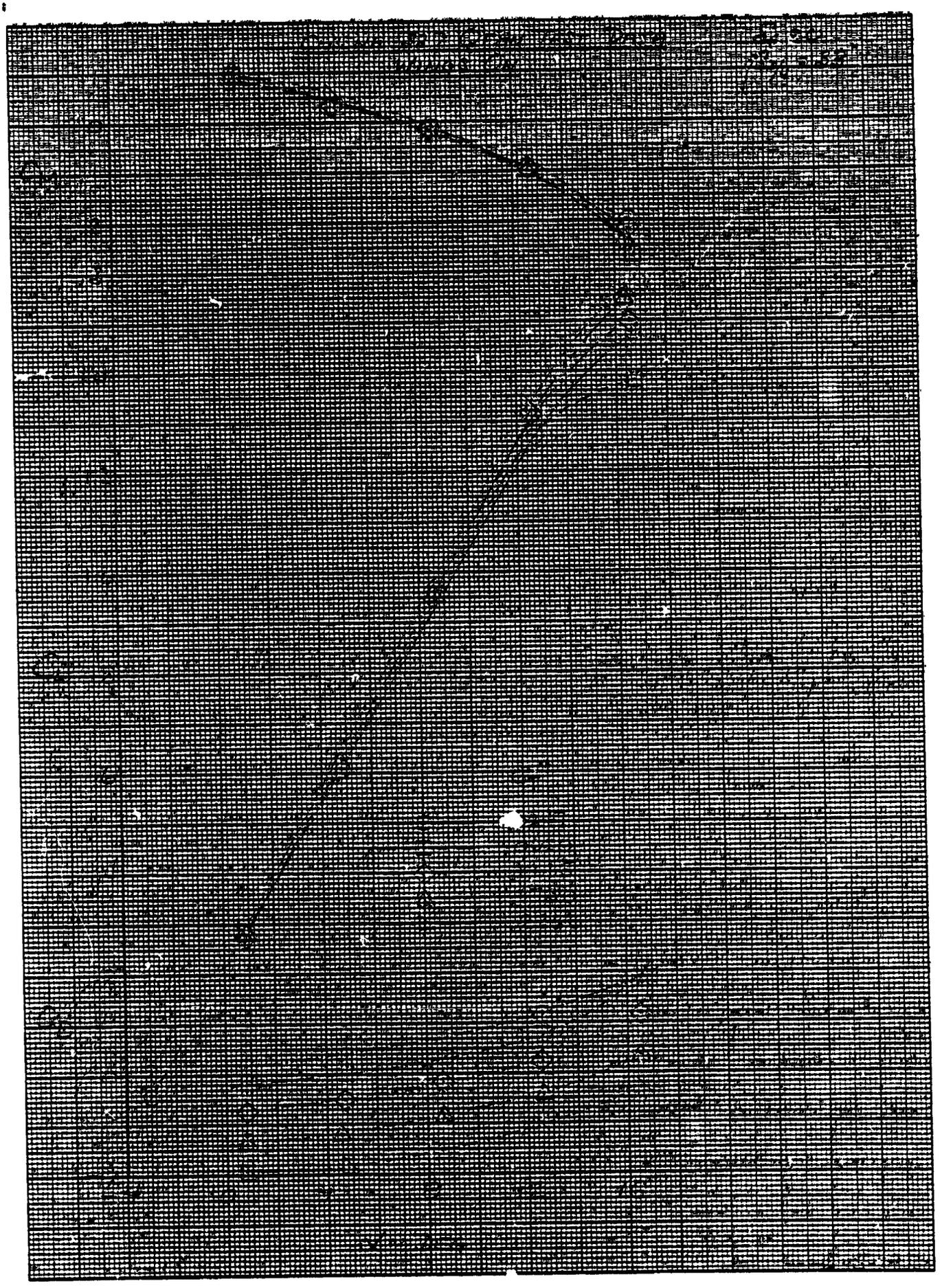

Figure 59

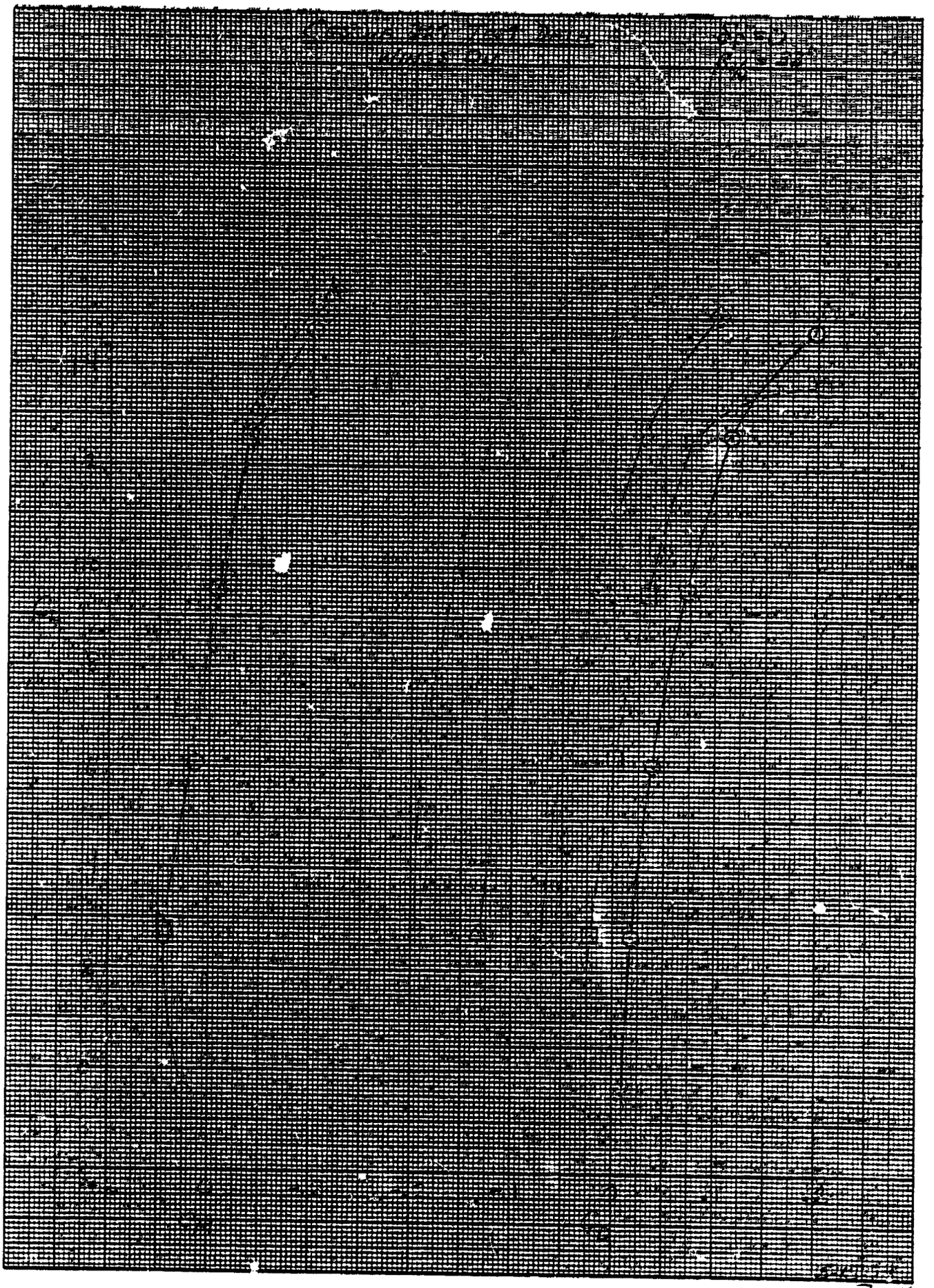

Figure 60

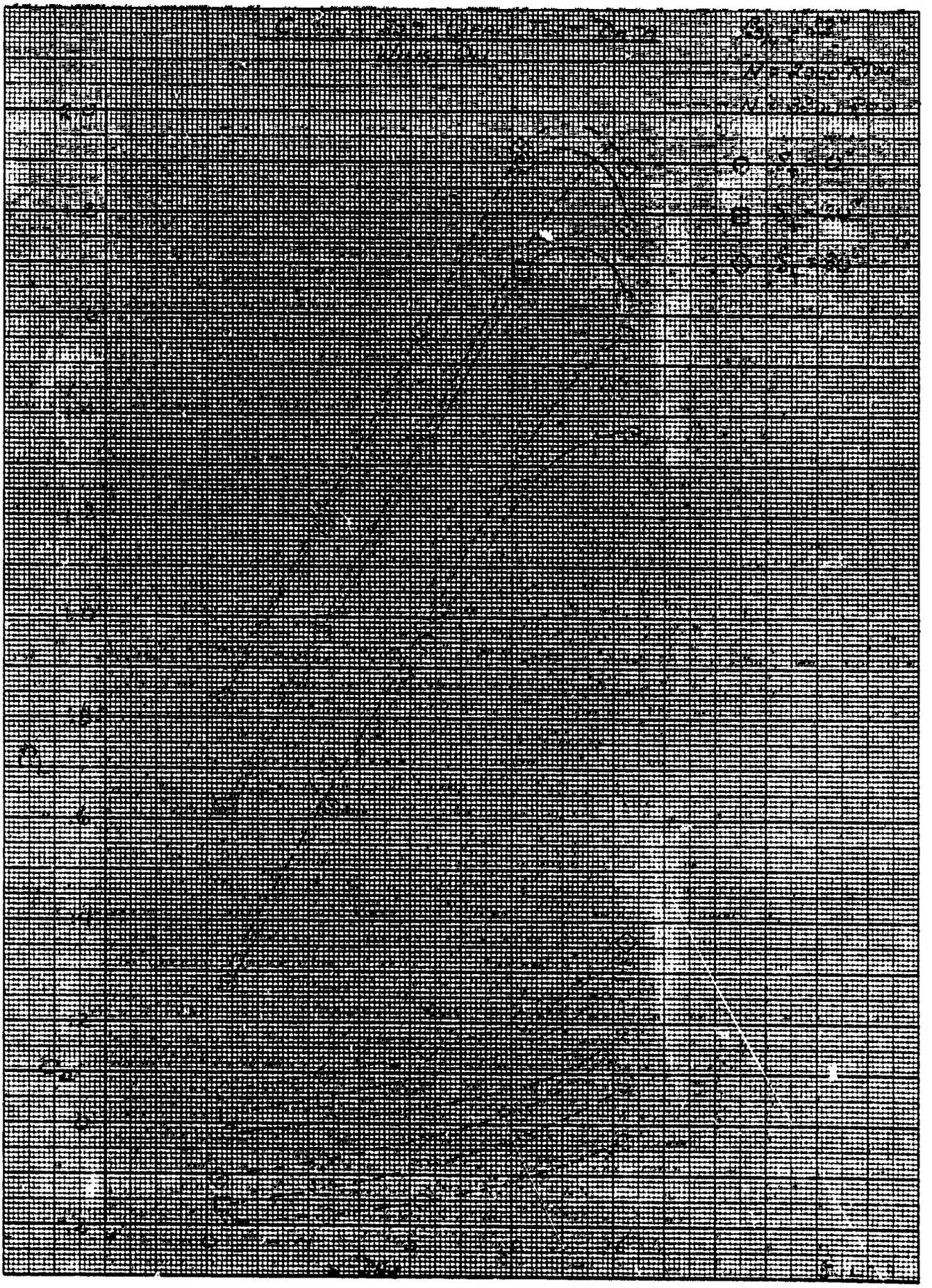

Figure 61

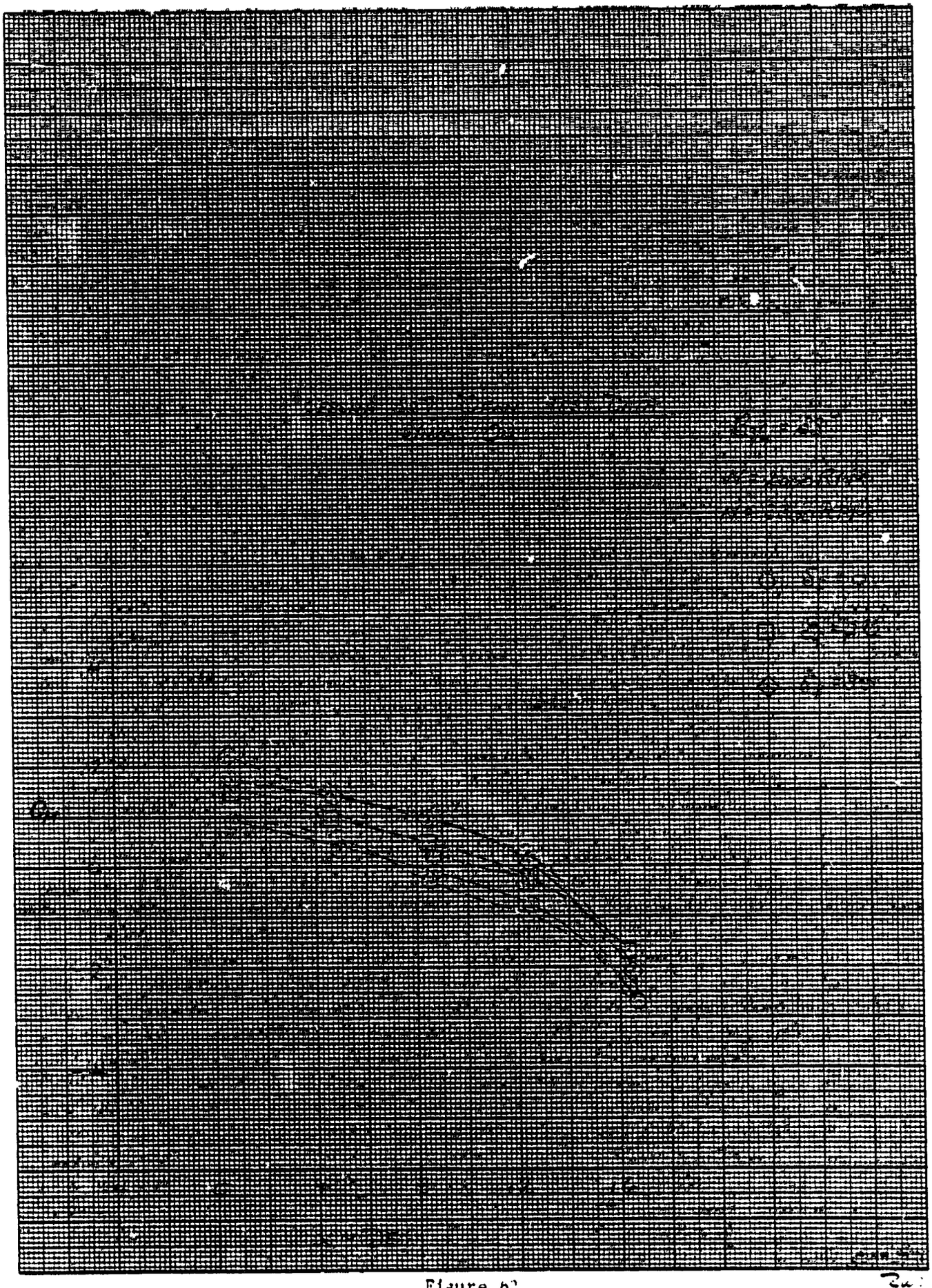

Figure 62

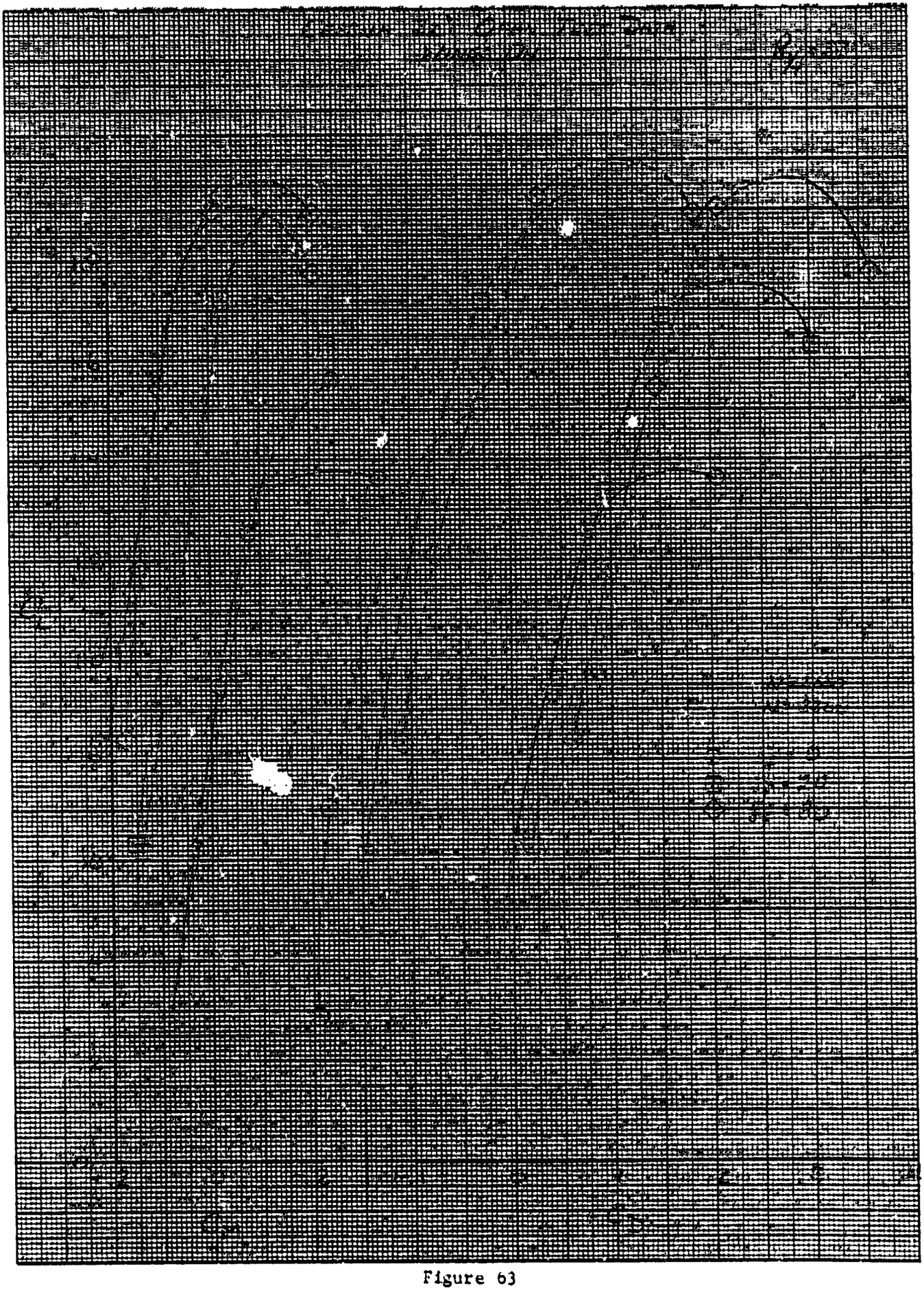

Figure 63

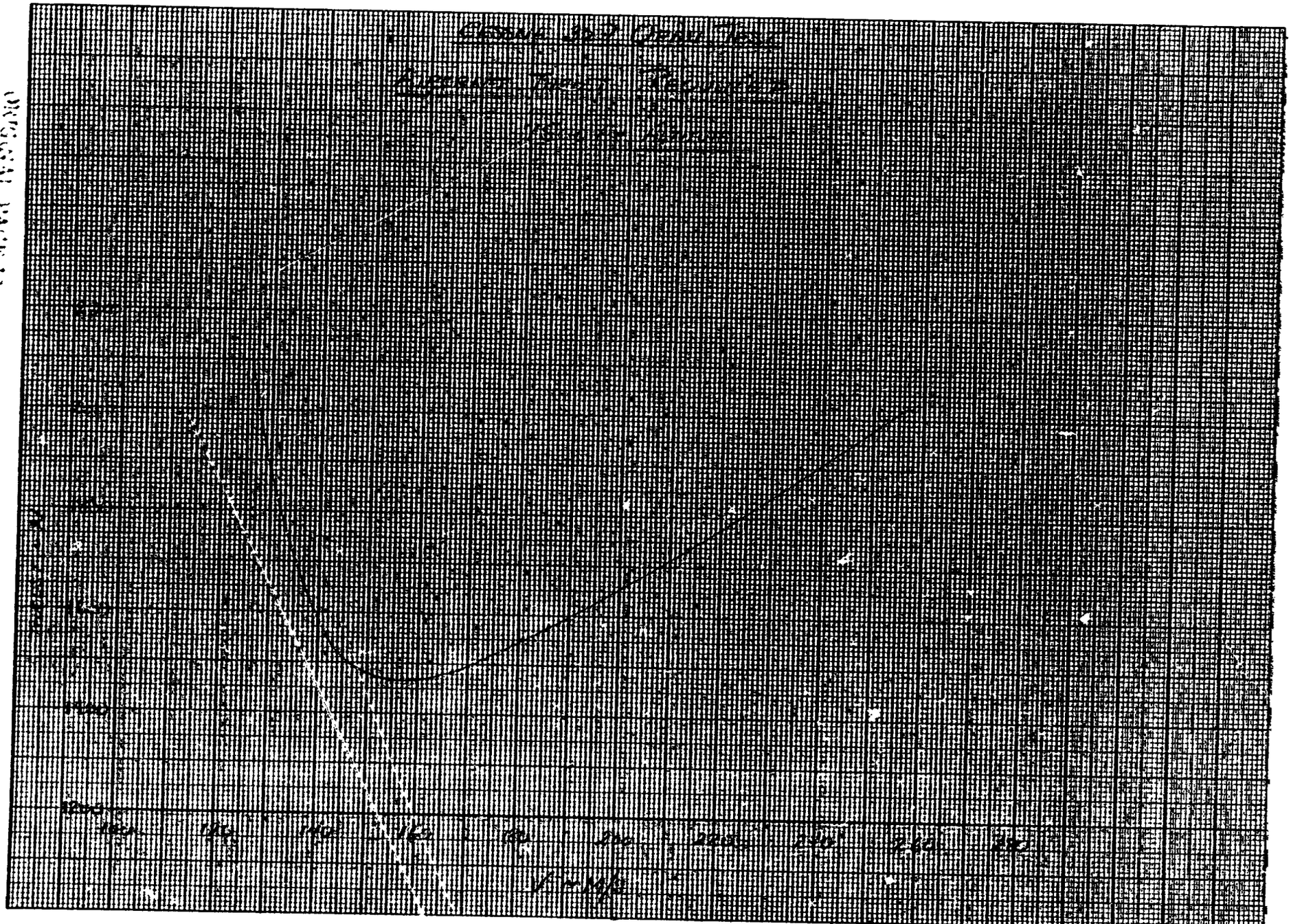

Figure 64